Auxin-induced degradation dynamics and plant development

Jessica Marie Guseman

A dissertation

submitted in partial fulfillment of the

requirements for the degree of

Doctor of Philosophy

University of Washington

2014

Reading Committee

Jennifer Nemhauser, Chair

Takato Imaizumi

Christine Queitsch

Program Authorized to Offer Degree:

Biology

University of Washington

Abstract

Auxin-induced degradation dynamics and plant development

Jessica Marie Guseman

Chair of the Supervisory Committee:
Associate Professor Jennifer Nemhauser
Biology

Development requires cells to send and receive information, often in the form of small molecules or peptides. An emerging theme in biology is that information can be encoded in the dynamics of signaling, not just in the relative abundance of signaling molecules. In plants, response to the hormone auxin is a useful tool for studying the role that signal dynamics play in development. Auxin triggers degradation of an Aux/IAA repressor protein, which activates transcription of a large number of genes. Auxin facilitates Aux/IAA degradation by mediating interaction between Aux/IAAs and auxin receptors called TIR1/AFBs. Each component in the auxin signaling pathway belongs to a gene family, and different family members play distinct roles throughout development. Our work building a synthetic auxin response system in yeast revealed that Aux/IAAs exhibit a range of degradation rates. I hypothesized that these IAA degradation rates act as biological pacemakers to coordinate developmental processes. To test this, I

characterized the effect of altered rates of Aux/IAA degradation on lateral root initiation. These studies demonstrate that Aux/IAA degradation dynamics determine the rate of progression through lateral root development in Arabidopsis. This work has revealed a molecular connection between the dynamics of auxin signaling and the dynamics of organogenesis, supporting the hypothesis that the Aux/IAAs act as auxin-induced pacemakers in plant development.

ACKNOWLEDGEMENTS

There are so many people that made this journey through graduate school possible. It's a difficult thing to do, and we all need quite a lot of help, whether we realize it or not.

The Biology Department has been very supportive, both financially and in providing many opportunities to learn, network, and present data. Our staff have constantly been amazing. Especially Judy and Marissa for dealing with graduate business; Rodney for helping me with payroll things for many years; Brianna for figuring out everything ordering; and Robert and Alex for making the buildings and equipment work. Several fantastic faculty members have been especially helpful in providing classes, seminars, advice, and conversation. In particular, Dave Parichy, Barbara Wakimoto, Billie Swalla, Cecilia Moens, Janneke Hille Ris Lambers, and Liz Van Volkenburgh. And additionally for teaching me how to teach: Ben Wiggins and Linda Martin-Morris.

The developmental biology community and the DBTG have been supportive of my research in many ways for many years. My three years on the Developmental Biology Training Grant have not only been financially helpful, but also mentally stimulating and incredibly useful for bringing a group of graduate students together who would otherwise not have interacted as much. I learned a lot about new research outside of my immediate field, and we had lots of practice communicating across disciplines. Thanks especially to Dave Raible for leading this group.

My graduate committee has been incredibly helpful and supportive through this whole process. They pushed me with thoughtful questions and it was clear that they cared about my success. It says a lot that I actually have quite fond memories of my general exam. Thank you for all of your advice and help over these past years, and I look forward to seeing the amazing work your labs do in the future, and hopefully running into you at meetings! Thank you Keiko Torii, Takato Imaizumi, Christine Queitsch, and Eric Klavins.

My cohort of incoming graduate students is a great group of positive, fun people. Talking and spending time with these people made the transition to graduate school much smoother, and I am very glad to have been able to keep up with most of them throughout my time here. I would like to especially thank Jaquan Horton, Kelsey Galimba, Heather Hunsperger, Hilary Hayford, and Olivia Woods.

Through our AuxSynBi/o collaboration, I spent a lot of time in the Klavins lab in the first few years of graduate school, and have continued to have the chance to interact with lab members through meetings. These interactions taught me so much about collaboration on many different levels, and I am grateful to have met and worked with some really great Klavins lab people through this project. And I would still totally be down for an AuxSynBi/o tattoo – or at least a t-shirt.

I have had the opportunity to work with several amazing undergraduate students over these years. I was fortunate to be able to teach and collaborate with these incredibly smart, thoughtful, and helpful individuals: Zachary McCauley, Autumn Walker, and Tamar Feldman. Each of these students will go on to do amazing things and I am very proud of their accomplishments.

The Nemhauser lab has been such a dynamic, positive group of people that have made my life so much more enjoyable. The science we do is super cool, but I like being around these people so much, that being at work is enjoyable even on the days when nothing works (i.e. when you realize you cloned a stop codon into the middle of you construct or something). I will really miss working with you, and I am happy to have made such a fantastic group of life-long friends and colleagues: Andrej Arsovski, Anahit Galstyan, Chris Gee, Amy Lanctot, Jodi Lilley, Britney Moss, Edith Pierre-Jerome, Cristy Walcher, Clay Wright.

Wonderful people that kept me sane and with whom I enjoyed many weekends and in-depth discussion about life, the universe, and everything:

Jodi and Travis, Britney and Rande, Edith and Nima, Kyle, Cat and Justin, Frank and Elizabeth, Dan and Autumn, Jen, Alan, Jena.

Increasingly through graduate school, I have become more and more grateful that I joined Jennifer Nemhauser's lab and that I had the opportunity to have Jennifer as a mentor. She has been an incredibly thoughtful, caring, generous person to learn from, and it was clear from the beginning that she would have my back.
Thank you for always pushing me, but at the same time giving great tools and advice for how to take care of myself in the face of stress. Meditation was the best thing I did for myself during grad school. I have grown so much during my time in your lab, and I especially want to thank you for helping me to remember to believe in myself.

My family have always been my biggest supporters. They taught me that I could be anything I wanted to be. Thank you Dad for always being so blown away by my descriptions of my research – it helps me remember that I am doing some pretty cool things. And thank you Mom for answering all of my late-night panic attack phone calls and listening to my grad school woes. And thank you Nick for reminding me that people do not always realize how talented they are – you are amazing and hopefully you realize it.

And finally, Adam: my wonderful, supportive, generous husband, who said five years ago, "Yeah, you should totally apply for grad school". And had no idea what he was getting into. Thank you for always being there for me, through all the craziness. I am happy to know we will go through these next phases together.

Chapter 1

Photomorphogenesis

Andrej A. Arsovski, Anahit Galstyan, Jessica M. Guseman and Jennifer L. Nemhauser (2012) Photomorphogenesis *The Arabidopsis Book* 10:e0147.

ABSTRACT

As photoautotrophs, plants are exquisitely sensitive to their light environment. Light affects many developmental and physiological responses throughout plants' life histories. The focus of this chapter is on light effects during the crucial period of time between seed germination and the development of the first true leaves. During this time, the seedling must determine the appropriate mode of action to best achieve photosynthetic and eventual reproductive success. Light exposure triggers several major developmental and physiological events. These include: growth inhibition and differentiation of the embryonic stem (hypocotyl); maturation of the embryonic leaves (cotyledons); and establishment and activation of the stem cell population in the shoot and root apical meristems. Recent studies have linked a number of photoreceptors, transcription factors, and phytohormones to each of these events.

INTRODUCTION

As photoautotrophs, plants are exquisitely sensitive to their light environment. Light affects many developmental and physiological responses throughout plants' life histories, including germination (Bentsink and Koornneef, 2008), flowering (Alvarez-Buylla et al., 2010), and direction of growth (Pedmale et al., 2010). In *Arabidopsis*, there are four major classes of photoreceptors: the phytochromes (phy) acting predominantly in red/far-red wavelengths (Wang and Deng, 2004), the cryptochromes (cry) responding in blue and UVA (Yu et al., 2010; Chaves et al., 2011), the phototropins (phot) responding in blue (Phototropism), and recently identified UVB photoreceptors (Rizzini et al., 2011).

The focus of this chapter will be on light effects during the crucial period of time between seed germination and the development of the first true leaves. During this time, the seedling must determine the appropriate mode of action to best achieve

photosynthetic and eventual reproductive success. If light is limiting, the seedling will exhibit etiolated growth —a developmentally arrested growth mode characterized by an elongated hypocotyl topped by tightly-closed, underdeveloped cotyledons and a limited root system (skotomorphogenesis). In contrast, *Arabidopsis* seedlings grown in bright light have: short hypocotyls; expanded and photosynthetically-active cotyledons; and self-regulating stem cell populations at root and shoot apices (photomorphogenesis) (Figure 1).

A number of inputs determine where along this growth spectrum a given plant will be found, including the quality, quantity, duration, and intensity of light, as well as genetic factors. It is perhaps not surprising that such a complex web of regulation controls photomorphogenesis. In this brief window of time, a plant matures from an seed reserve-dependent embryo to a self-sufficient photoautotroph—correct assessment of the environment is quite literally a matter of life and death. Information about resources and environment must be conveyed across the entire plant to optimally coordinate growth. In the following sections, the focus will be on the major developmental and physiological events specific to seedling exposure to light.

HYPOCOTYL DIFFERENTIATION AND GROWTH INHIBITION

The extent of hypocotyl elongation has been the basis for critical genetic screens identifying key components of photomorphogenetic signaling, as well as the basis for quantitatively classifying mutants from a variety of pathways implicated in light responses. In the dark, extremely rapid growth of the hypocotyl is a strategy to ensure the apex of the plant reaches the light before the seed reserves are exhausted. Hypocotyl growth is driven by cell expansion and is suppressed by less than one minute of blue or a few minutes of sustained red light (Parks et al., 1998; Parks and Spalding, 1999; Wu et al., 2010). Phys, crys and phots are all implicated in inhibition of hypocotyl elongation (Casal, 2000).

Reprogramming of the Genome

A screen for plants with reduced hypocotyl response to light yielded the first photomorphogenetic mutants (Koornneef et al., 1980). In addition to several mutants

affecting photoreceptors and showing wavelength-specific hypocotyl defects, one mutant called *long hypocotyl 5* (*hy5*) had an elongated hypocotyl in all light conditions tested. The gene affected in this mutant was found to encode a basic leucine zipper (bZIP) transcription factor that accumulates in the presence of light, implicating transcriptional changes in the photomorphogenetic response (Oyama et al., 1997). A recent study used a series of ChIP-chip assays to identify more than 9000 promoters as likely HY5 binding sites. Approximately one-third of these genes are differentially expressed in *hy5* mutants (Zhang et al., 2011). Gene Ontology (GO) analysis showed that transcription factors are enriched among the HY5-regulated genes, as well as genes related to auxin, cytokinin, ethylene and jasmonic acid pathways. Not surprisingly, genes related to cell elongation, cell division, and chloroplast development were also among the HY5-regulated target genes (Zhang et al., 2011).

Beyond these transcriptional changes, there is evidence for genome-wide reprogramming following light exposure. An examination of histone modification marks at the *HY5* and the *HY5 HOMOLOG* (*HYH*) loci revealed considerable differences in seedlings grown in the dark versus those experiencing a dark to light transition (Charron et al., 2009). H3K9 acetylation (H3K9ac), a histone mark associated with gene activation, showed a massive peak in the coding region of both *HY5* and *HYH* following transition to light. Additionally, 37% of putative HY5 binding sites identified in an earlier study (Lee et al., 2007) were targeted by H3K9ac in dark grown seedlings and this overlap increased to 52% in dark to light seedlings (Charron et al., 2009).

HY5 is degraded in the dark by association with the ubiquitin ligase CONSTITUTIVE PHOTOMORPHOGENIC 1 (COP1) (Osterlund et al., 2000). In the light, interaction between COP1 and HY5 is disrupted. This leads to accumulation of HY5 and inhibition of hypocotyl elongation. FIN219, a protein quickly induced by auxin and involved in regulation of jasmonic acid, has been shown to negatively regulate COP1 levels under continuous far-red light (Wang et al., 2011). In the absence of FIN219, COP1 accumulates in the nucleus resulting in an increase of HY5 degradation (Wang et al., 2011). Bimolecular fluorescence complementation, yeast two-hybrid and pull-down assays show that FIN219 can interact directly with the WD40 domain of COP1. Fluorescence experiments indicate that FIN219 can also modulate the subcellular

localization of COP1. A *fin219-2/cop1-6* double mutant shows greatly reduced HY5 levels in the dark as well as in far-red light. This suggests that FIN219 may have COP1-independent roles in HY5 stability (Wang et al., 2011).

In addition to HY5, a number of basic helix-loop-helix (bHLH) transcription factors have been implicated in regulation of hypocotyl growth control. Members of the PHYTOCHROME INTERACTING FACTOR (PIF) family of bHLH transcription factors are emerging as hubs of seedling growth control (Leivar and Quail, 2011). Recent examination of a quadruple *pif* mutant (*pif1 pif3 pif4 pif5*, also called *pifq)* has revealed a striking constitutively photomorphogenic (cop)-like phenotype in dark-grown seedlings (Leivar et al., 2008; Shin et al., 2009). In addition to directly promoting hypocotyl growth, PIFs antagonize photoreceptor function by stimulating COP1-catalyzed ubiquitylation and degradation of phyB (Jang et al., 2010). This leads to over-accumulation of phyB and light-hypersensitivity in *pifq* mutants.

LONG HYPOCOTYL IN FAR-RED1 (HFR1), an atypical bHLH, is required for both phy- and cry-dependent light signal transduction in seedlings (Fairchild et al., 2000; Duek et al., 2004). Similar to HY5, HFR1 is degraded in the dark by COP1-catalyzed ubiquitination, while light stabilizes HFR1 in the nucleus to promote photomorphogenesis (Pokhilko et al., 2011). Using ChIP assays, HFR1 was shown to act as a non-DNA binding transcription cofactor directly interacting with PIF4 and PIF5 to inhibit their activation of target genes (Hornitschek et al., 2009). This activity may be antagonized by yet another family of bHLH transcription factors called BANQUO1 (BNQ1), BNQ2, and BNQ3. Seedlings overexpressing any of the *BNQ* genes have elongated hypocotyls in red light (Mara et al., 2010). Overexpression of *BNQ* genes can suppress the short hypocotyl phenotype of seedlings overexpressing HFR1, perhaps through blocking HFR1 interaction with PIF proteins (Mara et al., 2010).

Hormones as Targets of the Photoreceptors

Hypocotyl growth has also been used to identify a large number of mutants involved in hormone biosynthesis and signaling. The pathways most closely associated with proper hypocotyl elongation include auxin, brassinosteroids, gibberellins, ethylene,

and cytokinin. Details of these pathways are reviewed elsewhere (Clouse, 2002; Kieber, 2002; Schaller and Kieber, 2002; Michniewicz et al., 2007; Sun, 2008; Stepanova and Alonso, 2009; Argueso et al., 2010; Kim and Wang, 2010; Stewart and Nemhauser, 2010). Here, we focus on a few recent examples of molecular mechanisms connecting light and hormone responses.

Many lines of evidence connect auxin transport and signaling to the seedling light response (Boerjan et al., 1995; Romano et al., 1995; Delarue et al., 1998; Collett et al., 2000; Zhao et al., 2001). For example, blue light acting through cry1 alters the expression of some *AUXIN RESPONSE FACTOR* (*ARF*) genes (Folta et al., 2003). Recently ABCB19, a member of a large family of ABC transporters, was shown to play a role in auxin distribution along the hypocotyl. Overexpression of *ABCB19* led to reduced inhibition of hypocotyl elongation in blue and red light and greater expression of an auxin-responsive reporter. Conversely, mutants in *ABCB19* (*b19-1*) were hypersensitive to high-fluence blue light and loss of ABCB19 strongly suppressed *phyB* and *cry1* long hypocotyl phenotypes. Mutations in either photoreceptor caused a substantial increase in ACBC19 protein, even in the absence of light (Wu et al., 2010). Despite this strong connection to the light response, high-resolution time course analysis of hypocotyl growth indicated that loss or gain of ABCB19 had only a modest effect on the initial 12 hours of hypocotyl growth inhibition by blue light (Wu et al., 2010).

One clue to this surprising result is that co-application of gibberellins with auxin is far more effective than auxin treatment alone in suppressing blue light-mediated growth inhibition (Folta et al., 2003). Defects in gibberellin biosynthesis or response result in light-grown phenotypes in dark-grown seedlings (Alabadi et al., 2004). Gibberellins play a role in photomorphogenesis through the destabilization of the growth repressing DELLA family of transcriptional regulators (Silverstone et al., 1997; Silverstone et al., 1998; Silverstone et al., 2001; Harberd, 2003; Alabadi et al., 2004; Feng et al., 2008; Achard and Genschik, 2009). One hour of light is sufficient to strongly repress expression of genes encoding gibberellin-biosynthesis enzymes, while up-regulating genes involved in gibberellin inactivation (Achard et al., 2007). Consequently, DELLAs accumulate to higher levels in light-exposed seedlings, resulting in shorter hypocotyls. Following exposure to light, phyB promotes the gradual accumulation of DELLAs in the

hypocotyl (Achard et al., 2007). In addition to direct regulation of PIF protein stability, phyB-mediated DELLA accumulation also antagonizes PIF function, as DELLAs directly inhibit PIF3 and PIF4 transcriptional activity (de Lucas et al., 2008; Feng et al., 2008).

Brassinosteroids are yet another class of small molecule hormones whose antagonism of light signaling has been recognized for some time (Li et al., 1996; Song et al., 2009; Li et al., 2010). Plants with defective production or response to BRs show an array of phenotypes specific to light-grown seedlings, even when they are grown in the dark. These phenotypes include a short hypocotyl, expanded cotyledons and expression of light-specific genes (Chory et al., 1991; Li et al., 1996). Brassinosteroid signaling is among the best-understood pathways in plants. Brassinosteroids regulate the activity of BES1 and BZR1 by modulating their phosphorylation status via a kinase cascade (Gampala et al., 2007; Ryu et al., 2010). Phosphorylation of BES1 or BZR1 inhibits DNA-binding and promotes the retention of these proteins in the cytoplasm. In the presence of brassinosteroids, BES1/BZR1 family members are hypophosphorylated and bind to BR-responsive gene promoters (Yin et al., 2005). Loss of brassinosteroid signaling in dark-grown seedlings was recently shown to cause a highly similar transcriptional response as exposure to red light (Sun et al., 2010). Moreover, there is a significant overlap of the BZR1 (Sun et al., 2010) and BES1/BZR2 (Yu et al., 2011) targets with the targets of light-signaling transcription factors PIF1 and HY5, as well as with genes differentially expressed between light and dark conditions (Oh et al., 2009). In addition, BZR1 negatively regulates the expression of the transcription factor GATA2, a positive regulator of photomorphogenesis, by binding to its promoter (Luo et al., 2010).

As more information becomes available describing the interaction of these various hormones in response to light, a complex picture emerges. Hormones affect levels of other hormones, as well as impacting downstream signaling events. For example, both auxin and GA effects on growth appear to converge on HY5, PIFs and DELLAs. As described above, these transcription factors are central to the genomic reprogramming during photomorphogenesis. Additionally, transcription factors regulated by specific hormone pathways may interact on gene promoters. Many brassinosteroid-responsive genes contain Auxin Response Factor binding sites, suggesting a link between auxin and brassinosteroid responses (Vert et al., 2005; Vert et al., 2008).

Outside of the nucleus

Ultimately, the cell wall is the fundamental determinant of cell shape and form. As a result of their dramatic growth potential, cell walls of hypocotyl cells have been extensively analyzed. The cell wall is composed of cellulose microfibrils tethered together by cross-linking hemicelluloses. This fundamental framework lies embedded in a second network of matrix polysaccharides, glycoproteins, proteoglycans and various low molecular weight compounds (Carpita and McCann, 2000). The continuous modification of the cell wall during growth and development requires the hydrolysis and alteration of existing cell wall material, as well as *de novo* synthesis and secretion of cell wall components. During etiolated growth, cells of the hypocotyl undergo rapid cell expansion at right angles to the predominant orientation of cellulose microfibrils. Several lines of evidence support a model where deposition of cellulose is oriented by an interaction between cellulose synthase complexes (CSCs) and microtubules (reviewed in Baskin, 2001). For example, one study used a fluorescently-labeled cellulose synthase subunit to show CSCs delivered to the plasma membrane at sites coincident with cortical microtubules (Gutierrez et al., 2009).

Another indication of the key role of the cytoskeleton in scaffolding growth comes from studies of the MICROTUBULE ASSOCIATED PROTEINS (MAPs) (Lucas et al., 2011). MAPs work alongside a number of other proteins to balance assembly and disassembly of microtubules (Hamada, 2007; Sedbrook and Kaloriti, 2008). A genetic screen for aberrant microtubule patterns identified the temperature-sensitive *mor1* mutant, carrying a mutation in a MAP215/Dis1 family member (Whittington et al., 2001). *mor1* mutants grown at the restrictive temperature show severe morphological abnormalities, including isotropic cell expansion. Mutations in the *MAP65-2* gene cause a modest but significant reduction in the height of dark-grown seedlings. Additional loss of *MAP65-1* leads to a 40% decrease in elongation of dark-grown hypocotyls, as well as defects in hypocotyl growth in light-grown seedlings. Expression of fluorescent *MAP65-1* and *MAP65-2* reporters showed expression in all hypocotyl epidermal cells, cotyledons and root tips. When examined in combination with fluorescently-labeled tubulin, both

MAPs localized to regions of structured antiparallel microtubules rather than unbundled microtubules. This association is not absolutely necessary for proper microtubule assembly, as transversely aligned arrays could still be detected in *map65-1 map65-2* double mutants (Lucas et al., 2011).

Temperature is known to increase hypocotyl cell elongation (Gray et al., 1998), and a recent study examined the effects of temperature on the cell wall (Fujita et al. 2011). Higher growth temperatures were found to decrease crystallinity of cellulose, a measure of the overall mechanical properties of cellulose microfibrils. High cellulose crystallinity makes microfibrils inextensible and limits cross-linking by hemicelluloses, a crucial factor for resisting mechanical stress during rapid cell expansion (Chambat et al., 2005). After exposure to only three hours at increased temperature, CSC velocity increased more than 4-fold, suggesting that temperature can stimulate cell growth by increasing the rate of cellulose production. In the temperature-sensitive *mor1* mutant, elevated temperature causes microtubules to shorten and lose parallel order. As a result of disordered microtubules, cellulose crystallinity remains relatively high even at the elongation-promoting higher temperature (Kawamura and Wasteneys, 2008; Allard et al., 2010; Fujita et al., 2011) . By labeling microtubules with another fluorescent reporter, the authors could detect a significant reduction in total area covered by microtubules in *mor1* mutants grown at elevated temperature. Consistent with this finding, *mor1* mutants exposed to 29^{o}C also had an increased proportion of CSCs in microtubule-free domains. Somewhat surprisingly, the microfibril pattern in the *mor1* mutant was consistent with the transverse parallel orientation observed in wild type hypocotyls (Fujita et al., 2011). These findings strongly suggest that microtubules are not essential for guiding cellulose deposition, although it should be noted that only one cellulose synthase subunit was examined in these studies. Rather than directly affecting cellulose deposition, microtubules might alter the proportion of crystalline and amorphous cellulose by guiding secretion of non-cellulosic polysaccharides or enzymes that modify polysaccharides in the vicinity of the cell wall (Lai-Kee-Him et al., 2002). It is also worth noting that previous studies have demonstrated that increased temperature elevates auxin levels and increases sensitivity to brassinosteroids (Gray et al., 1998; Zhao et al., 2002;

Nemhauser et al., 2004). Whether these diverse effects of temperature are related to one another would be an interesting area for future investigation.

A recent observation that growth can be uncoupled from cellulose synthesis provides a possible alternative explanation for the apparent lack of connection between CSC trajectory and microfibril orientation. Hypocotyls of seedlings growing in the dark for 20 hours following germination have been shown to elongate with a velocity of < 0.1 mm h^{-1}. After 40 hours of dark growth, growth rate increases to 0.3mm h^{-1}. This rapid growth is maintained for the following 3 days (Refregier et al., 2004). Surprisingly, growth can be inhibited by a CSC-targeting drug called isohaxben only if seedlings are exposed during the early, slow-growth phase. This differential effect on growth was particularly striking as several lines of evidence indicated that isohaxben was equally able to inhibit cellulose synthesis at both time points (Pelletier et al., 2010).

A microarray analysis of transcriptional changes in dark-grown, isolated hypocotyls during growth acceleration identified nearly 600 differentially regulated genes (Pelletier et al., 2010). Among the overrepresented categories were genes involved in cell wall related processes, including four putative pectin methyl-esterase inhibitors (PMEIs). Fourier Transformed-Infrared (FT-IR) microspectroscopy of hypocotyl cells undergoing growth acceleration suggests a significant increase in the global amount of cellulose and/or xyloglucan, along with an increase in the degree of de-methylesterified pectin (Pelletier et al., 2010). The degree of pectin methyl-esterification in the cell wall is controlled by pectin methyl-esterases and can be inhibited by PMEIs. De-methylesterified pectins can form Ca^{2+}-crosslinks and lead to wall stiffening (Willats et al., 2001; Willats et al., 2006). The gene encoding PMEI4 shows the strongest growth-associated induction, and when overexpressed causes significantly delayed hypocotyl growth acceleration (Pelletier et al., 2010). Once acceleration is initiated, *PMEI4* overexpressing lines show the same acceleration rate as wild type (Pelletier et al. 2010). This suggests pectin de-methylesterification controls the initiation of the acceleration rather than growth itself. Heterologous expression of the *Aspergillus aculeatus PME1* gene resulted in a clear decrease in degree of esterification and a 20% decrease in hypocotyl length (Derbyshire et al., 2007). Phytohormones may be possible mediators of this cell wall restructuring, as there are clear differences in the degree of esterification in

primary cell walls of gibberellin mutants (Derbyshire et al., 2007). Wild-type hypocotyls have a 60% degree of esterification, compared to only 40% in the gibberellin-deficient *ga1-3* mutant. This deficiency can be largely rescued by gibberellin treatment.

COTYLEDON DEVELOPMENT

At the same time that light is inhibiting hypocotyl growth, it is promoting growth of the cotyledons. Many of the same factors control growth in both tissues—often with opposite effects—presenting an intriguing question of how tissue-specific cellular responses are achieved. Recent work has led to a model of seedling photomorphogenesis with two distinct stages of growth dynamics: before and after full opening of the cotyledons (Stewart et al., 2011).

Cotyledon Opening

A young seedling expands its cotyledons to increase the light capturing surface and uses petioles to position blades towards the light source. Similar to hypocotyl growth, many mutants show defects in cotyledon expansion. Among the strongest phenotypes are those of the *cop/det/fus* class (Chory, 2010). The genes affected in these mutants are all negative regulators of response to light. As mentioned previously, *cop1* displays a nearly complete de-etiolated phenotype when grown in the dark as a result of aberrant accumulation of transcription factors such as HY5 and HFR1 (Pokhilko et al., 2011). To degrade HY5, COP1 forms a heterodimeric tetramer complex with SUPPRESSOR OF *phytochromeA* (SPA) proteins (SPA1-4 in *Arabidopsis*). A quadruple *spa* mutant closely resembles a *cop1* mutant and some single mutants show hypersensitivity to light (Balcerowicz et al., 2011). There is also evidence for some specialization among the SPA family (Ranjan et al., 2011). For example, SPA1 plays additional roles in leaf size, stomatal development and flowering time. Interestingly, SPA1 needed to be expressed in both phloem and mesophyll cells to fully rescue leaf phenotypes, suggesting a possible route of signal transmission through the phloem to achieve coordinated growth across the seedling (Ranjan et al., 2011).

Further evidence for long-distance coordination of growth comes from experiments where expression of phyB is limited to the cotyledon mesophyll (Endo et al., 2005). The

long hypocotyl phenotype of *phyB* mutants is completely suppressed in these lines. Similarly, specific inhibition of phy function in cotyledon mesophyll cells is sufficient to cause hypocotyl elongation (Warnasooriya and Montgomery, 2009). Fiber-optic-directed illumination of cotyledons but not hypocotyls has been shown to trigger full de-etiolation in both organs (Tanaka et al., 2002).

Opening of the Apical Hook

Upon emergence from the seed, the upper hypocotyl and immature cotyledons form a hooked structure to protect the shoot apical meristem while the seedling pushes towards the soil surface. Mutant seedlings lacking a hook fail to emerge when their seeds are buried in soil (Gallego-Bartolome et al., 2011). Light triggers complete and irreversible cotyledon opening within six hours (Wu et al., 2010). To fully maintain an apical hook in the light requires near complete loss of cry and phy function (Lopez-Juez et al., 2008).

In the absence of light, the hook must be actively maintained through differential cell growth. Differential growth is established by a gradient of auxin activity and refined by the coordinated action of auxin and ethylene (Lehman et al., 1996; Gallego-Bartolome et al., 2011). Etiolated *hookless1* (*hls1*) mutants show a dramatically reduced expression of an auxin-responsive reporter (Li et al., 2004). *HLS1* encodes a putative aminotransferase and is proposed to cause asymmetric auxin-distribution and/or response. Mutations in a negative regulator of auxin response called *Auxin Response Factor 2* (*ARF2*) partially suppress *hls1* mutants, possibly by restoring balance to auxin response in the hook (Li et al., 2004; Hamaguchi et al., 2008).This is supported by a partial restoration of expression of the auxin-responsive reporter. Auxin moves into the hook cells through regulated transport under the control of a number of proteins (Grunewald and Friml, 2010). Overexpression of the auxin transporter ABCB19 in *cry1* or *phyB* mutants can also affect hook opening, likely by preventing modification of the auxin gradient needed to restore symmetric growth (Wu et al., 2010)

Gibberellins also play a role in hook maintenance. Seedlings treated with the gibberellin biosynthesis inhibitor paclobutazol (PAC) fail to form an apical hook (Gallego-Bartolome et al., 2011) and expression of a stabilized DELLA protein in the endodermis but not the epidermis impairs hook formation (Gallego-Bartolome et al.,

2011). Gibberellins promote hook development in several ways, including through transcriptional regulation of several genes in the ethylene and auxin pathways (e.g., *HLS1* and *PIN-FORMED* auxin efflux carriers). Moreover, gibberellins cooperate with ethylene in preventing hook opening, at least in part through interactions with the PIF family (Gallego-Bartolome et al., 2011). PIF5 requires gibberellin-mediated release from the DELLA repressors to bind to the promoter of ethylene biosynthetic genes. *pifq* mutants begin to open their cotyledons immediately upon germination, but this opening can be delayed by gibberellin treatment (Gallego-Bartolome et al., 2011).

Chloroplast Development

As primary sites of seedling photosynthesis, cotyledons have additional developmental programs beyond growth. Light triggers cotyledon greening through conversion of largely undifferentiated etioplasts into photosynthetically active chloroplasts. In preparation for this switch, dark-grown seedlings accumulate the chlorophyll precursor protochlorophyllide (Stephenson et al., 2009). This allows for rapid assembly of functional photosynthetic machinery once exposed to light. Dark-grown *cop1* and *pifq* mutants have partially developed chloroplasts and accumulation of chlorophyll precursor, largely phenocopying wild-type seedlings grown in light (Stephenson et al., 2009). The transcriptome of *pifq* mutants reflects these morphological effects, showing aberrant expression of numerous genes related to the biogenesis of active chloroplasts and metabolic genes required for the transition from heterotrophic to autotrophic growth (Leivar et al., 2009).

One noticeable difference between dark-grown constitutively photomorphogenic mutants and light-grown wild-type seedlings is the absence of greening. Greening is blocked because one of the last steps in chlorophyll synthesis--the conversion of protochlorophyllide into chlorophyllide--is catalyzed by the photon-activated enzyme phrotochlorophyllide oxidoreductase. In Arabidopsis, chlorophyll production is largely independent of the phytochromes. Even in the quintuple phytochrome mutant, a red light pulse increases chlorophyllide levels (Strasser et al., 2010). In contrast, rice mutants lacking phytochrome function are also deficient in chlorophyll (Takano et al., 2009).

The DELLA-PIF interaction acts as a key regulator of chloroplast development. Dark-grown plants with reduced gibberellin levels contain chloroplasts with many similar attributes to those of light-grown wild-type plants (Cheminant et al., 2011). Many of the same light-regulated genes are up-regulated in dark-grown *ga1* (Cheminant et al., 2011) and *pifq* (Leivar et al., 2009) seedlings. Moreover, PIF1 binds in a gibberellin-dependent manner to promoters of several light-induced (*LHB1B1*, *LHCB1* and *2*), photosynthetic (*PSAG* and *PSAE-1*) and chlorophyll biosynthesis (*CAO* and *CHLH*) genes. In particular, DELLA-dependent up-regulation of the photoprotective enzyme protochlorophyllide oxidoreductase in dark-grown seedlings facilitates rapid adaptation upon light exposure (Cheminant et al., 2011).

In addition to genes involved in chlorophyll production and photosystem assembly, genes encoding enzymes needed for carotenoid biosynthesis are strongly up-regulated when seedlings are exposed to light (Rodriguez-Villalon et al., 2009). Carotenoids play a critical photoprotective role by quenching excess excitation energy generated during photosynthesis. Recently, several members of the PIF family have been shown to directly repress expression of phytoene synthase and thereby decrease the accumulation of carotenoids (Toledo-Ortiz et al., 2010). This PIF activity is countered by DELLAs (Cheminant et al., 2011). At least 50 genes show correlated expression with phytoene synthase, including *PIF*s, genes involved in chlorophyll and carotenoid biosynthesis, and genes involved in the production and perception of brassinosteroids, auxins, abscisic acid and jasmonate (Meier et al., 2011). Current models suggest that light-triggered degradation of PIFs leads to a rapid transition to photoautotrophy, at least in part through coordinated production of carotenoids and chlorophyll.

MERISTEM ESTABLISHMENT AND ACTIVATION

While the hypocotyl is elongating and the cotyledons are opening towards the light, stem cells located in the shoot and root apical meristems (SAM and RAM, respectively) are also undergoing significant developmental changes. Both meristems are established during embryogenesis before seedset. In the days following germination, both meristems achieve their mature size and initiate production of new biomass. In the shoot, production of leaves is a direct outcome of the transition to light. Root development is at least

initially light-independent, although it cannot continue indefinitely without shoot-derived photosynthate. Appearance of the first true leaves is the endpoint of seedling photomorphogenesis.

Events in the Seedling Shoot Apical Meristem

SAM activity must balance the need for photosynthetic tissue with resources that are frequently in limited supply. In the game "Extinct! Are you smarter than a plant?" (http://www.joecutting.com/extinct.php), the strategy for the seedling is clear and absolute—make enough root biomass to get the nutrients and water to support production of leaves or die early. Of course, without light, there is no point in making leaves at all. Once a seedling experiences even a short pulse of light, a wave of SAM-specific gene expression is initiated which depends on phys or crys (Lopez-Juez et al., 2008). Microarrays on dissected shoot apices identified nearly 6000 differentially regulated genes within the first six hours after light exposure (Lopez-Juez et al., 2008). Several hypotheses about SAM activation emerged from this analysis. First, cell division is initiated. Genes involved in the cell-cycle and translational machinery are induced early after the dark-to-light transition. Second, hormones need to be re-balanced. Genes associated with auxin and ethylene activity are down-regulated by light, whereas genes associated with cytokinin and gibberellin action are up-regulated. Third, cell walls need to be modified to allow for emergence of lateral organs. A substantial number of genes encoding cell-wall loosening enzymes, as well as cellulose synthases, show increased expression at the later time points when leaf primordia begin expanding.

After activation by light, the SAM grows until it reaches its mature size and is then maintained by a feedback loop comprised of WUSCHEL and the CLAVATA proteins (Barton, 2010). Cytokinin plays a critical role in SAM establishment and is thought to do so through activation of STIMPY/WUSCHEL HOMEOBOX 9 (STIP) (reviewed in Argueso et al., 2010; Skylar et al., 2010). *STIP* expression requires cytokinin receptor function, and *stip* mutants show a similar retarded growth phenotype and cytokinin insensitivity as triple cytokinin receptor mutants. In the triple cytokinin receptor mutant, *STIP* overexpression can partially rescue SAM size and substantially prolong growth (Skylar et al., 2010; Skylar and Wu, 2010). There is also likely a

feedback loop between STIP and the cytokinin response pathway. Expression of several negative regulators of cytokinin response called ARABIDOPSIS RESPONSE REGULATORS (ARRs) is reduced in *stip* mutants. However, these genes retain cytokinin response in a *stip* background, suggesting a branched rather than linear pathway. An interesting recent report shows that contrary to the sharp reduction in cytokinin sensitivity of light-grown *stip* mutants, mutants grown in the dark have increased cytokinin sensitivity (Skylar and Wu, 2010). Exogenous cytokinin treatment provoked a severe de-etiolated phenotype in *stip* mutants, a phenotype not observed in wild-type plants. The rescue of *stip* by exogenous sucrose may point to additional connections between photosynthetic activity, cell division, and the balance between division and differentiation (Wu et al., 2005).

Events in the Root Apical Meristem

Several recent studies have led to a provocative and persuasive model for how the RAM reaches its mature size during a critical window three to five days post-germination. While it is interesting that this occurs during the same short time frame as photomorphogenesis, a link between the two processes remains unclear, as all root studies have been performed in light conditions. Over this time, the RAM slows its rate of cell division and arrives at a stable balance between rates of division and differentiation. Expression levels of the gene encoding the auxin-regulated transcriptional co-repressor SHORT HYPOCOTYL 2/IAA3 (SHY2/IAA3) appear to be key to this transition. *SHY2/IAA3* levels rise as the RAM slows its rate of division, and heat-shock induced expression of *SHY2/IAA3* can prematurely arrest RAM expansion (Moubayidin et al., 2010). While no direct link has been made between the maturation of the RAM and photomorphogenesis, it is intriguing that this same timing—five days post germination—is coincident with full cotyledon opening (Stewart et al., 2011).

For the few days immediately after germination, a positive regulator of the cytokinin response called ARR12 weakly induces *SHY2/IAA3* (Moubayidin et al., 2010). Low levels of *SHY2/IAA3* lead to high division rates in the RAM. By day 5, *SHY2/IAA3* expression is induced by both ARR1 and ARR12, causing division rates to slow. The major target of SHY2/IAA3 function appears to be the auxin transporters *PIN1*, *PIN3*,

and *PIN7* (Moubayidin et al., 2010). All three are negatively regulated by *SHY2/IAA3* and have increased expression in an *arr12* mutant. A SUMO E3 ligase called AtMMS21/HPY2 provides an additional potential link between cytokinin and auxin signaling in the root. Mutants defective in *AtMMS21/HPY2* display fewer and smaller meristematic cells, as well as a reduced sensitivity to cytokinins and reduced expression of cytokinin-induced genes (Huang et al., 2009; Zhang et al., 2010). AtMMS21/HPY2 has been linked to cell-cycle progression via the PLETHORA (PLT)-dependent auxin signaling pathway. PLTs are AP2-domain transcription factors required to maintain stem cell activity by regulation of polar auxin transport in both RAM and SAM (Galinha et al., 2007; Prasad et al., 2011).

Cytokinin-auxin balance has long been associated with meristem function, but recent work has added gibberellins and brassinosteroids to the mix. Gibberellins act through DELLAs to keep *ARR1* expression low early in meristem development, promoting cell division (Moubayidin et al., 2010). Ubeda-Tomas and colleagues determined that gibberellin biosynthesis mutants have a smaller meristem with fewer cells. This can be rescued by addition of gibberellins or loss of multiple DELLAs. Gibberellin-directed turnover of the DELLAs is required specifically in the endodermis to maintain a wild-type RAM (Ubeda-Tomas et al., 2009) and requires the GRAS transcription factor SCARECROW-LIKE 3 (SCL3). *SCL3* endodermal expression decreases in response to both exogenous gibberellin application and DELLA loss-of-function mutations (Heo et al., 2011). The rate of cell elongation and division in the endodermis may physically dictate what occurs in surrounding tissues.

Brassinosteroids also influence RAM size and maintenance. One mechanism for brassinosteroid action is a feedback loop involving both SHY2/IAA3 and PIN3. Previous work on the root has shown that BREVIS RADIX (BRX) functionally connects brassinosteroid biosynthesis and auxin signaling to promote growth (Mouchel et al., 2006). A recent study revealed that *BRX* is expressed in the developing protophloem of the RAM and is a target of the auxin-regulated transcription factor MP/ARF5 (Scacchi et al., 2010). MP/ARF5 is negatively regulated by SHY2/IAA3 (Weijers et al., 2005). BRX appears to bind to MP/ARF5 to increase its activity, including inducing expression of *SHY2/IAA3*. This ARF5-BRX-SHY2 feedback loop is critical for regulation of auxin

transport. *BRX* may play a further integrative role, as cytokinin also induces *BRX* expression, and roots of *brx* mutants are largely cytokinin insensitive (Scacchi et al., 2010). Contrary to gibberellin signaling, the site of brassinosteroid action appears to be the root epidermis (Weijers et al., 2005; Scacchi et al., 2010). Using null and gain-of-function brassinosteroid signaling mutants, two groups found that brassinosteroids control meristem size through regulation of cell-cycle progression (Gonzalez-Garcia et al., 2011; Hacham et al., 2011). In contrast to the work in BRX, these studies found that brassinosteroid influence on meristem size was not via regulation of expression of *PIN1*, *PIN3* or *PIN7*.

CONCLUSION

Plants are marvelously and maddeningly complex. By analyzing the morphologically simple seedling during the brief window of initial photomorphogenesis, we observe many of the events that will re-occur throughout the rest of the life cycle. These events include: the integration of development and physiology, the rapid reprogramming of the genome, large-scale changes in cellular structure and function, and re-wiring of metabolism. All of these events are coordinated in a tissue and organ-specific manner, yet also coordinated across the entire organism. All green seedlings undergo photomorphogenesis. The spaghetti diagrams of molecular networks from several years ago (Nemhauser and Chory, 2002) are beginning to resolve into maps with major regulatory hubs, like the PIFs. The next challenges will be to test how universal these networks are among flowering plants, and how they are tweaked to fit diverse ecological niches.

ACKNOWLEDGEMENTS

The authors would like to thank Jodi Stewart, Edith Pierre-Jerome, and Cristina Walcher for careful reading of the manuscript. This work was supported by funds contributed by the National Science Foundation grants IOS-0919021 and MCB-0929046. JG was supported by the Developmental Biology Predoctoral Training Grant T32HD007183 from the National Institute of Child Health and Human Development.

REFERENCES

Achard, P., and Genschik, P. (2009). Releasing the brakes of plant growth: how GAs shutdown DELLA proteins. J Exp Bot **60,** 1085-1092.

Achard, P., Baghour, M., Chapple, A., Hedden, P., Van Der Straeten, D., Genschik, P., Moritz, T., and Harberd, N.P. (2007). The plant stress hormone ethylene controls floral transition via DELLA-dependent regulation of floral meristem-identity genes. Proc Natl Acad Sci U S A **104,** 6484-6489.

Alabadi, D., Gil, J., Blazquez, M.A., and Garcia-Martinez, J.L. (2004). Gibberellins repress photomorphogenesis in darkness. Plant Physiol **134,** 1050-1057.

Alvarez-Buylla, E.R., Benítez, M., Corvera-Poiré, A., Chaos Cador, A., de Folter, S., Gamboa de Buen, A., Garay-Arroyo, A., García-Ponce, B., Jaimes-Miranda, F., Pérez-Ruiz, R.V., Piñeyro-Nelson, A., and Y.E., S.-C. (2010). Flower Development. The Arabidopsis Book **8**.

Allard, J.F., Ambrose, J.C., Wasteneys, G.O., and Cytrynbaum, E.N. (2010). A mechanochemical model explains interactions between cortical microtubules in plants. Biophys J **99,** 1082-1090.

Argueso, C.T., Raines, T., and Kieber, J.J. (2010). Cytokinin signaling and transcriptional networks. Curr Opin Plant Biol **13,** 533-539.

Balcerowicz, M., Fittinghoff, K., Wirthmueller, L., Maier, A., Fackendahl, P., Fiene, G., Koncz, C., and Hoecker, U. (2011). Light exposure of Arabidopsis seedlings causes rapid de-stabilization as well as selective post-translational inactivation of the repressor of photomorphogenesis SPA2. Plant J **65,** 712-723.

Barton, M.K. (2010). Twenty years on: the inner workings of the shoot apical meristem, a developmental dynamo. Dev Biol **341,** 95-113.

Baskin, T.I. (2001). On the alignment of cellulose microfibrils by cortical microtubules: a review and a model. Protoplasma **215,** 150-150.

Bentsink, L., and Koornneef, M. (2008). Seed Dormancy and Germination. The Arabidopsis Book **6**.

Boerjan, W., Cervera, M.T., Delarue, M., Beeckman, T., Dewitte, W., Bellini, C., Caboche, M., Van Onckelen, H., Van Montagu, M., and Inze, D. (1995). Superroot, a recessive mutation in Arabidopsis, confers auxin overproduction. Plant Cell **7,** 1405-1419.

Carpita, N., and McCann, M. (2000). The Cell Wall. In Biochemistry & Molecular Biology of Plants, Chapter 2.

Casal, J.J. (2000). Phytochromes, cryptochromes, phototropin: photoreceptor interactions in plants. Photochem Photobiol **71,** 1-11.

Clouse, S.D. (2002). Brassinosteroids. The Arabidopsis Book **1**.

Collett, C.E., Harberd, N.P., and Leyser, O. (2000). Hormonal interactions in the control of Arabidopsis hypocotyl elongation. Plant Physiol **124,** 553-562.

Chambat, G.r., Karmous, M., Costes, M., Picard, M., and Joseleau, J.-P. (2005). Variation of xyloglucan substitution pattern affects the sorption on celluloses with different degrees of crystallinity. Cellulose **12,** 117-125.

Charron, J.B., He, H., Elling, A.A., and Deng, X.W. (2009). Dynamic landscapes of four histone modifications during deetiolation in Arabidopsis. Plant Cell **21,** 3732-3748.

Chaves, I., Pokorny, R., Byrdin, M., Hoang, N., Ritz, T., Brettel, K., Essen, L.O., van der Horst, G.T., Batschauer, A., and Ahmad, M. (2011). The cryptochromes: blue light photoreceptors in plants and animals. Annu Rev Plant Biol **62,** 335-364.

Cheminant, S., Wild, M., Bouvier, F., Pelletier, S., Renou, J.P., Erhardt, M., Hayes, S., Terry, M.J., Genschik, P., and Achard, P. (2011). DELLAs Regulate Chlorophyll and Carotenoid Biosynthesis to Prevent Photooxidative Damage during Seedling Deetiolation in Arabidopsis. Plant Cell.

Chory, J. (2010). Light signal transduction: an infinite spectrum of possibilities. Plant J **61,** 982-991.

Chory, J., Nagpal, P., and Peto, C.A. (1991). Phenotypic and Genetic Analysis of det2, a New Mutant That Affects Light-Regulated Seedling Development in Arabidopsis. Plant Cell **3,** 445-459.

de Lucas, M., Daviere, J.M., Rodriguez-Falcon, M., Pontin, M., Iglesias-Pedraz, J.M., Lorrain, S., Fankhauser, C., Blazquez, M.A., Titarenko, E., and Prat, S. (2008). A molecular framework for light and gibberellin control of cell elongation. Nature **451,** 480-484.

Delarue, M., Prinsen, E., Onckelen, H.V., Caboche, M., and Bellini, C. (1998). Sur2 mutations of Arabidopsis thaliana define a new locus involved in the control of auxin homeostasis. Plant J **14,** 603-611.

Derbyshire, P., McCann, M.C., and Roberts, K. (2007). Restricted cell elongation in Arabidopsis hypocotyls is associated with a reduced average pectin esterification level. BMC Plant Biol **7,** 31.

Duek, P.D., Elmer, M.V., van Oosten, V.R., and Fankhauser, C. (2004). The degradation of HFR1, a putative bHLH class transcription factor involved in light signaling, is regulated by phosphorylation and requires COP1. Curr Biol **14,** 2296-2301.

Endo, M., Nakamura, S., Araki, T., Mochizuki, N., and Nagatani, A. (2005). Phytochrome B in the mesophyll delays flowering by suppressing FLOWERING LOCUS T expression in Arabidopsis vascular bundles. Plant Cell **17,** 1941-1952.

Fairchild, C.D., Schumaker, M.A., and Quail, P.H. (2000). HFR1 encodes an atypical bHLH protein that acts in phytochrome A signal transduction. Genes Dev **14,** 2377-2391.

Feng, S., Martinez, C., Gusmaroli, G., Wang, Y., Zhou, J., Wang, F., Chen, L., Yu, L., Iglesias-Pedraz, J.M., Kircher, S., Schafer, E., Fu, X., Fan, L.M., and Deng, X.W. (2008). Coordinated regulation of Arabidopsis thaliana development by light and gibberellins. Nature **451,** 475-479.

Folta, K.M., Pontin, M.A., Karlin-Neumann, G., Bottini, R., and Spalding, E.P. (2003). Genomic and physiological studies of early cryptochrome 1 action demonstrate roles for auxin and gibberellin in the control of hypocotyl growth by blue light. Plant J **36,** 203-214.

Fujita, M., Himmelspach, R., Hocart, C.H., Williamson, R.E., Mansfield, S.D., and Wasteneys, G.O. (2011). Cortical microtubules optimize cell-wall crystallinity to drive unidirectional growth in Arabidopsis. The Plant Journal.

Galinha, C., Hofhuis, H., Luijten, M., Willemsen, V., Blilou, I., Heidstra, R., and Scheres, B. (2007). PLETHORA proteins as dose-dependent master regulators of Arabidopsis root development. Nature **449,** 1053-1057.

Gallego-Bartolome, J., Arana, M.V., Vandenbussche, F., Zadnikova, P., Minguet, E.G., Guardiola, V., Van Der Straeten, D., Benkova, E., Alabadi, D., and Blazquez, M.A. (2011). Hierarchy of hormone action controlling apical hook development in Arabidopsis. Plant J.

Gampala, S.S., Kim, T.W., He, J.X., Tang, W., Deng, Z., Bai, M.Y., Guan, S., Lalonde, S., Sun, Y., Gendron, J.M., Chen, H., Shibagaki, N., Ferl, R.J., Ehrhardt, D., Chong, K., Burlingame, A.L., and Wang, Z.Y. (2007). An essential role for 14-3-3 proteins in brassinosteroid signal transduction in Arabidopsis. Dev Cell **13,** 177-189.

Gonzalez-Garcia, M.P., Vilarrasa-Blasi, J., Zhiponova, M., Divol, F., Mora-Garcia, S., Russinova, E., and Cano-Delgado, A.I. (2011). Brassinosteroids control meristem size by promoting cell cycle progression in Arabidopsis roots. Development **138,** 849-859.

Gray, W.M., Ostin, A., Sandberg, G.r., Romano, C.P., and Estelle, M. (1998). High temperature promotes auxin-mediated hypocotyl elongation in Arabidopsis. Proceedings of the National Academy of Sciences **95,** 7197-7202.

Grunewald, W., and Friml, J. (2010). The march of the PINs: developmental plasticity by dynamic polar targeting in plant cells. Embo J **29,** 2700-2714.

Gutierrez, R., Lindeboom, J.J., Paredez, A.R., Emons, A.M.C., and Ehrhardt, D.W. (2009). Arabidopsis cortical microtubules position cellulose synthase delivery to the plasma membrane and interact with cellulose synthase trafficking compartments. Nature Cell Biology **11,** 797-806.

Hacham, Y., Holland, N., Butterfield, C., Ubeda-Tomas, S., Bennett, M.J., Chory, J., and Savaldi-Goldstein, S. (2011). Brassinosteroid perception in the epidermis controls root meristem size. Development **138,** 839-848.

Hamada, T. (2007). Microtubule-associated proteins in higher plants. J Plant Res **120,** 79-98.

Hamaguchi, A., Yamashino, T., Koizumi, N., Kiba, T., Kojima, M., Sakakibara, H., and Mizuno, T. (2008). A small subfamily of Arabidopsis RADIALIS-LIKE SANT/MYB genes: a link to HOOKLESS1-mediated signal transduction during early morphogenesis. Biosci Biotechnol Biochem **72,** 2687-2696.

Harberd, N.P. (2003). Botany. Relieving DELLA restraint. Science **299,** 1853-1854.

Heo, J.O., Chang, K.S., Kim, I.A., Lee, M.H., Lee, S.A., Song, S.K., Lee, M.M., and Lim, J. (2011). Funneling of gibberellin signaling by the GRAS transcription regulator scarecrow-like 3 in the Arabidopsis root. Proc Natl Acad Sci U S A **108,** 2166-2171.

Hornitschek, P., Lorrain, S., Zoete, V., Michielin, O., and Fankhauser, C. (2009). Inhibition of the shade avoidance response by formation of non-DNA binding bHLH heterodimers. Embo J **28,** 3893-3902.

Huang, L., Yang, S., Zhang, S., Liu, M., Lai, J., Qi, Y., Shi, S., Wang, J., Wang, Y., Xie, Q., and Yang, C. (2009). The Arabidopsis SUMO E3 ligase AtMMS21, a homologue of NSE2/MMS21, regulates cell proliferation in the root. Plant J **60,** 666-678.

Jang, I.C., Henriques, R., Seo, H.S., Nagatani, A., and Chua, N.H. (2010). Arabidopsis PHYTOCHROME INTERACTING FACTOR proteins promote phytochrome B polyubiquitination by COP1 E3 ligase in the nucleus. Plant Cell **22,** 2370-2383.

Kawamura, E., and Wasteneys, G.O. (2008). MOR1, the Arabidopsis thaliana homologue of Xenopus MAP215, promotes rapid growth and shrinkage, and suppresses the pausing of microtubules in vivo. J Cell Sci **121,** 4114-4123.

Kieber, J.J. (2002). Cytokinins. The Arabidopsis Book **1**.

Kim, T.W., and Wang, Z.Y. (2010). Brassinosteroid signal transduction from receptor kinases to transcription factors. Annu Rev Plant Biol **61,** 681-704.

Koornneef, M., Rolff, E., and Spruit, C.J.P. (1980). Genetic control of light-inhibited hypocotyl elongation in Arabidopsis thaliana (L.) L. Heynh. Zeitschrift Pflanzenphysiologie **100,** 147–160.

Lai-Kee-Him, J.p., Chanzy, H., MÃ¼ller, M., Putaux, J.-L., Imai, T., and Bulone, V. (2002). In Vitro Versus in VivoCellulose Microfibrils from Plant Primary Wall Synthases: Structural Differences. Journal of Biological Chemistry **277,** 36931-36939.

Lee, J., He, K., Stolc, V., Lee, H., Figueroa, P., Gao, Y., Tongprasit, W., Zhao, H., Lee, I., and Deng, X.W. (2007). Analysis of transcription factor HY5 genomic binding sites revealed its hierarchical role in light regulation of development. Plant Cell **19,** 731-749.

Lehman, A., Black, R., and Ecker, J.R. (1996). HOOKLESS1, an ethylene response gene, is required for differential cell elongation in the Arabidopsis hypocotyl. Cell **85,** 183-194.

Leivar, P., and Quail, P.H. (2011). PIFs: pivotal components in a cellular signaling hub. Trends Plant Sci **16,** 19-28.

Leivar, P., Tepperman, J.M., Monte, E., Calderon, R.H., Liu, T.L., and Quail, P.H. (2009). Definition of early transcriptional circuitry involved in light-induced reversal of PIF-imposed repression of photomorphogenesis in young Arabidopsis seedlings. Plant Cell **21,** 3535-3553.

Leivar, P., Monte, E., Oka, Y., Liu, T., Carle, C., Castillon, A., Huq, E., and Quail, P.H. (2008). Multiple phytochrome-interacting bHLH transcription factors repress premature seedling photomorphogenesis in darkness. Curr Biol **18,** 1815-1823.

Li, H., Johnson, P., Stepanova, A., Alonso, J.M., and Ecker, J.R. (2004). Convergence of signaling pathways in the control of differential cell growth in Arabidopsis. Dev Cell **7,** 193-204.

Li, J., Nagpal, P., Vitart, V., McMorris, T.C., and Chory, J. (1996). A role for brassinosteroids in light-dependent development of Arabidopsis. Science **272,** 398-401.

Li, J., Li, G., Gao, S., Martinez, C., He, G., Zhou, Z., Huang, X., Lee, J.H., Zhang, H., Shen, Y., Wang, H., and Deng, X.W. (2010). Arabidopsis transcription factor ELONGATED HYPOCOTYL5 plays a role in the feedback regulation of phytochrome A signaling. Plant Cell **22,** 3634-3649.

Lopez-Juez, E., Dillon, E., Magyar, Z., Khan, S., Hazeldine, S., de Jager, S.M., Murray, J.A., Beemster, G.T., Bogre, L., and Shanahan, H. (2008). Distinct

light-initiated gene expression and cell cycle programs in the shoot apex and cotyledons of Arabidopsis. Plant Cell **20,** 947-968.

Lucas, J.R., Courtney, S., Hassfurder, M., Dhingra, S., Bryant, A., and Shaw, S.L. (2011). Microtubule-Associated Proteins cand MAP65-2 Positively Regulate Axial Cell Growth in Etiolated Arabidopsis Hypocotyls. The Plant Cell Online.

Luo, X.M., Lin, W.H., Zhu, S., Zhu, J.Y., Sun, Y., Fan, X.Y., Cheng, M., Hao, Y., Oh, E., Tian, M., Liu, L., Zhang, M., Xie, Q., Chong, K., and Wang, Z.Y. (2010). Integration of light- and brassinosteroid-signaling pathways by a GATA transcription factor in Arabidopsis. Dev Cell **19,** 872-883.

Mara, C.D., Huang, T., and Irish, V.F. (2010). The Arabidopsis floral homeotic proteins APETALA3 and PISTILLATA negatively regulate the BANQUO genes implicated in light signaling. Plant Cell **22,** 690-702.

Meier, S., Tzfadia, O., Vallabhaneni, R., Gehring, C., and Wurtzel, E.T. (2011). A transcriptional analysis of carotenoid, chlorophyll and plastidial isoprenoid biosynthesis genes during development and osmotic stress responses in Arabidopsis thaliana. BMC Syst Biol **5,** 77.

Michniewicz, M., Brewer, P.B., and Friml, J. (2007). Polar Auxin Transport and Asymmetric Auxin Distribution. The Arabidopsis Book **5**.

Moubayidin, L., Perilli, S., Dello Ioio, R., Di Mambro, R., Costantino, P., and Sabatini, S. (2010). The rate of cell differentiation controls the Arabidopsis root meristem growth phase. Curr Biol **20,** 1138-1143.

Mouchel, C.F., Osmont, K.S., and Hardtke, C.S. (2006). BRX mediates feedback between brassinosteroid levels and auxin signalling in root growth. Nature **443,** 458-461.

Nemhauser, J., and Chory, J. (2002). Photomorphogenesis. The Arabidopsis Book **1,** e0054. doi:0010.1199/tab.0054.

Nemhauser, J.L., Mockler, T.C., and Chory, J. (2004). Interdependency of brassinosteroid and auxin signaling in Arabidopsis. PLoS Biol **2,** E258.

Oh, E., Kang, H., Yamaguchi, S., Park, J., Lee, D., Kamiya, Y., and Choi, G. (2009). Genome-wide analysis of genes targeted by PHYTOCHROME INTERACTING FACTOR 3-LIKE5 during seed germination in Arabidopsis. Plant Cell **21,** 403-419.

Osterlund, M.T., Hardtke, C.S., Wei, N., and Deng, X.W. (2000). Targeted destabilization of HY5 during light-regulated development of Arabidopsis. Nature **405,** 462-466.

Oyama, T., Shimura, Y., and Okada, K. (1997). The Arabidopsis HY5 gene encodes a bZIP protein that regulates stimulus-induced development of root and hypocotyl. Genes Dev **11,** 2983-2995.

Parks, B.M., and Spalding, E.P. (1999). Sequential and coordinated action of phytochromes A and B during Arabidopsis stem growth revealed by kinetic analysis. Proc Natl Acad Sci U S A **96,** 14142-14146.

Parks, B.M., Cho, M.H., and Spalding, E.P. (1998). Two genetically separable phases of growth inhibition induced by blue light in Arabidopsis seedlings. Plant Physiol **118,** 609-615.

Pedmale, U.V., Celaya, R.B., and Liscum, E. (2010). Phototropism: Mechanism and Outcomes. The Arabidopsis Book **8**.

Pelletier, S., Van Orden, J., Wolf, S., Vissenberg, K., Delacourt, J., Ndong, Y.A., Pelloux, J., Bischoff, V., Urbain, A., Mouille, G., Lemonnier, G., Renou, J.P., and Hofte, H. (2010). A role for pectin de-methylesterification in a developmentally regulated growth acceleration in dark-grown Arabidopsis hypocotyls. New Phytol **188,** 726-739.

Pokhilko, A., Ramos, J.A., Holtan, H., Maszle, D.R., Khanna, R., and Millar, A.J. (2011). Ubiquitin ligase switch in plant photomorphogenesis: A hypothesis. J Theor Biol **270,** 31-41.

Prasad, K., Grigg, S.P., Barkoulas, M., Yadav, R.K., Sanchez-Perez, G.F., Pinon, V., Blilou, I., Hofhuis, H., Dhonukshe, P., Galinha, C., Mahonen, A.P., Muller, W.H., Raman, S., Verkleij, A.J., Snel, B., Reddy, G.V., Tsiantis, M., and Scheres, B. (2011). Arabidopsis PLETHORA Transcription Factors Control Phyllotaxis. Curr Biol.

Ranjan, A., Fiene, G., Fackendahl, P., and Hoecker, U. (2011). The Arabidopsis repressor of light signaling SPA1 acts in the phloem to regulate seedling de-etiolation, leaf expansion and flowering time. Development **138,** 1851-1862.

Refregier, G., Pelletier, S., Jaillard, D., and Hofte, H. (2004). Interaction between wall deposition and cell elongation in dark-grown hypocotyl cells in Arabidopsis. Plant Physiol **135,** 959-968.

Rizzini, L., Favory, J.J., Cloix, C., Faggionato, D., O'Hara, A., Kaiserli, E., Baumeister, R., Schafer, E., Nagy, F., Jenkins, G.I., and Ulm, R. (2011). Perception of UV-B by the Arabidopsis UVR8 protein. Science **332,** 103-106.

Rodriguez-Villalon, A., Gas, E., and Rodriguez-Concepcion, M. (2009). Colors in the dark: a model for the regulation of carotenoid biosynthesis in etioplasts. Plant Signal Behav **4,** 965-967.

Romano, C.P., Robson, P.R., Smith, H., Estelle, M., and Klee, H. (1995). Transgene-mediated auxin overproduction in Arabidopsis: hypocotyl elongation phenotype and interactions with the hy6-1 hypocotyl elongation and axr1 auxin-resistant mutants. Plant Mol Biol **27,** 1071-1083.

Ryu, H., Cho, H., Kim, K., and Hwang, I. (2010). Phosphorylation dependent nucleocytoplasmic shuttling of BES1 is a key regulatory event in brassinosteroid signaling. Mol Cells **29,** 283-290.

Scacchi, E., Salinas, P., Gujas, B., Santuari, L., Krogan, N., Ragni, L., Berleth, T., and Hardtke, C.S. (2010). Spatio-temporal sequence of cross-regulatory events in root meristem growth. Proc Natl Acad Sci U S A **107,** 22734-22739.

Schaller, G.E., and Kieber, J.J. (2002). Ethylene. The Arabidopsis Book **1**.

Sedbrook, J.C., and Kaloriti, D. (2008). Microtubules, MAPs and plant directional cell expansion. Trends Plant Sci **13,** 303-310.

Shin, J., Kim, K., Kang, H., Zulfugarov, I.S., Bae, G., Lee, C.H., Lee, D., and Choi, G. (2009). Phytochromes promote seedling light responses by inhibiting four negatively-acting phytochrome-interacting factors. Proc Natl Acad Sci U S A **106,** 7660-7665.

Silverstone, A.L., Ciampaglio, C.N., and Sun, T. (1998). The Arabidopsis RGA gene encodes a transcriptional regulator repressing the gibberellin signal transduction pathway. Plant Cell **10,** 155-169.

Silverstone, A.L., Mak, P.Y., Martinez, E.C., and Sun, T.P. (1997). The new RGA locus encodes a negative regulator of gibberellin response in Arabidopsis thaliana. Genetics **146,** 1087-1099.

Silverstone, A.L., Jung, H.S., Dill, A., Kawaide, H., Kamiya, Y., and Sun, T.P. (2001). Repressing a repressor: gibberellin-induced rapid reduction of the RGA protein in Arabidopsis. Plant Cell **13,** 1555-1566.

Skylar, A., and Wu, X. (2010). STIMPY mutants have increased cytokinin sensitivity during dark germination. Plant Signal Behav **5,** 1437-1439.

Skylar, A., Hong, F., Chory, J., Weigel, D., and Wu, X. (2010). STIMPY mediates cytokinin signaling during shoot meristem establishment in Arabidopsis seedlings. Development **137,** 541-549.

Song, L., Zhou, X.Y., Li, L., Xue, L.J., Yang, X., and Xue, H.W. (2009). Genome-wide analysis revealed the complex regulatory network of brassinosteroid effects in photomorphogenesis. Mol Plant **2,** 755-772.

Stepanova, A.N., and Alonso, J.M. (2009). Ethylene signaling and response: where different regulatory modules meet. Curr Opin Plant Biol **12,** 548-555.

Stephenson, P.G., Fankhauser, C., and Terry, M.J. (2009). PIF3 is a repressor of chloroplast development. Proc Natl Acad Sci U S A **106,** 7654-7659.

Stewart, J.L., and Nemhauser, J.L. (2010). Do trees grow on money? Auxin as the currency of the cellular economy. Cold Spring Harb Perspect Biol **2,** a001420.

Stewart, J.L., Maloof, J.N., and Nemhauser, J.L. (2011). PIF Genes Mediate the Effect of Sucrose on Seedling Growth Dynamics. PLoS One **6,** e19894.

Strasser, B., Sanchez-Lamas, M., Yanovsky, M.J., Casal, J.J., and Cerdan, P.D. (2010). Arabidopsis thaliana life without phytochromes. Proc Natl Acad Sci U S A **107,** 4776-4781.

Sun, T. (2008). Gibberellin Metabolism, Perception and Signaling Pathways in Arabidopsis. The Arabidopsis Book **6**.

Sun, Y., Fan, X.Y., Cao, D.M., Tang, W., He, K., Zhu, J.Y., He, J.X., Bai, M.Y., Zhu, S., Oh, E., Patil, S., Kim, T.W., Ji, H., Wong, W.H., Rhee, S.Y., and Wang, Z.Y. (2010). Integration of brassinosteroid signal transduction with the transcription network for plant growth regulation in Arabidopsis. Dev Cell **19,** 765-777.

Takano, M., Inagaki, N., Xie, X., Kiyota, S., Baba-Kasai, A., Tanabata, T., and Shinomura, T. (2009). Phytochromes are the sole photoreceptors for perceiving red/far-red light in rice. Proc Natl Acad Sci U S A **106,** 14705-14710.

Tanaka, S., Nakamura, S., Mochizuki, N., and Nagatani, A. (2002). Phytochrome in cotyledons regulates the expression of genes in the hypocotyl through auxin-dependent and -independent pathways. Plant Cell Physiol **43,** 1171-1181.

Toledo-Ortiz, G., Huq, E., and Rodriguez-Concepcion, M. (2010). Direct regulation of phytoene synthase gene expression and carotenoid biosynthesis by phytochrome-interacting factors. Proc Natl Acad Sci U S A **107,** 11626-11631.

Ubeda-Tomas, S., Federici, F., Casimiro, I., Beemster, G.T., Bhalerao, R., Swarup, R., Doerner, P., Haseloff, J., and Bennett, M.J. (2009). Gibberellin signaling in the endodermis controls Arabidopsis root meristem size. Curr Biol **19,** 1194-1199.

Vert, G., Walcher, C.L., Chory, J., and Nemhauser, J.L. (2008). Integration of auxin and brassinosteroid pathways by Auxin Response Factor 2. Proc Natl Acad Sci U S A **105,** 9829-9834.

Vert, G., Nemhauser, J.L., Geldner, N., Hong, F., and Chory, J. (2005). Molecular mechanisms of steroid hormone signaling in plants. Annu Rev Cell Dev Biol **21,** 177-201.

Wang, H., and Deng, X.W. (2004). Phytochrome Signaling Mechanism. The Arabidopsis Book **3**.

Wang, J.G., Chen, C.H., Chien, C.T., and Hsieh, H.L. (2011). FAR-RED INSENSITIVE219 Modulates CONSTITUTIVE PHOTOMORPHOGENIC1 Activity via Physical Interaction to Regulate Hypocotyl Elongation in Arabidopsis. Plant Physiol **156,** 631-646.

Warnasooriya, S.N., and Montgomery, B.L. (2009). Detection of spatial-specific phytochrome responses using targeted expression of biliverdin reductase in Arabidopsis. Plant Physiol **149,** 424-433.

Weijers, D., Benkova, E., Jager, K.E., Schlereth, A., Hamann, T., Kientz, M., Wilmoth, J.C., Reed, J.W., and Jurgens, G. (2005). Developmental specificity of auxin response by pairs of ARF and Aux/IAA transcriptional regulators. Embo J **24,** 1874-1885.

Whittington, A.T., Vugrek, O., Wei, K.J., Hasenbein, N.G., Sugimoto, K., Rashbrooke, M.C., and Wasteneys, G.O. (2001). MOR1 is essential for organizing cortical microtubules in plants. Nature **411,** 610-613.

Willats, W., McCartney, L., Mackie, W., and Knox, J.P. (2001). Pectin: cell biology and prospects for functional analysis. Plant Molecular Biology **47,** 9-27.

Willats, W.G.T., Knox, J.P., and Dalgaard Mikkelsen, J. (2006). Pectin: new insights into an old polymer are starting to gel. Trends in Food Science and Technology **17,** 97-104.

Wu, G., Cameron, J.N., Ljung, K., and Spalding, E.P. (2010). A role for ABCB19-mediated polar auxin transport in seedling photomorphogenesis mediated by cryptochrome 1 and phytochrome B. Plant J **62,** 179-191.

Wu, X., Dabi, T., and Weigel, D. (2005). Requirement of homeobox gene STIMPY/WOX9 for Arabidopsis meristem growth and maintenance. Curr Biol **15,** 436-440.

Yin, Y., Vafeados, D., Tao, Y., Yoshida, S., Asami, T., and Chory, J. (2005). A new class of transcription factors mediates brassinosteroid-regulated gene expression in Arabidopsis. Cell **120,** 249-259.

Yu, X., Liu, H., Klejnot, J., and Lin, C. (2010). The Cryptochrome Blue Light Receptors. The Arabidopsis Book **8**.

Yu, X., Li, L., Zola, J., Aluru, M., Ye, H., Foudree, A., Guo, H., Anderson, S., Aluru, S., Liu, P., Rodermel, S., and Yin, Y. (2011). A brassinosteroid transcriptional network revealed by genome-wide identification of BESI target genes in Arabidopsis thaliana. Plant J **65,** 634-646.

Zhang, H., He, H., Wang, X., Wang, X., Yang, X., Li, L., and Deng, X.W. (2011). Genome-wide mapping of the HY5-mediated gene networks in Arabidopsis that involve both transcriptional and post-transcriptional regulation. Plant J **65,** 346-358.

Zhang, S., Qi, Y., and Yang, C. (2010). Arabidopsis SUMO E3 ligase AtMMS21 regulates root meristem development. Plant Signal Behav **5**.

Zhao, Y., Christensen, S.K., Fankhauser, C., Cashman, J.R., Cohen, J.D., Weigel, D., and Chory, J. (2001). A role for flavin monooxygenase-like enzymes in auxin biosynthesis. Science **291,** 306-309.

Zhao, Y., Hull, A.K., Gupta, N.R., Goss, K.A., Alonso, J., Ecker, J.R., Normanly, J., Chory, J., and Celenza, J.L. (2002). Trp-dependent auxin biosynthesis in Arabidopsis: involvement of cytochrome P450s CYP79B2 and CYP79B3. Genes & Development **16,** 3100-3112.

Figure 1A

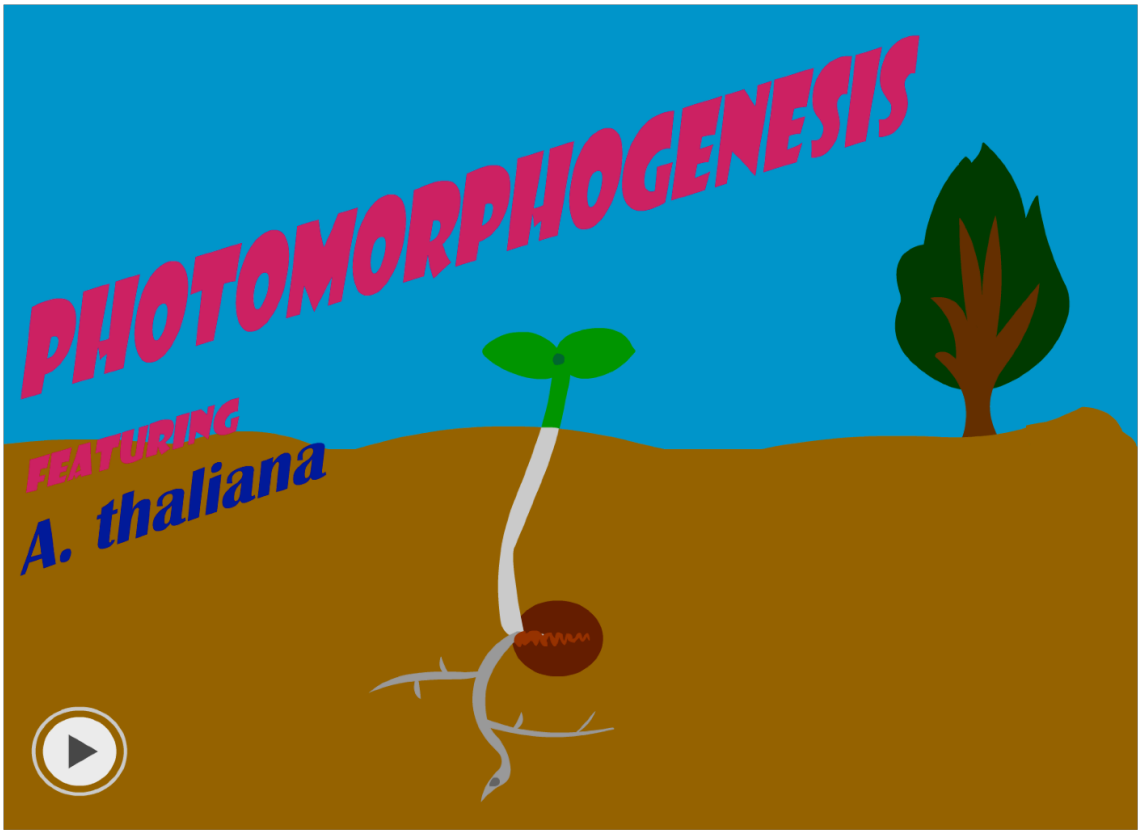

Figure 1B

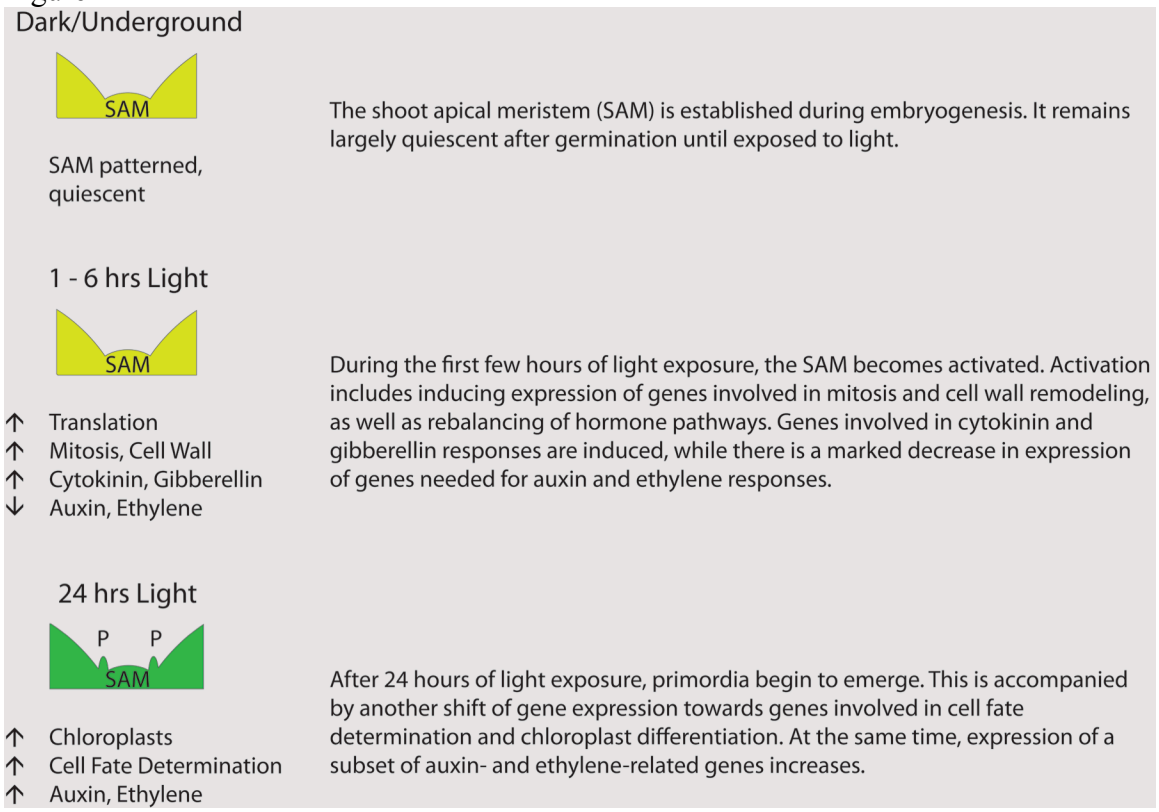
Dark/Underground
SAM
SAM patterned, quiescent
The shoot apical meristem (SAM) is established during embryogenesis. It remains largely quiescent after germination until exposed to light.
1 - 6 hrs Light
SAM
↑ Translation
↑ Mitosis, Cell Wall
↑ Cytokinin, Gibberellin
↓ Auxin, Ethylene
During the first few hours of light exposure, the SAM becomes activated. Activation includes inducing expression of genes involved in mitosis and cell wall remodeling, as well as rebalancing of hormone pathways. Genes involved in cytokinin and gibberellin responses are induced, while there is a marked decrease in expression of genes needed for auxin and ethylene responses.
24 hrs Light
P
P
SAM
↑ Chloroplasts
↑ Cell Fate Determination
↑ Auxin, Ethylene
After 24 hours of light exposure, primordia begin to emerge. This is accompanied by another shift of gene expression towards genes involved in cell fate determination and chloroplast differentiation. At the same time, expression of a subset of auxin- and ethylene-related genes increases.

Figure 1C

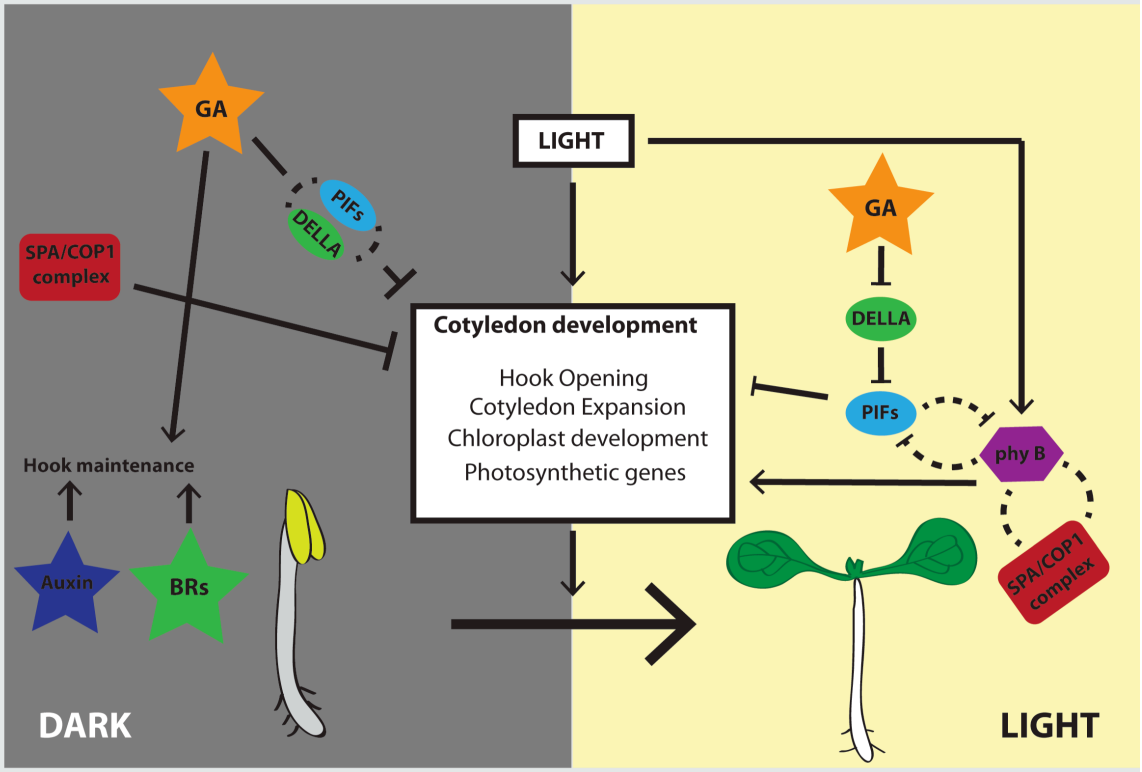

Dashed lines refer to protein interactions, arrows to up-regulation, T-bar to repression.

A seedling growing underground keeps its embryonic leaves (cotyledons) tightly-closed and hooked to protect the stem cells in the shoot apical meristem. Once it breaks free of the soil, a seedling expands its cotyledons to increase the light capturing surface. To elicit this response, light triggers a a number of dramatic changes. Transcriptional changes include induction of genes needed for photosynthesis, pigment production and chloroplast biogenesis. Photoreceptors, the PIF family of transcription factors, and a number of hormones are critical for this transition to photoautotrophy.

Figure 1D

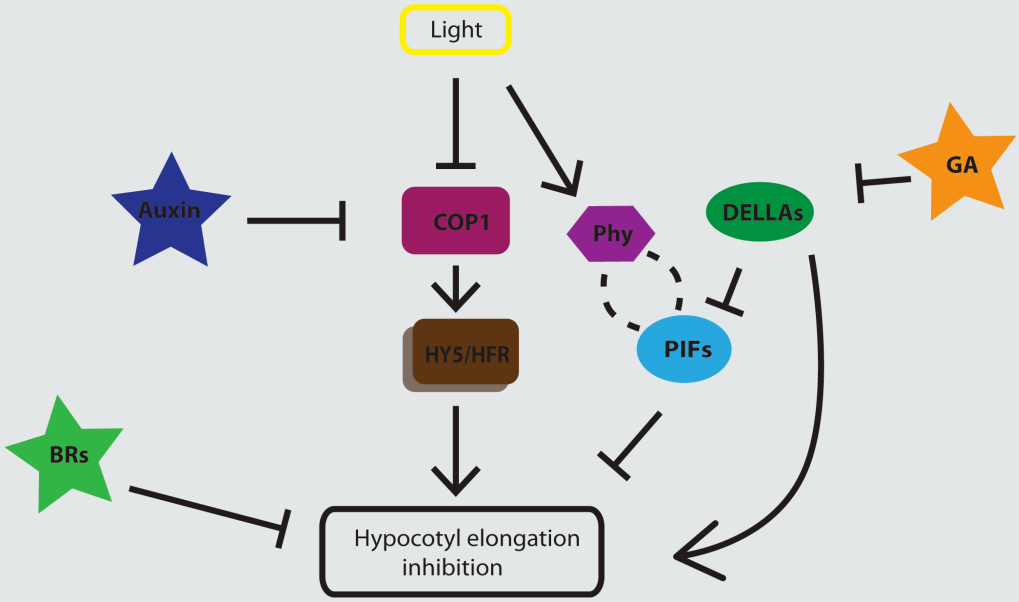

In the dark, *Arabidopsis* hypocotyls elongate rapidly, reaching a rate of up to 0.1mm/h. A number of phytohormones are required for this growth, including auxin, gibberellins (GA), and brassinosteroids (BRs). In addition, hypocotyl growth requires *de novo* synthesis and secretion of cell wall components. Cellulose production is increased, and microtubules have been suggested to provide scaffolding for cellulose deposition. Other modifications to the cell wall, like pectin modifications, are also required for stable cell expansion.

Following exposure to light, a massive reprogramming of the genome takes place. Transcription factors, such as LONG HYPOCOTYL 5 (*HY5*), target genes related to cell elongation, proliferation and chloroplast development. Members of the PHYTOCHROME INTERACTING FACTOR (PIF) family of transcription factors promote hypocotyl growth and antagonize photoreceptor function.

Figure 1E

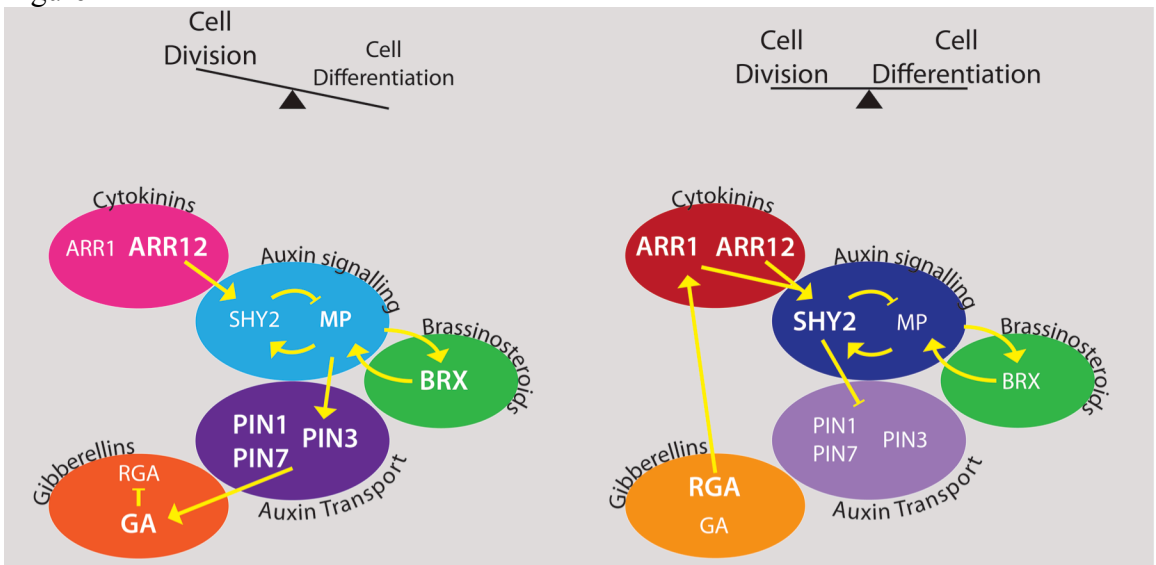

The root apical meristem (RAM) is established during embryogenesis. In the first few days following germination, the RAM is growing in size as cell proliferation outpaces cell differentiation. The molecular mechanism to maintain this balance relies on high levels of local auxin. This is achieved through elevated levels of the transcription factors MP/ARF5 and BRX, which together induce expression of PIN genes encoding auxin efflux carriers. High auxin levels trigger turnover of the corepressor SHY2/IAA3. High auxin levels also lead to increased gibberellin biosynthesis and subsequent degradation of the DELLA repressor RGA. In the absence of RGA, levels of the cytokinin-regulated transcription factor ARR1 are low.

At five days after germination, the RAM has reached its stable size by balancing the rates of cell division and differentiation. Gibberellin biosynthesis drops, causing an elevation in the levels of RGA. This leads to elevated levels of ARR1, allowing SHY2/IAA3 to accumulate. Expression of MP/ARF5, BRX, and PIN genes decrease, leading to lower local levels of auxin.

Chapter 2

A synthetic approach reveals extensive tunability of auxin signaling

Kyle A. Havens, Jessica M. Guseman, Seunghee S. Jang, Edith Pierre-Jerome, Nick Bolten, Eric Klavins, Jennifer L. Nemhauser (2012) A synthetic approach reveals extensive tunability of auxin signaling. Plant Physiol. 160:135–142.

ABSTRACT

Explaining how the small molecule auxin triggers diverse yet specific responses is a long-standing challenge in plant biology. An essential step in auxin response is degradation of IAA repressor proteins through interaction with auxin receptors. To systematically characterize diversity in degradation behaviors among IAA|receptor pairs, we engineered auxin-induced degradation of plant IAA proteins in yeast. We found that IAA degradation dynamics vary widely, depend on which receptor is present, and are not encoded solely by the degron-containing domain II. To facilitate this and future studies, we identified a mathematical model able to quantitatively describe IAA degradation behavior in a single parameter. Together, our results demonstrate the remarkable tunability conferred by specific configurations of the auxin response pathway.

INTRODUCTION

Auxin directs almost every aspect of plant biology, yet how specificity is generated from auxin signaling components remains largely unresolved. A range of auxin-associated phenotypes, including profound disruptions in development and severely compromised responses to environmental signals, are caused by single amino acid substitutions that stabilize transcriptional co-repressors called the Aux/IAAs or IAAs (Chapman & Estelle, 2009). The diversity of these phenotypes and the size of the IAA family suggest IAAs may provide specificity in auxin responses (Lokerse & Weijers, 2009). Functional studies support this idea, as stabilized IAAs provoke different phenotypes even when expressed from the same promoter (Weijers et al., 2005; Muto et al., 2007).

Auxin activates gene expression by enhancing IAA turnover through interaction with auxin receptors, a family of F-box proteins called TRANSPORT INHIBITOR RESISTANT 1 (TIR1) / AUXIN SIGNALING F-BOX PROTEINS (AFBs) (Dharmasiri et al., 2005a; Kepinski & Leyser, 2005), referred to here collectively as AFBs. Variation in the affinities of IAA|AFB pairs has recently been observed (Calderón Villalobos et al., 2012). How such differences relate to degradation kinetics is still unclear. Labor-intensive seedling studies on a small number of IAA proteins, in combination with analysis of stabilized IAA mutants, uncovered the importance of a conserved region, termed domain II, in determining protein stability. The degron-containing IAA domain II is both necessary and sufficient for interaction with TIR1 and the resulting auxin-induced degradation (Ramos et al., 2001; Dharmasiri et al., 2005a; Kepinski and Leyser, 2005; Tan et al., 2007). In addition, IAA-reporter fusions with diverse domain II sequences show a range of degradation rates when over-expressed in *Arabidopsis* seedlings (Dreher et al., 2006). However, the ubiquity of the auxin pathway in plants and the difficulty in reconstituting the complete degradation machinery *in vitro* have hindered further characterization of the molecular determinants of IAA degradation rates.

As a complement to existing systems and to systematically characterize the potential tunability of different IAA|AFB pairs, we engineered the auxin-induced degradation of IAA proteins in *Saccharomyces cerevisiae* (yeast). Our synthetic system has several advantages: precise control of auxin input levels, the ability to study IAA|AFB pairs in isolation, and the absence of the many other plant pathways known to impact auxin signaling (Stewart & Nemhauser, 2010). Our system allowed a comprehensive survey of IAA turnover while recapitulating behaviors observed in plants. We discovered that the particular AFB receptor used greatly impacted the rate of degradation and that sequences outside of the degron-containing domain II accelerated or decelerated IAA degradation in an IAA-specific manner. Moreover, we identified a mathematical model that provides a single parameter to quantitatively describe degradation behavior. The synthetic toolkit described here will facilitate rapid testing of hypotheses about ubiquitylation of IAA proteins and suggests a means to characterize other hormone-induced protein degradation pathways.

RESULTS

A synthetic yeast system recapitulates auxin-induced IAA degradation dynamics

Our engineered auxin response system consisted of pairwise matings of yeast expressing either YFP-IAA fusion proteins or AFBs (Fig. 1A). In the presence of a functional AFB, YFP fluorescence (a proxy for IAA levels) could be both up- and down-regulated by modulating levels of indole-3-acetic acid, hereafter referred to as auxin (Fig. 1B, S1). The timing and extent of degradation was comparable to experimental systems relying on a much higher concentration of a synthetic auxin (Nishimura et al., 2009). Flow cytometry provided high-resolution IAA degradation profiles for each IAA|AFB pair with improved time-resolution measurements at the single cell level (Fig. 1C). In contrast to the 'basal degradation' rates observed in plants (Dreher et al., 2006), YFP-IAA proteins were essentially stable in yeast in the absence of auxin or a functional AFB (Fig. S2, S3). This may reflect the difficulty of completely clearing auxin from plant cells or the presence of additional components in plants that are absent from our synthetic system. Following the major auxin-induced degradation events, a more gradual decline in YFP can be observed. As this behavior was also observed in strains expressing mTIR1, we believe that this decrease in fluorescence is caused by physiological changes associated with increasing culture density and not auxin-induced degradation of YFP-IAAs.

The fine time-resolution of our measurements resulted in complex degradation profiles that included an initial delay in degradation prior to an exponential decay of YFP levels (Fig.1B). Standard half-life calculations were therefore insufficient to describe the dynamics of degradation in our system. In order to quantitatively characterize the degradation behavior of every IAA|AFB pair, we identified a second-order nonlinear model that captures the dynamic auxin response in both time-course and dose-response experimental data (Fig. 2A, Supp. File 1). This model accounts for the complex degradation behavior we observed and the nonlinear relationship between auxin concentration and steady-state YFP intensity (Fig. S1). Among the candidate models tested, this model had the least complexity while still fitting the data with low residual error (Supp. File 1). Auxin response is represented by YFP-IAA fluorescence intensity output y and a hypothesized internal state x, dependent on the auxin input

concentration u. The hypothesized internal state x is not directly measured in our experiments and does not necessarily equate with specific active species, although one interpretation is that x is a complex formed between auxin and an AFB. Similarly, parameters k_1, k_2, k_3, k_4, and k_5 are not intended to have direct association with physical values in the system. One possibility is that these rates correlate with synthesis (k_1 for the internal state and k_3 for the IAA), degradation of the internal state (k_2), basal degradation/dilution of the IAA (k_4), and AFB-induced degradation (k_5). With this interpretation and applying the principles of global curve fitting, we reduced the total number of parameters needed to fit the entire data set (Supp. File 1).

Modeling distilled the differences observed in degradation between the IAA|AFB pairs into a single parameter: k_5. Importantly, the k_5 value for each IAA|AFB pair is consistent with the qualitative behaviors present in the experimental data (Fig. 1C, 2C). For example, the faster degrading IAAs had the largest k_5 values while more stable IAAs had the lowest k_5 values. Of all the parameters, k_5 best captures IAA|AFB degradation behavior and is hereafter called the degradation rate.

IAA proteins exhibit a range of degradation rates

In our system, auxin-induced degradation differs across IAA|AFB pairs (Fig. 1C, 2C). This is consistent with previous work in *Arabidopsis* seedlings, where half-lives of over-expressed IAA:LUC fusions were calculated by blocking new protein production with cycloheximide and treating exogenously with the synthetic auxin 2,4-D (Dreher et al., 2006; Table S1). In these assays, a strong match to the consensus domain II sequence was correlated with a short protein half-life in the presence of 2,4-D. For example IAA17 and IAA28 have strong matches to the consensus domain II and half-lives of five and fifteen minutes, respectively. In contrast IAA31, with a diverged domain II, has a half-life of approximately four hours. IAA20 lacks a recognizable domain II sequence and is highly stable. We observed similar patterns of degradation in yeast (Fig. 1C, 2C). In yeast expressing either TIR1 or AFB2, IAAs with consensus-matching domain II sequences degraded rapidly, IAA31 was slow to degrade and IAA20 showed no degradation. Of the IAAs with consensus domain II sequences, most

IAA|TIR1 pairs had rates similar to the fast degrading IAA17|TIR1 (Fig. 2C). We observed a few IAAs outside of this general trend, including the slow degrading IAA11.

Despite being expressed from the same promoter and singly integrated in the same genomic location, IAAs displayed different basal fluorescence levels in yeast (Fig. S3). Our model predicts that rates of IAA expression and degradation are independent of each other (Supp. File 1). To test this prediction, we synthesized a variant allele of IAA1 (IAA1.1) with yeast-optimized codons. Basal expression of IAA1.1 was twice that of IAA1 (Fig. 2A) with a similar fold change in the estimated k_3 values (Fig. 2B). In contrast, normalized degradation curves and k_5 values overlapped (Fig. 2B, C). This result validates our model and demonstrates that IAA degradation rates are indeed robust to fluctuations in IAA expression levels. Challenges in plant assays—including random location of insertions and multiple cell types contributing to variation in transgene expression—make this type of quantitative analysis quite difficult and highlight the benefits of using yeast as an additional resource for dynamic analysis of auxin responses.

IAA degradation rates are receptor specific

For the majority of IAAs tested, AFB2 promoted faster degradation than TIR1 (Fig. 1C, 2C). This resulted in IAA|AFB2 pairs having degradation rates up to three times higher than IAA|TIR1 pairs. AFB2 pairs also had a wider range of degradation rates between all IAAs. Excluding the IAAs with divergent domain IIs, the fastest IAA|TIR1 (IAA8) pair had a degradation rate 3.3 fold higher than the slowest, IAA11. In contrast, the fastest IAA|AFB2 pair (IAA17) had a degradation rate 5.5 fold higher than IAA11. Strikingly, the rank-order of degradation rates was not maintained between strains expressing different receptors. IAA6 showed one of the slowest rates of degradation with TIR1, yet had among the fastest degradation rates for IAA|AFB2 pairs. A subset of IAAs showed little difference in degradation between auxin receptors leading to some of the widest discrepancies in relative rank order. For example, there was little or no change in IAA1 degradation when the receptor was switched from TIR1 to AFB2. This resulted in IAA1 being one of the fastest degrading IAAs in combination with TIR1, yet among the slowest when expressed with AFB2. While it is possible that AFB2 functions more efficiently than TIR1 in yeast, the identification of a subset of

IAAs that show no change in degradation between the two receptors suggests these two proteins are intrinsically different in their IAA interactions.

While TIR1 and AFB2 conferred rapid auxin-induced degradation of IAAs, AFB1 and AFB3 had little effect on IAA degradation rates (Fig. S4). Genetic analysis suggests that TIR1 and AFB2 are the major auxin receptors in *Arabidopsis,* but it is still unclear the degree to which each TIR1/AFB protein contributes to specific auxin responses (Dharmasiri et al., 2005b, Parry et al., 2009). Mutations in *TIR1* or *AFB2* lead to stronger overall auxin-related phenotypes than mutations in *AFB1* or *AFB3* , although loss of *AFB1* or *AFB3* can enhance mutations in other AFB family members (Dharmasiri et al., 2005b, Parry et al., 2009). We reasoned that AFBs might differ in their ability to interact with IAAs. This hypothesis is consistent with our findings, as well as with *in vitro* pull-down assays showing AFB1 and AFB3 have lower levels of interaction with IAAs than TIR1 and AFB2 (Parry et al., 2009). In addition, IAA-reporter fusions are strongly stabilized in *afb2* mutants, while loss of *AFB1* or *AFB3* alone has little effect on turnover rates (Dharmasiri *et al*, 2005b). An additional factor may be that our heterologous degradation assay is less sensitive than other assays to weak or transient IAA|AFB interactions. Indeed, *in vitro* pull-down assays and yeast two-hybrid screens have shown low levels of interaction between some IAA|AFB pairs even in the absence of auxin (Kepinski & Leyser, 2005; Dharmasiri et al., 2005a, 2005b; Parry et al., 2009; Calderón Villalobos et al., 2012), while we did not see any change in IAA stability without auxin addition (Fig. S2, S3). Moreover, auxin can increase interactions between AFB1-DNA-binding domain fusion proteins and IAA-activation domain fusion proteins when both constructs are highly expressed in yeast (Calderón Villalobos et al., 2012), suggesting that these weaker interactions may contribute to auxin responses in plants. Additional work in plants will be needed to discriminate among these different possibilities.

Receptor expression levels did not influence IAA degradation in our yeast assays. Degradation rates were not correlated with receptor abundance (Fig. S5) nor could they be increased by adding a second copy of the same receptor to the genome (Fig. S6). In addition, when TIR1 and AFB2 were co-expressed, the degradation rate of IAA6 closely matched that of AFB2 alone (Fig. S6). Genetic studies indicate that TIR1 is the primary

auxin receptor and AFB2 is not able to substitute for TIR1 even when expressed from the TIR1 promoter (Parry et al., 2009). This suggests that degradation rate differences are not the sole distinguishing characteristic of receptors and that further functional studies of the dynamics of IAA degradation in receptor mutant backgrounds could be fruitful.

Residues outside of domain II differentially affect degradation rates

Residues outside of domain II have been found to contribute to AFB|IAA auxin binding affinity *in vitro* (Calderón Villalobos et al., 2012) and high basal IAA degradation rates in seedlings (Dreher et al., 2006). We engineered truncations in IAAs with disparate degradation rates (Fig. 3A and S7) to directly test the role of non-domain II residues in auxin-induced degradation. The N-terminal half of the protein (T1) or a smaller region restricted to domain II (T2) were fused to an SV40 nuclear localization signal (NLS) (Table S2). Degradation rates of truncated proteins were compared to full-length constructs fused to the same NLS (Fig. 3B, 3C). We found that sequences outside of domain II could accelerate or decelerate degradation rates in an IAA-specific manner. Relative rank order of full-length IAA degradation rates was not conserved in the truncations. IAA28.T2 was the fastest degrading of the T2 truncations, yet IAA28 showed much slower degradation rates than IAA1 or IAA6. Moreover, parallel truncations in different IAAs did not have the same effect on degradation rates. IAA6.T1 was slower than full-length IAA6, but IAA28.T1 was faster than full-length IAA28.

The recently reported DII-VENUS auxin sensor is similar to IAA28.T2, but shifted 15 amino acids towards the IAA28 N-terminus (Vernoux et al, 2011; Brunoud et al, 2012). To test whether this small difference in sequence had any effect on degradation rates, we engineered the identical IAA28 truncation into our system (IAA28.T2V) (Fig. 3A, Table S2). IAA28.T2V degraded far slower than all other constructs tested (Fig. 3B). This effect is opposite to what we observed with IAA28.T1 and IAA28.T2, both of which had increased rates of degradation compared with the full-length protein. The markedly slower degradation rate we observed for IAA28.T2V could explain why it was the brightest reporter tested (Brunoud et al., 2012). In fact, our analysis predicted that IAA8 and IAA9, the other IAA truncations tested in that study,

would degrade faster than IAA28 (Fig. 2, Table S1). This is consistent with the much dimmer fluorescence observed for the DII reporters made with these IAA proteins (Brunoud et al., 2012). To directly test whether our yeast assays could predict relative degradation rates in plants, we generated transgenic seedlings expressing a modified DII-VENUS reporter where we replaced the IAA28.T2V sequence with the IAA28.T2 sequence. Consistent with the higher rate of turnover of the IAA28.T2 fusion protein in yeast, we observed significantly lower levels of fluorescence of the IAA28.T2 reporter in transgenic plants (Fig. S8).

DISCUSSION

The size and diversity of the IAA and AFB protein families suggest that auxin specificity can be conferred by specific configurations of IAA and AFB family members (Lokerse & Weijers, 2009). In this study, we present a new method for investigating the range of diversity encoded by these large families. By porting plant proteins into yeast, we could directly test the variability in degradation rates between specific IAA|AFB pairs. We were able to reproduce auxin-induced degradation and generate high-resolution real-time data. Our yeast platform was able to recapitulate behaviors previously observed in studies of IAA turnover and allowed for an extensive survey of IAA degradation behavior.

Assessing degradation with each receptor individually, we showed that IAA degradation is highly influenced by which receptor is present, and that these receptor effects are IAA-specific (Fig. 1C, 2C). Our data provide evidence of receptor choice on regulating the turnover of IAAs, and show that each member of the IAA|AFB pair plays a role in determining auxin sensitivity. The high sequence similarity between TIR1 and AFB2, in combination with their shared substrates, should provide a platform to dissect how F-box proteins influence the rate of ubiquitylation, a factor known to vary among other F-box proteins (Pierce et al., 2009). The lack of detectable IAA degradation in yeast expressing AFB1 or AFB3, despite their ability to bind auxin, may have important implications for calibrating auxin responses. This implies that different combinations of receptors may produce varied response thresholds, which may each trigger a specific auxin-regulated process (Del Bianco & Kepinski, 2011; Reinhardt et al., 2003).

Surprisingly, IAA degradation rates were not strongly correlated with the few recently reported *in vitro* dissociation constants (K_d) (Calderón Villalobos et al., 2012; Table S1). This lack of correlation could simply be the result of the artificial nature of both systems: K_ds are a measure of complex formation and are determined independent of a complete ubiquitin complex, and our heterologous system has a mixture of yeast and plant components (Fig. 1A). However, a testable alternative hypothesis is that the interaction strength between TIR1 and an IAA is not a direct reflection of how quickly the IAA is degraded. Conserved sequences outside of the interaction domain have recently been shown to impact the rate of degradation of a number of substrates of the anaphase-promoting complex (Williamson et al., 2011). While similar sequences have not been identified in IAA proteins, the fact that truncations have such varied degradation rates clearly shows that additional residues play a crucial role in modulating interaction with the ubiquitin machinery (Fig. 3; Dreher et al., 2006). Identification of IAA degradation rate determinants could be accelerated by combining information from studies in yeast, *in vitro*, and in plants.

By utilizing a small, data-driven model we were able to quantitatively characterize the complex degradation behavior of each IAA|AFB in response to auxin (Fig. 2). Mathematical modeling allowed us to distinguish IAA and AFB contributions to degradation and thereby demonstrate how auxin perception can be tuned. We chose a small, empirical model because large mechanistic models (e.g. Bridge et al., 2011) require more parameters than could be identified from the low-dimensional output available in our experiments. Small models can nevertheless be quite useful. For example, a new negative feedback loop was discovered in yeast osmo-adaptation using a small model approach (Mettetal et al., 2008). Similarly, our simple model showed that unknown molecular interactions beyond complex affinity are required to describe IAA degradation dynamics. Moreover, small models such as ours can provide a simple description of the input-output properties of a module and facilitate the rational design of new systems in synthetic biology.

In this study, we have demonstrated the utility of porting a pathway to an orthogonal organism to characterize its function. As a single-celled eukaryote with conserved cellular machinery, yeast provides a semi-natural context that facilitates study

of complex signaling pathways. The rapid generation time, control of insertion site and number, and high throughput methods for quantitative analysis—combined with the absence of other known confounding factors like auxin transport, auxin metabolism, and the co-expression of AFB and IAA family members—make studies in yeast a strong complement to plant studies. Given the obvious artificiality of our system, it is quite promising that the rank order of auxin induced degradation rates parallels the limited number of half-lives observed in plants (Table S1). The fact that the IAA28.T2 construct behaved as predicted when expressed in seedlings (Fig. 3, S8) also points to overall conservation in degradation determinants between plant cells and engineered yeast. A full analysis of the similarities and differences between the systems will require more plant studies and likely better tools for measuring dynamic behaviors in plants. Our heterologous system provides a new method to investigate auxin signaling, as well as suggesting a means to study the many other plant pathways that rely on ubiquitin-mediated protein degradation.

MATERIALS AND METHODS

Yeast Methods

Yeast transformations were performed using a standard lithium acetate protocol (Gietz & Woods, 2002) into *MAT***a** W303-1A or *MATα* W814-29B, a gift from the Gottschling lab. YPAD and synthetic media supplemented with 80mg/ml adenine (SC) were made according to standard protocols. All strains used in this study are listed in Table S9.

Strain Construction

IAAs, TIR1 and AFB were amplified from *A. thaliana* cDNA (Columbia eco-type) using primers listed in Table S8. A partial attB1 site and Kozak sequence (*AAA*) were added to the 5' end of each forward primer (5'-*AAAAAGCAGGCTTCAAA*-3'), and a partial attB2 site was added to the 5' end of each reverse primer, (*AGAAAGCTGGGTG*). The remaining attB1 and attB2 sequences were added with a second PCR using generic forward and reverse adapter primers (GGGGACAAGTTTGTACAAAAAAGCAGGCT) and (GGGGACCACTTTGTACAAGAAAGCTGGGT). Products were sub-cloned into a Gateway® pDONR221 plasmid using a standard BP reaction (BP Clonase® II, Life

Technologies). Each cDNA was fully sequenced and then cloned into destination vectors with an LR reaction (LR Clonase® II, Life Technologies). IAAs were cloned into pGP4GY-ccdB (TRP selection) and auxin receptors were cloned into pGP5G-ccdB (LEU selection) (Havens et al., in preparation). Approximately 300 ng of each plasmid was digested with PmeI and transformed: pGP4GY-IAA into W303-1A, pGP5G-AFB into W814-29B. Integrations were confirmed by PCR. Strains to be mated were co-inoculated at low density into YPAD medium, grown overnight at 30^{o}C, and struck out to single colonies on SC-HIS,-TRP to select for diploids.

IAA truncations were fused to an N-terminal YFP and C-terminal SV40 nuclear localization signal repeat using glycine-alanine linkers (GAGAGAGAGAGP and GAGA, respectively) (Nishimura et al., 2009). The IAA17.T1 construct was synthesized with partial EYFP and the complete NLS sequence (www.genewiz.com) and then cloned into the pGP4GY-ccdB vector backbone via Gibson assembly (Gibson et al., 2009). The cloning scheme is outlined in Fig. S7. Primers are listed in Table S8. Gateway® acceptor sites were removed by this process. Further truncation constructs were amplified from full-length IAA sequences and cloned in place of IAA17 using Gibson assembly (Gibson et al., 2009).

The DII-VENUS plasmid was a gift from Teva Vernoux. The IAA28.T2-VENUS plasmid was constructed by replacing the DII region of DII-VENUS with the IAA28.T2 degron region using Gibson assembly (Gibson et al., 2009).

Flow Cytometry

YFP intensity measurements were taken with a BD Accuri C6 flow cytometer with a CSampler plate adapter using excitation wavelengths of 488 and 640 nm and an emission detection filter at 533 nm (FL1 channel). 10,000 events above a 400,000 FSC-H threshold (to exclude debris) were measured for each sample at a flow rate of 66 μL/min and core size of 22 μm using the Accuri C6 CFlow Sampler software. Cytometry data were exported as FCS 3.0 files and processed using the flowCore R software package and custom R scripts to obtain the mean FL1-A value at each time point. The script applies two polygon gates on the data to isolate single yeast cells. One

gate separates the total yeast population from debris on the SSC-A and FSC-A channels. The second gate isolates single cells from cell aggregates (doublet discrimination) via their higher FSC-H (peak height) to FSC-A (peak area) ratio. Scripts are available upon request.

Degradation Assays

Cells were prepared by transferring a freshly grown colony from YPD plates into SC. The cell density (in events/µl) was estimated using cytometry data gated for yeast by a custom R script. Each culture was then diluted to 0.5 events/µl in 15 mL of SC. This dilution was split into duplicate 4 mL aliquots with the exception of controls. For IAA17 without a YFP tag and YFP without an IAA, only a single 4 mL aliquot was prepared. YFP-IAA17 was split into 3 aliquots to serve as an internal replicate control within each experiment. Aliquots were incubated for 16 hours at 30°C with shaking. At 16 hours, duplicate aliquots of each strain were mixed and split again into two tubes. Cultures were in log-phase at the beginning of each experiment (density measured in cytometer at ~ 500 events/µl) and remained in log phase for the duration of each experiment (Fig. S2).

Measurements were taken at two time points prior to the addition of any treatment. For each strain, one replicate was mock treated (95% Et0H) and one replicate was treated with 10 µM indole-3-acetic acid [the minimal concentration of auxin needed to promote complete IAA degradation during log-phase growth of the yeast (Fig. S1 and S2)]. As soon as possible after addition of auxin, fluorescence for the t=0 min time point was recorded. Subsequent measurements were acquired at 10 min intervals for the first 2 hr after auxin addition and every 30 min thereafter until the fluorescence level in most strains had plateaued (approximately 3.5 hours). Controls were measured every hour for the duration of the experiment.

Modeling and Quantitative Analysis

Modeling methods and quantitative analysis are described in Supplementary File 1.

Microscopy

Yeast cells grown overnight in SC at 30ºC were diluted 1:100 in SC, incubated for 4-5hrs, then diluted 1:20 before loading into a Y04D plate (CellASIC). Using the CellASIC-ONIX^{TM} microfluidic system and associated software, cells were pulsed with a square wave of 10μM auxin in SC media over a period of 2 hours. An inverted Nikon Eclipse Ti microscope with a 60x, NA 1.4 oil objective was used to image the yeast cells at 5 min intervals using a YFP-HYQ 535 bandpass filter (Nikon) (excitation at 515nm, detection from 520nm to 550nm), and a CoolSNAP HQ2 14 bit camera. Image processing was done with custom MATLAB scripts, available upon request. Briefly, a segmentation algorithm was applied to brightfield images to produce a binary mask for each microcolony. This binary mask was then applied to the YFP image to calculate the average YFP intensity value within the colony. Background fluorescence level was estimated using the average fluorescence of a 100x100 pixel square away from the yeast colony and subtracted from total fluorescence values.

Generation and analysis of transgenic plants

Col-0 plants were transformed using the floral dip method (Clough & Bent, 1998). T1 plants were selected on 0.5x LS agar plates containing 30 μg ml^{-1} Hygromycin B. Plates were stratified for two days, exposed to light for 6 hours, the grown in the dark for 3 days following a modification of the method of Harrison et al. (2006). Resistant seedlings were transferred to plates containing no antibiotics and allowed to recover for 3 additional days. DII-VENUS seeds provided generously by Teva Vernoux were grown in the identical conditions to allow a direct comparison of the IAA28.T2 and IAA28.T2V constructs in plants.

Plants were imaged using a Leica DMI 3000B microscope fitted with a Leica long-working 20X HCX PL FLUORTAR objective and illuminated with a Lumencor SOLA light source. Images were captured using Leica LAS AF version 2.6.0 software and a Leica DFC 345FX camera. Seven independent IAA28.T2 transformants were examined and compared to ten DII-VENUS seedlings. Fiji software was used to quantify fluorescence in a region of interest centered on each image.

ACKNOWLEDGEMENTS

We thank Mark Estelle, Ning Zheng and members of the Nemhauser and Klavins Groups for helpful discussions; Alec Nielson, Selma Alkafeef and Brandi House for technical assistance.

AUTHOR CONTRIBUTIONS

All authors conceived and designed experiments. KAH, JMG, SSJ, EPJ and NB performed experiments. KAH, JMG, SSJ, EPJ, EK, and JLN wrote the paper.

REFERENCES

Del Bianco M & Kepinski S (2011) Context, specificity, and self-organization in auxin response. *Cold Spring Harb Perspect Biol* **3:** a001578

Bridge LJ, Mirams GR, Kieffer ML, King JR & Kepinski S (2011) Distinguishing possible mechanisms for auxin-mediated developmental control in Arabidopsis: Models with two Aux/IAA and ARF proteins, and two target gene-sets. *Math Biosci* **235**: 32-44

Brunoud G, Wells DM, Oliva M, Larrieu A, Mirabet V, Burrow AH, Beeckman T, Kepinski S, Traas J, Bennett MJ & Vernoux T (2012) A novel sensor to map auxin response and distribution at high spatio-temporal resolution. *Nature* **482:** 103-106

Calderón Villalobos LI a, Lee S, De Oliveira C, Ivetac A, Brandt W, Armitage L, Sheard LB, Tan X, Parry G, Mao H, Zheng N, Napier R, Kepinski S & Estelle M (2012) A combinatorial TIR1/AFB-Aux/IAA co-receptor system for differential sensing of auxin. *Nat Chem Biol* **8:** 477-485

Chapman EJ & Estelle M (2009) Mechanism of auxin-regulated gene expression in plants. *Annu Rev Genet* **43:** 265-285

Clough SJ & Bent AF (1998) Floral dip: a simplified method for Agrobacterium-mediated transformation of Arabidopsis thaliana. *Plant J* **16:** 735-743

Dharmasiri N, Dharmasiri S & Estelle M (2005a) The F-box protein TIR1 is an auxin receptor. *Nature* **435:** 441-445

Dharmasiri N, Dharmasiri S, Weijers D, Lechner E, Yamada M, Hobbie L, Ehrismann JS, Jürgens G & Estelle M (2005b) Plant development is regulated by a family of auxin receptor F box proteins. *Dev Cell* **9:** 109-119

Dreher KA, Brown J, Saw RE & Callis J (2006) The Arabidopsis Aux / IAA Protein Family Has Diversified in Degradation and Auxin Responsiveness. *Plant Cell* **18:** 699-714

Gibson DG, Young L, Chuang R-Y, Venter JC, Hutchison CA & Smith HO (2009) Enzymatic assembly of DNA molecules up to several hundred kilobases. *Nat Methods* **6:** 343-345

Gietz RD & Woods RA (2002) Transformation of yeast by lithium acetate/single-stranded carrier DNA/polyethylene glycol method. *Methods Enzymol* **350:** 87-96

Harrison SJ, Mott EK, Parsley K, Aspinall S, Gray JC & Cottage A (2006) A rapid and robust method of identifying transformed Arabidopsis thaliana seedlings following floral dip transformation. *Plant Methods 2:19* **2:** 19.

Kepinski S & Leyser O (2005) The Arabidopsis F-box protein TIR1 is an auxin receptor. *Nature* **435:** 446-451

Lokerse AS & Weijers D (2009) Auxin enters the matrix--assembly of response machineries for specific outputs. *Current Opin Plant Biol* **12:** 520-526

Mettetal JT, Muzzey D, Gómez-Uribe C & van Oudenaarden A (2008) The frequency dependence of osmo-adaptation in Saccharomyces cerevisiae. *Science* **319:** 482-484

Muto H, Watahiki MK, Nakamoto D, Kinjo M & Yamamoto KT (2007) Specificity and Similarity of Functions of the Aux/IAA Genes in Auxin Signaling of Arabidopsis Revealed by Promoter-Exchange Experiments among MSG2/IAA19, AXR2/IAA7, and SLR/IAA14. *Plant Phys* **144:** 187-196

Nishimura K, Fukagawa T, Takisawa H, Kakimoto T & Kanemaki M (2009) An auxin-based degron system for the rapid depletion of proteins in nonplant cells. *Nat Methods* **6:** 917-922

Parry G, Calderon-Villalobos LI, Prigge M, Peret B, Dharmasiri S, Itoh H, Lechner E, Gray WM, Bennett M & Estelle M (2009) Complex regulation of the TIR1/AFB family of auxin receptors. *Proc Natl Acad Sci U S A* **106:** 22540-22545

Pierce NW, Kleiger G, Shan S-ou & Deshaies RJ (2009) Detection of sequential polyubiquitylation on a millisecond timescale. *Nature* **462:** 615-619

Ramos J, Zenser N, Leyser O & Callis J (2001) Rapid degradation of auxin/indoleacetic acid proteins requires conserved amino acids of domain II and is proteasome dependent. *Plant Cell* **13:** 2349-2360

Reinhardt D, Pesce E-R, Stieger P, Mandel T, Baltensperger K, Bennett M, Traas J, Friml J & Kuhlemeier C (2003) Regulation of phyllotaxis by polar auxin transport. *Nature* **426:** 255-260

Stewart JL & Nemhauser JL (2010) Do trees grow on money? Auxin as the currency of the cellular economy. *Cold Spring Harb Perspect Biol* **2:** a001420

Tan X, Calderon-Villalobos LI, Sharon M, Zheng C, Robinson CV, Estelle M, Zheng N (2007) Mechanism of auxin perception by the TIR1 ubiquitin ligase. *Nature* **446:** 640-645

Vernoux T, Brunoud G, Farcot E, Morin V, Van den Daele H, Legrand J, Oliva M, Das P, Larrieu A, Wells D, Guédon Y, Armitage L, Picard F, Guyomarc'h S, Cellier C, Parry G, Koumproglou R, Doonan JH, Estelle M, Godin C, Kepinski S, Bennett M, De Veylder L, Traas J (2011) The auxin signalling network translates dynamic input into robust patterning at the shoot apex. *Mol Syst Biol* **7:** 508

Weijers D, Benkova E, Jäger KE, Schlereth A, Hamann T, Kientz M, Wilmoth JC, Reed JW & Jürgens G (2005) Developmental specificity of auxin response by pairs of ARF and Aux/IAA transcriptional regulators. *EMBO J* **24:** 1874-1885

Williamson A, Banerjee S, Zhu X, Philipp I, Iavarone AT & Rape M (2011) Regulation of ubiquitin chain initiation to control the timing of substrate degradation. *Mol Cell* **42:** 744-757

FIGURE LEGENDS

Figure 1: IAA degradation is highly variable
(A) Plant auxin receptors (TIR1 or AFB2) and YFP-tagged IAA repressors were integrated into the yeast ubiquitin pathway, shown in grey. **(B)** Yeast cells were imaged while exposed to a square wave of auxin. Auxin leads to a rapid decrease in YFP (fluorescence of individual microcolonies in blue, average value in black), which can be recovered with auxin removal. **(C)** A range of IAA|receptor degradation rates were obtained using time-lapse flow cytometry. Degradation curves were normalized to starting fluorescence. IAAs are listed in order of the relative difference in degradation in the presence of TIR1 (light blue) versus AFB2 (dark blue). Strains expressing the F-box deficient mTIR1 (grey) show no auxin-dependent degradation.

Figure 2: Degradation dynamics can be described using few parameters
(A) Our model is described by two ODEs. Degradation curves for AFB2 strains expressing IAA1 (blue) or yeast codon-optimized IAA1.1 (purple) are shown. **(B)** k_5 is largely independent of expression levels. IAA1 and IAA1.1 degradation curves overlap after normalization, although there is an approximately 2-fold difference in k_3 values. **(C)** IAA|AFB2 pairs have increased degradation rates (k_5), a different rank order when compared to IAA|TIR1 pairs, and an increased dynamic range between the slowest and fastest pairs. Parameters were estimated for two independent replicates. All error bars represent one standard deviation. Additional parameters are listed in Tables S4 and S5.

Figure 3: Residues outside of domain II contribute to auxin-induced degradation rates
(A) Schematic of IAA truncations. **(B, C)** Degradation dynamics of full-length proteins are not maintained in truncations. (B) Degradation rates of truncations expressed with TIR1 or AFB2, normalized to starting fluorescence for each strain. (C) Parameters k_3 and k_5 were determined, using parameters k_1, k_2, and k_4 from previous model fitting. Additional parameters are listed in Table S6.

Figure 1

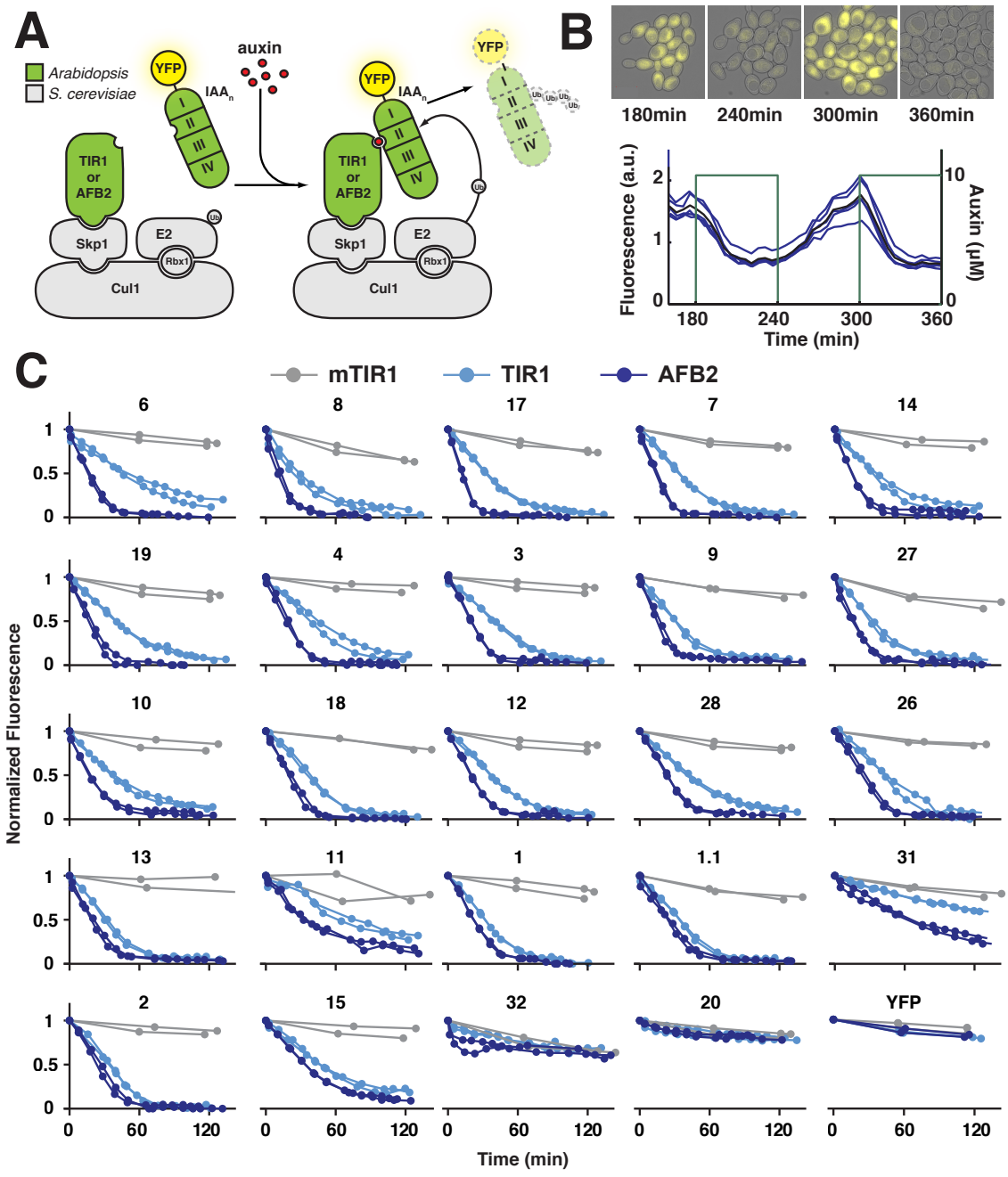
A
Arabidopsis
S. cerevisiae
auxin
YFP
IAA
TIR1 or AFB2
Skp1
E2
Rbx1
Cul1
Ub
B
180min
240min
300min
360min
Fluorescence (a.u.)
Auxin (μM)
Time (min)
C
mTIR1
TIR1
AFB2
Normalized Fluorescence
Time (min)
6
8
17
7
14
19
4
3
9
27
10
18
12
28
26
13
11
1
1.1
31
2
15
32
20
YFP

Figure 2

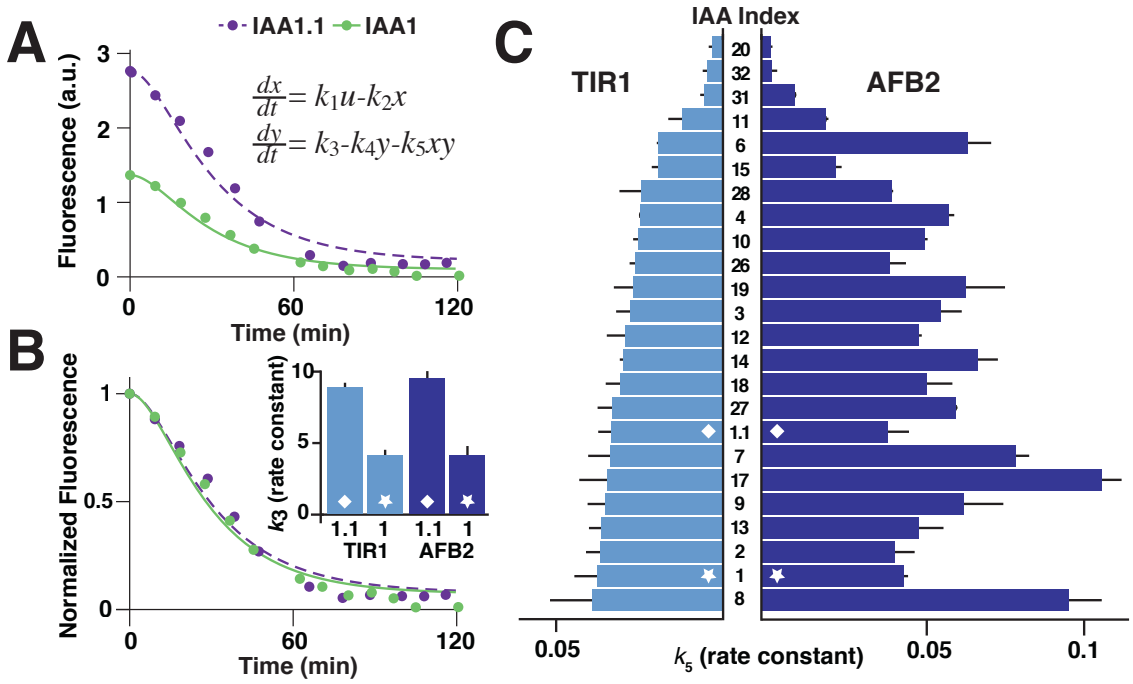
A
IAA1.1
IAA1
$\frac{dx}{dt} = k_1u - k_2x$
$\frac{dy}{dt} = k_3 - k_4y - k_5xy$
Fluorescence (a.u.)
Time (min)
B
Normalized Fluorescence
Time (min)
k_3 (rate constant)
1.1 1 1.1 1
TIR1 AFB2
C
IAA Index
TIR1
AFB2
20 32 31 11 6 15 28 4 10 26 19 3 12 14 18 27 1.1 7 17 9 13 2 1 8
0.05
k_5 (rate constant)
0.05
0.1

Figure 3

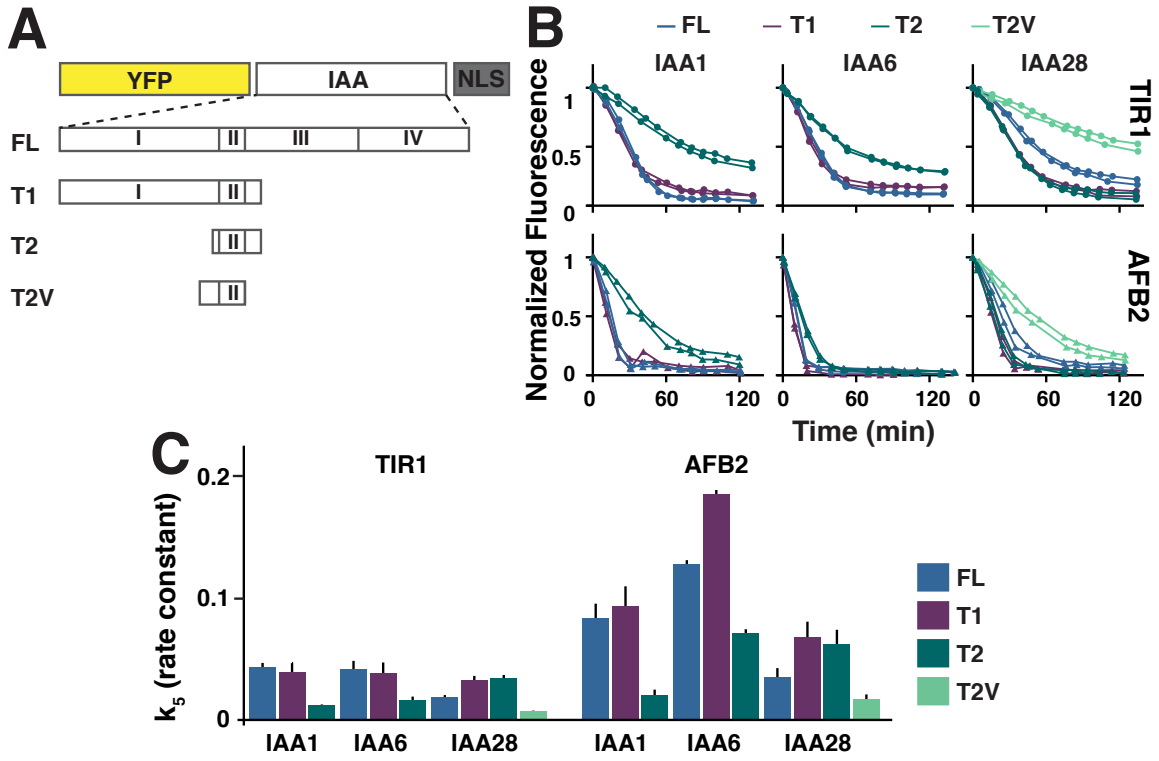
A
YFP
IAA
NLS
FL
T1
T2
T2V
I
II
III
IV
B
FL
T1
T2
T2V
IAA1
IAA6
IAA28
TIR1
AFB2
Normalized Fluorescence
Time (min)
C
TIR1
AFB2
k_5 (rate constant)
IAA1
IAA6
IAA28
FL
T1
T2
T2V

Supplementary Information for

A synthetic approach reveals extensive tunability of auxin signaling

Kyle A. Havens[1*], Jessica M. Guseman[2*], Seunghee S. Jang[1*], Edith Pierre-Jerome[2*], Nick Bolten[1], Eric Klavins[1#], and Jennifer L. Nemhauser[2#]

[1]Department of Electrical Engineering
[2]Department of Biology
University of Washington, Seattle, WA, 98195
[*]co-first authors
[#]correspondence should be addressed to klavins@uw.edu or jn7@uw.edu

Contents

Supplementary Figures

Supplementary Tables

1 Quantitative Analysis

1.1 Objectives and Approach

The primary objective of our quantitative analysis is to identify a small model, with as few parameters as possible, that describes the differential degradation of IAA|AFB pairs observed in experiments. Having few parameters avoids over-fitting, facilitates comparison among available pairs, and provides a guide for the selection of parts during the rational design of new networks. A computationally intractable number of candidate models can be generated by, for example, various assumptions about the mechanism of degradation and the many molecular species involved. Computational limits, therefore, require that we limit the number of candidate models by employing current knowledge of the auxin signal pathway, basic assumptions about protein synthesis, and simple input-output concepts.

We assess candidate models by fitting their parameters to the entire data set, analyzing their qualitative fit, and then computing their residual fit. We fit our models to experimental data using the nonlinear optimization function `FindFit` in *Mathematica* (Wolfram) where the cost function is defined as

$$J(\theta^{(s)}, M_s) \quad = \quad \sum_{i,j} \sum_{t_m \in \mathrm{T}} \left\| y_{ij}(t_m) - \hat{y}_{ij}(t_m, \theta_{ij}^{(s)}, M_s) \right\|_2, \tag{1}$$

where i denotes the index of an IAA, j denotes the index of a AFB, s denotes the index of a model, $y_{ij}(t_m)$ denotes the measured output at $t = t_m$, T denotes the set of measurement times, $\theta_{ij}^{(s)}$ denotes the parameter vector for a model M_s and $\mathrm{IAA}_i|\mathrm{AFB}_j$, $\hat{y}_{ij}(t_m, \theta_{ij}, M_s)$ denotes the predicted output using the model M_s and its parameter vector θ_{ij} at $t = t_m$, $\theta^{(s)}$ denotes the union of all parameter vectors of IAA|AFB pairs under the model M_s and $\|\cdot\|_2$ denotes the 2-norm[1] of the given vector. Following the estimation, the residual of a model is defined as

$$G(M_s) = \sum_{i,j} \sum_{t_m \in \mathrm{T}} \frac{1}{dim\ y_{ij}} \left\| \frac{y_{ij}(t_m) - \hat{y}_{ij}\left(t_m, M_s, \theta_{ij}^{(s)*}\right)}{y_{ij}(t_m)} \right\|_2 \tag{2}$$

where $\theta^{(s)*}$ denotes the optimal estimated parameter vector obtained from minimizing the cost function (1), and *dim* denotes the dimension of the vector (e.g. numbers of data points in the time course).

1.2 Model Development and Discrimination

Our approach is to develop candidate models with good qualitative fits, low residuals, and a small number of parameters by incrementally increasing complexity via refinements that are based on known mechanisms. In the model discrimination step, both quantitative and qualitative metrics of each model are evaluated. It is true that quantitatively low residual is desired in general, however, the analytical metric takes precedence. If a model is shown to be analytically incapable of fitting critical features of experimental observation, the

[1] $\|x\|_p = \left(\sum_{i=1}^{n} |x_i|^p\right)^{1/p}$

model is deemed structurally flawed, and is eliminated, even if the quantitative metric is relatively low. Following are the two general qualitative features observed in the experimental data.

1. Each degradation time-course includes an inflection point, such that the curve switches from concave to convex (Figure 1C).

2. Each dose-response curve (steady-state fluorescence measurement vs auxin concentration) is nonlinear (Supplementary Figure 1).

These two features were used as qualitative criteria to which all models were subjected to. The number of parameters for the model is computed over all experimental data sets, such that the total number of parameters equals the number of parameters in the model multiplied by the number of experiments (i.e. the number of distinct IAA|AFB pairs). After a model has been selected, we reduced the total number of parameters by assuming that some of the parameters can be consolidated for a specific group of experiments.

1.2.1 M_0

We first consider the synthetic yeast system as a grey-box with a single input (auxin) and a single output (YFP intensity). Therefore, we propose the following model, M_0, which is a combination of simple synthesis/degradation dynamics and exponential decay:

$$\frac{d\,y(t)}{dt} = k_1 - k_2\,y(t) - k_3\,u(t)\,y(t), \tag{3}$$

where t denotes time, y denotes the output, and u denotes the input. This model encodes the hypothesis that the YFP-IAA fusion protein is subject to zeroth-order synthesis and first-order degradation, and that the output degrades at a rate proportional to the input. The first two terms, k_1 and $k_2\,y(t)$, represent the input-independent synthesis and degradation of the output, respectively. The last term represents the degradation of output with the overall rate proportional to itself and the input. Thus, k_1 is the synthesis rate, k_2 is the basal degradation rate, and k_3 is the input mediated degradation rate.

This model has residual $G(M_0) = 49.31$, and requires 144 distinct parameters (3 per IAA|AFB pair) to fit the entire data set. The model has a closed form analytical solution,

$$y(t) \;=\; \frac{k_1}{k_2 + k_3 u}\left(1 + \frac{e^{-t(k_2+k_3u)}k_3u}{k_2}\right), \tag{4}$$

which demonstrates the nonlinear relationship between u and the y^*, which is consistent with the qualitative observation of the experimental data (Supplementary Figure 9, purple curve). However, the model cannot capture the inflection of the curve (Supplementary Figure 9, purple curve). For a function to have change in its convexity, the second derivative has to equal zero at some $t > 0$ (and that t is the inflection point). However, M_0 has second-order derivative,

$$\frac{d^2y}{dt^2} \;=\; \frac{k_1k_3u\,(k_2 + k_3u)}{k_2}e^{-t(k_2+k_3u)} \tag{5}$$

which shows that for all parameters $k_1, k_2, k_3 > 0$ and $u \geq 0$, $d^2y/dt^2 > 0$. This represents M_0 is fundamentally unable to capture one of the crucial features of the system.

1.2.2 M_1

The inflection point and the related initial delay in the degradation curves suggest that the IAA degradation mechanism comprises additional intermediate processes (e.g. formation of an intermediate species). To model this feature, we add an internal state x. At this point, we do not assume that x is any specific

species or combination of species – just that it is formed and degraded. In particular, we assume that the rate at which x is synthesized is proportional to the input, and that x affects the non-basal degradation of y. This second-order linear model, M_1, is defined by

$$\begin{aligned}\frac{d\,x(t)}{dt} &= k_1\,u(t) - k_2\,x(t)\\ \frac{d\,y(t)}{dt} &= k_3 - k_4\,y(t) - k_5\,x(t).\end{aligned} \tag{6}$$

The model has residual $G(M_1) = 81.68$, and requires 240 distinct parameters (5 per IAA|AFB pair) to fit the entire data set. The model captures the inflection point in time-course degradation curve (Supplementary Figure 9, blue curve). However, the dose-response predicted by M_1 is qualitatively different from our observations. Analytically, the steady-state solution of M_1 has a closed form,

$$\begin{aligned}x^* &= \frac{k_1\,u}{k_2}\\ y^* &= \frac{k_3}{k_4} - \frac{k_5\,k_1}{k_2\,k_4}u,\end{aligned} \tag{7}$$

which demonstrates that y^* has a linear relationship to u. Furthermore, because of this linear relationship, the model predicts that the steady-state fluorescence decreases indiscriminately with increasing amount of input, to the point where negative fluorescence is predicted (Supplementary Figure 10, blue curve). The fact that M_2 makes predictions that starkly contradict physical constraints demonstrates that M_1 is qualitatively unfit for the given experimental data.

1.2.3 M_2

Since the dose-response is nonlinear, we modify M_1 by introducing a nonlinear term, making the degradation term dependent on $y(t)$. This second-order nonlinear model, M_2, is,

$$\begin{aligned}\frac{dx(t)}{dt} &= k_1\,u(t) - k_2\,x(t)\\ \frac{dy(t)}{dt} &= k_3 - k_4\,y(t) - k_5\,x(t)\,y(t),\end{aligned} \tag{8}$$

which has a residual of $G(M_2) = 24.54$ and requires 240 distinct parameters (5 per IAA|AFB pair) to fit the entire data set. The steady-state of output predicted by M_2 are,

$$\begin{aligned}x^* &= \frac{k_1\,u}{k_2}\\ y^* &= \frac{k_2 k_3}{k_2 k_4 + k_1 k_5 u},\end{aligned} \tag{9}$$

which demonstrates a nonlinear relationship between y^* and u, which satisfies one of the qualitative features. There is no closed-form solution for the model because it is nonlinear, however, numerical solution demonstrates that the model captures the inflection point in the predicted time-course curves (Supplementary Figures 9 and 10, green curve).

1.2.4 M_3

As mentioned before, the internal state x represents an unknown intermediate species (or combination of species) that interacts with auxin input and the YFP-IAA output. It is feasible that more than a single intermediate species is required to encompass the underlying dynamics. To investigate whether this might

be the case, we added a second internal state, z, as an intermediate state between x and y. This third-order nonlinear model, M_3, is

$$\begin{aligned}\frac{dx(t)}{dt} &= k_1\,u(t) - k_2\,x(t),\\ \frac{dz(t)}{dt} &= k_3\,x(t) - k_4\,z(t),\\ \frac{dy(t)}{dt} &= k_5 - k_6\,y(t) - k_7\,z(t)\,y(t),\end{aligned} \tag{10}$$

which has a residual of $G(M_3) = 33.30$ and requires 336 distinct parameters (7 parameters per IAA|AFB pair) to fit the entire data set. As in the case with M_2, M_3 captures the two qualitative features of the system (Supplementary Figures 9 and 10, red curve). It is notable that the computed residual is larger than $G(M_2)$, however, this is most likely the result of standard estimation error (e.g. non-optimal initial condition or insufficient search space). Alternatively, M_3 may represent a point at which the saturation of model benefit gained by increasing model complexity is saturated.

1.2.5 Summary

We generated and evaluated four candidate models, M_0, M_1, M_2, and M_3, with respect to how well each model captures the experimental observation, both quantitatively and qualitatively. M_0 did not capture the inflection observed in time-course degradation curves; M_1 did capture the inflection, but did not capture the nonlinear dose-response behavior; M_2 captures both the time-course and dose-response data qualitatively; and M_3 matches these behaviors with comparable quantitative metric to M_2. However, given the limitations of the experimental dataset (time-course to auxin step-input and auxin dose response), M_3, nor any more complex models, may not provide verifiable insights to the system. Said differently, more complex models may result in lower quantitative fit metric, however, to balance the estimation uncertainty associated with higher complexity models, we require richer perturbation of the system that reveals the appropriately higher complexity of the internal mechanism. Therefore, M_2 is arguably the simplest explanation for the observed phenomenon.

1.3 Parameter Reduction

Aside from M_0, the model candidates considered in the previous section include one or more internal states, x (and z), that are not readily associated with biological complexes. One way to approach this is to consider the internal state simply as a mathematical necessity for fitting the experimental observation. Another approach is to consider hypotheses as to what biological complex – that we know to exist in the auxin-mediated IAA degradation pathway – can be associated with x, and examine whether these hypotheses lend a useful quality to our model. One of the hypothetical interpretations of x is that it is a complex formed between auxin and AFB. A simple description of the mechanism in which IAA degrades in the presence of auxin and AFB is shown in Figure 1A, where auxin serves as a molecular glue, binding with an AFB and allowing the protein to bind with IAA, further triggering the ubiquitylation of IAA. Therefore, we postulate that x is a proxy of such a species.

Building on the hypothesis of model interpretation that x is a proxy of the auxin-bound AFB complex, we associate each of the model parameters to the identity of the two different proteins, IAA and AFB. Firstly, parameters k_1 and k_2 are rates associated with synthesis and degradation of auxin-bound receptor protein, where the synthesis is directly proportional to the input. In which case, we further hypothesized that these two parameters are dependent on the identity of AFB but are independent of the identity of the co-expressed IAA. Secondly, analogous interpretations are given to k_3 and k_4; these are rates of synthesis and basal (input-independent) degradation of IAA-YFP, and they are only dependent on the identity of the IAA and not on the identity of the AFB. Finally, k_5 is unique among the model parameters such that it is dependent on the identities of both proteins. Mathematically, k_5 is the rate constant for how

fast the output degrades, and such a degradation process is proportional to the amount of x and y in the system. One can then assign a biochemically feasible interpretation to the term, "when active AFB and IAA interact, the IAA degrades at a rate proportional to k_5". As shown in Figure 1C, the unifying feature of all IAA|AFB pairs is that they degrade when auxin is added to the system in varying degrees. Such variation in degradation among the IAA|AFB pairs can serve as a unique identifier for each pair, and we investigated whether a subset of parameters can serve as the quantitative identifier. Note that these association of parameters to reaction rates are based on a possible interpretation of the model, and should not be taken as a direct representation of a "true system". The parameters may be crude amalgamations of multiple biochemical processes but the resulting model is an elegant abstraction rid of unwieldy details.

In the previous section, when we fit candidate models to experimental data, all five of the M_2 parameters,

$$\theta_{ij}^{(2)} = \{k_1^{(i,j)}, k_2^{(i,j)}, k_3^{(i,j)}, k_4^{(i,j)}, k_5^{(i,j)}\}, \tag{11}$$

were allowed to vary, resulting in five different parameter values for each IAA|AFB pair[2]. This method, which allowed us to easily compare candidate models, makes it difficult to compare the parameters of one IAA|AFB pair to another. For example, suppose we want to directly compare the degradation rates of IAA17|TIR1 and IAA17|AFB2, which have mean fitted k_5 values of 0.034 and 0.21, respectively. The large discrepancy in the two values suggests a large difference in the respective degradation dynamics, but because each pair has other parameters that vary as well, the differences in k_5 are not the only explanation for the variation.

Therefore, we asked if some parameters may be common to a subset of the IAA|AFB pairs, and if consolidating these common parameters would reduce estimation uncertainty. This approach is often called global curve fitting. A systematic generation of all possible global fitting hypotheses for parameter reduction (identifying all possible combinations of common parameters across the 48 IAA|AFB pair, and five parameter model) would have been computationally expensive. Fortunately, the model interpretation provides a feasible guide as to which hypotheses are more likely than others, such as dividing the 48 pairs into smaller subsets. With this estimation approach, we can reduce the variability caused by other parameters and fairly compare parameter values. As mentioned before, k_5 is unique to the identity of each IAA|AFB pair, therefore, the parameter is the primary quantity of interest in comparing the differential degradation among the pairs.

First of all, we address an extreme case of parameter reduction, where we only let k_5 vary for all IAA|AFB pairs, and fix the rest of the parameters to be the same across all pairs. We denote this hypothesis H_1, which provides an additional constraint on the optimization problem, defined by

$$\begin{aligned} \min J(\theta^{(s)}, M_s) \quad &= \quad \sum_{i,j} \sum_{t_m \in \mathrm{T}} \left\| y_{ij}(t_m) - \hat{y}_{ij}(t_m, \theta_{ij}^{(s)}, M_s) \right\|_2, \\ \text{subject to} \qquad & k_l^{(i,j)} = k_l^{(i',j')} \qquad \forall i, i' \in \mathcal{I},\ \forall j, j' \in \mathcal{J},\ \text{and } l = 1,2,3,4, \end{aligned} \tag{12}$$

where, $\mathcal{I}$ and $\mathcal{J}$ denote the sets of IAA and AFB indices, respectively, and l denotes the parameter index. The resulting parameter vector, θ_{H_1}, has 52 distinct parameters (4 + 48 per pair) and results in $G(M_2, \theta_{H_1}) = 48.9$. Thus, H_1 reduces the cardinality of the parameter vector to the point where an IAA|AFB pair has only one parameter that differs from another pair. However, because H_1 makes both k_3 and k_4 be the same for all IAA|AFB pairs, it implies that the initial output value at $t = 0$ for all IAA|AFB pairs are equal ($y_{ij}(0) = k_3^{(i,j)}/k_4^{(i,j)}$). This is inconsistent with the experimental data where initial levels of expression vary (Figure S4). Therefore, H_1 is invalidated based on its conflict between the interpretation of the model and the experimental data.

[2] $k_l^{(i,j)}$ denotes the k_l value for $\mathrm{IAA}_i|\mathrm{AFB}_j$, where $l = 1,2,3,4,5$.

Next, we propose an alternative hypothesis to H_1 in which k_1, k_2, k_3 and k_4 are constrained, but across a smaller subset of IAA|AFB pairs. For example, it was shown that the AFBs do not have differential effect on basal dynamics of IAA (Supplementary Figure S4). Therefore, two IAA|AFB pairs with the same IAA have a similar initial output - suggesting equal k_3 and k_4 values for these two pairs. For this hypothesis, H_{11}, we have the following optimization constraints.

$$\text{subject to} \qquad k_l^{(i,j)} = k_l^{(i,j')} \qquad \forall j, j' \in \mathcal{J}, \text{ and } l = 1, 2, 3, 4. \tag{13}$$

The resulting parameter vector, denoted $\theta_{H_{11}}$, has 144 distinct parameters, and results in $G(M_2, \theta_{H_{11}}) = 24.33$. This decreased residual is a validation in which we let the model interpretation and the fundamental details of the system guide our hypotheses generation. To verify this approach, we generated an alternative hypothesis, H_{12}, where IAA|AFB pairs with the same AFB, versus those with the same IAA (H_{11}), have equal k_1, k_2, k_3 and k_4. This hypothesis has the same cost function as Eq 13 but with the following optimization constraint,

$$\text{subject to} \qquad k_l^{(i,j)} = k_l^{(i',j)} \qquad \forall i, i' \in \mathcal{I}, \text{ and } l = 1, 2, 3, 4. \tag{14}$$

Note that H_{12} was not generated based on the model interpretation as H_{11}, but was proposed as a counter example to our approach. The resulting residual is $G(M_2, \theta_{H_{12}}) = 36.62$, where $\theta_{H_{12}}$ has 56 distinct parameters. The increased residual validates our approach. Comparing H_1, H_{11} and H_{12} suggests that 1) larger numbers of distinct parameters tend to decrease the residual, and 2) when constraining the parameters across a smaller subset of IAA|AFB pairs, the model interpretation serves as a helpful guide in generating reasonable hypotheses.

The higher residuals of H_1 hypotheses family also suggest that for any two IAA|AFB pairs, more than one parameter ought to be allowed to vary (increasing degrees-of-freedom in the parameter estimation) to fit both data sets. Therefore, we further investigate whether a specific grouping of experimental data and parameter reduction hypotheses is possible. Each case of varying parameter (in addition to k_5), k_1, k_2, k_3 or k_4, is denoted with H_{21}, H_{22}, H_{23} or H_{24}, respectively (the four hypotheses are elements of the set $H_{2\kappa}$, where $\kappa = 1, 2, 3,$ or 4). Each hypothesis, depending on the parameter allowed to vary, is associated with data grouping that are supported by the model interpretation.

1. For H_{21} and H_{22}, the additional parameter allowed to vary is dependent on the identity of AFB and independent of the identity of the IAA. Therefore, IAA|AFB pairs are grouped by their IAAs (each group containing two pairs, IAA_i|TIR1 and IAA_i|AFB2), resulting in 24 distinct groups. For each group, the parameters are estimated under the constraint,

$$\text{subject to} \qquad k_l^{(i,j)} = k_l^{(i,j')} \qquad \forall j, j' \in \mathcal{J}, \ l \in \{1, 2, 3, 4\} \backslash \{\kappa\}, \text{ and } \kappa = 1, 2. \tag{15}$$

   These hypotheses imply that a group of IAA|AFB pairs that have the same IAA have the same basal synthesis and degradation rates (k_3 and k_4) of the output. Furthermore, they imply that the variations among each group can be captured by varying k_5 and k_1 for H_{21}, or k_5 and k_2 for H_{22}.

2. For H_{23} and H_{24}, the additional parameter allowed to vary is dependent on the identity of IAA and independent of the identity of the AFB. Therefore, IAA|AFB pairs are grouped by their AFBs (each group containing 24 pairs, IAA_i|AFB, where $i = [1, \cdots, 24]$), resulting in two groups. For each group, the parameters are estimated under the constraint,

$$\text{subject to} \qquad k_l^{(i,j)} = k_l^{(i',j)} \qquad \forall i, i' \in \mathcal{I}, \ l \in \{1, 2, 3, 4\} \backslash \{\kappa\}, \text{ and } \kappa = 3, 4. \tag{16}$$

   The hypotheses imply that a group of IAA|AFB pairs that have the same AFB has the same synthesis and degradation rates of the internal state (k_1 and k_2). Furthermore, they imply that the variations among each group can be captured by varying k_5 and k_3 for H_{23}, or k_5 and k_4 for H_{24}.

Supplementary Table 3 shows the residuals and the number of distinct parameters for various hypotheses investigated. Compared to H_1 hypotheses, H_2 hypotheses tend to have lower residuals, owing to the larger degrees-of-freedom given in the estimation constraints. Additionally, H_{24} has the lowest residual even with the lowest number of distinct parameters. This suggests that for any two IAA|AFB pairs, the differential dynamics between the two can be captured through varying the basal rate parameters of IAA and the input-mediated degradation by the AFBs (k_5). These two dynamics, however, are independent of one another as discussed previously (Results, Figure 2). Also, single parameter variation studies suggests that a set of time-courses predicted by varying k_3 or k_4 have identical degradation profiles when normalized to their initial conditions (Supplementary Figure 11, Supplementary Table 7). The simulation study is also supported by experimental data of IAA1 and IAA1.1, where IAA1.1 is a codon-optimized version of IAA1. This results in higher expression level for IAA1.1 relative to IAA1, which under the model interpretation, is equivalent to increasing k_3 and leaving other parameters the same. When the two curves are normalized to their initial conditions (Supplementary Figure 9), the curves overlap closely. This is reflected by the close k_5 values of IAA1 and IAA1.1 (Supplementary Table 4 and 5).

The normalized degradation curves in Supplementary Figure 11 further provide two notable features of the model. First, they suggest that the two parameter k_3 and k_4 are, in fact, dependent parameters that can be consolidated into a single parameter by normalizing the output. The normalized version of M_2 is

$$\frac{dx(t)}{dt} = k_1\, u(t) - k_2\, x(t) \tag{17}$$

$$\frac{dz(t)}{dt} = k_4 - k_4\, z(t) - k_5\, x(t)\, z(t), \tag{18}$$

where $z = \frac{y}{y_0} = \frac{k_4}{k_3}\, y$, the output normalized to its initial value. This procedure further reduces the number of parameters to be estimated and decreases computational cost in estimation. The differences in the estimated values of k_5 are negligible between the two versions of model. A second notable feature of the model is that the range of degradation profiles in experimental data can be fitted just as well by varying k_1 instead of k_5. This feature is not surprising as varying k_1 increase the rate at which x increases, ultimately having the same effect on the output. However, because of the way we interpret the model parameters, k_1 is independent of the identity of IAA. This conflicts with our objective of identifying a degradation rate parameter that are unique to each IAA|AFB pair. Therefore, we choose k_5 as the single parameter that captures the differential degradation range we observe among the IAA|AFB pairs.

1.4 Summary

Through iterative searches in model discrimination and parameter reduction, we identified a single parameter that captures the differential degradation exhibited by the family of IAA|AFB pairs. The reasoning behind finding a single parameter is largely inspired by the engineering principles of modularity and composable parts. For example, an electric circuit is composed of individual modular parts, such as resistors and transistors. The function of the circuit is tunable by swapping out these modular parts, where the electrical functionality of each type of modular part is specified by a number (i.e. a resistor is specified by its resistance). Casting this principle on the auxin signaling pathway, we ask whether the IAA|AFB pair degradation module (in the larger scheme of the auxin signal pathway) is a modular part, and if so, whether the biological functionality of the module can be specified by a number. The functional feature of the IAA|AFB module, degradation, demonstrates a large range of responses. Therefore, we hypothesize that the number that specifies each IAA|AFB pair's unique biological functionality is its degradation rate (k_5).

Now that we have a data-sheet of k_5 for a large group of IAA|AFB pair, the hypothesis regarding the modularity of these pairs must be verified. It will require an auxin synthetic network containing an IAA|AFB pair, where the part can be easily replaced with another pair. Using a similar approach, a succinct mathematical representation of such a network can be devised, and preferably, the k_5 identified

in this work will be a part of such a model. If a coherent function that maps the differential degradation rates (caused by using different IAA|AFB pairs) and the differential outputs of the larger network can be identified, it will allow us to test to what extent and under what context these pairs are modular. And if this is not the case, the question remains whether there is another set of identifiable quantities for the IAA|AFB pairs that is a better specification of their biological functionality and predictors of the composite network output. Furthermore, the relationship between the k_5 and the output of the network will illuminate the core interactions within the network, aiding in increasingly accurate mathematical representations of the synthetic network. These approaches will not only answer questions regarding the engineerability of auxin signaling pathway, but also provide the basis for novel ways of system identification in biology.

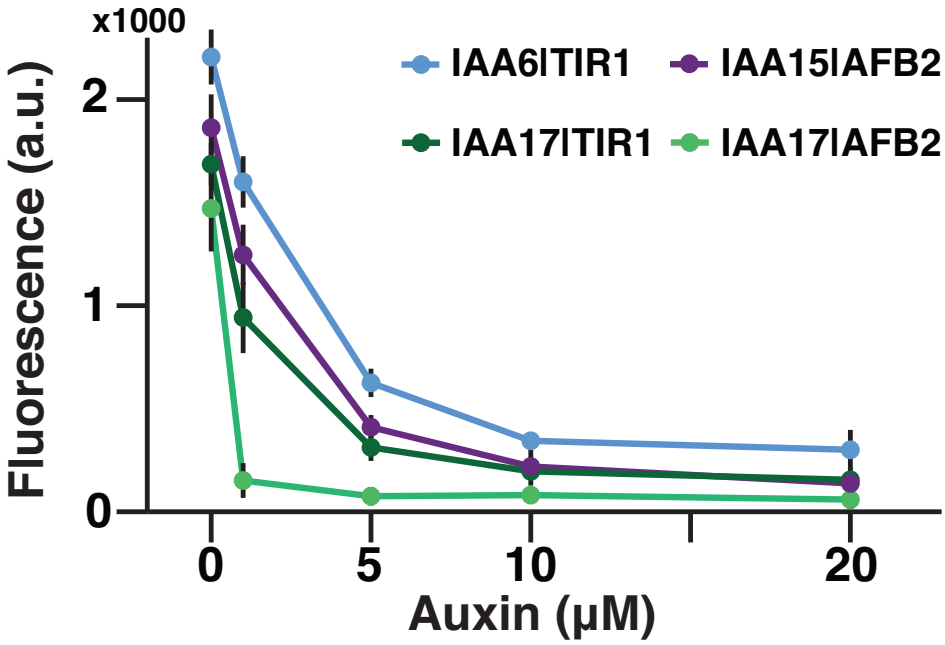

Supplementary Figure 1: Addition of 10μM auxin is sufficient for maximal degradation of IAAs. IAAs with the slowest and fastest degradation rates for TIR1 (IAA6 and IAA17, respectively) and AFB2 (IAA15 and IAA17, respectively) were treated with increasing concentrations of auxin. Fluorescence levels were measured two hours after auxin treatment. Doses of 10μM and 20μM resulted similar levels of degradation. Error bars represent $\pm$ one standard deviation between two experiments performed on different days.

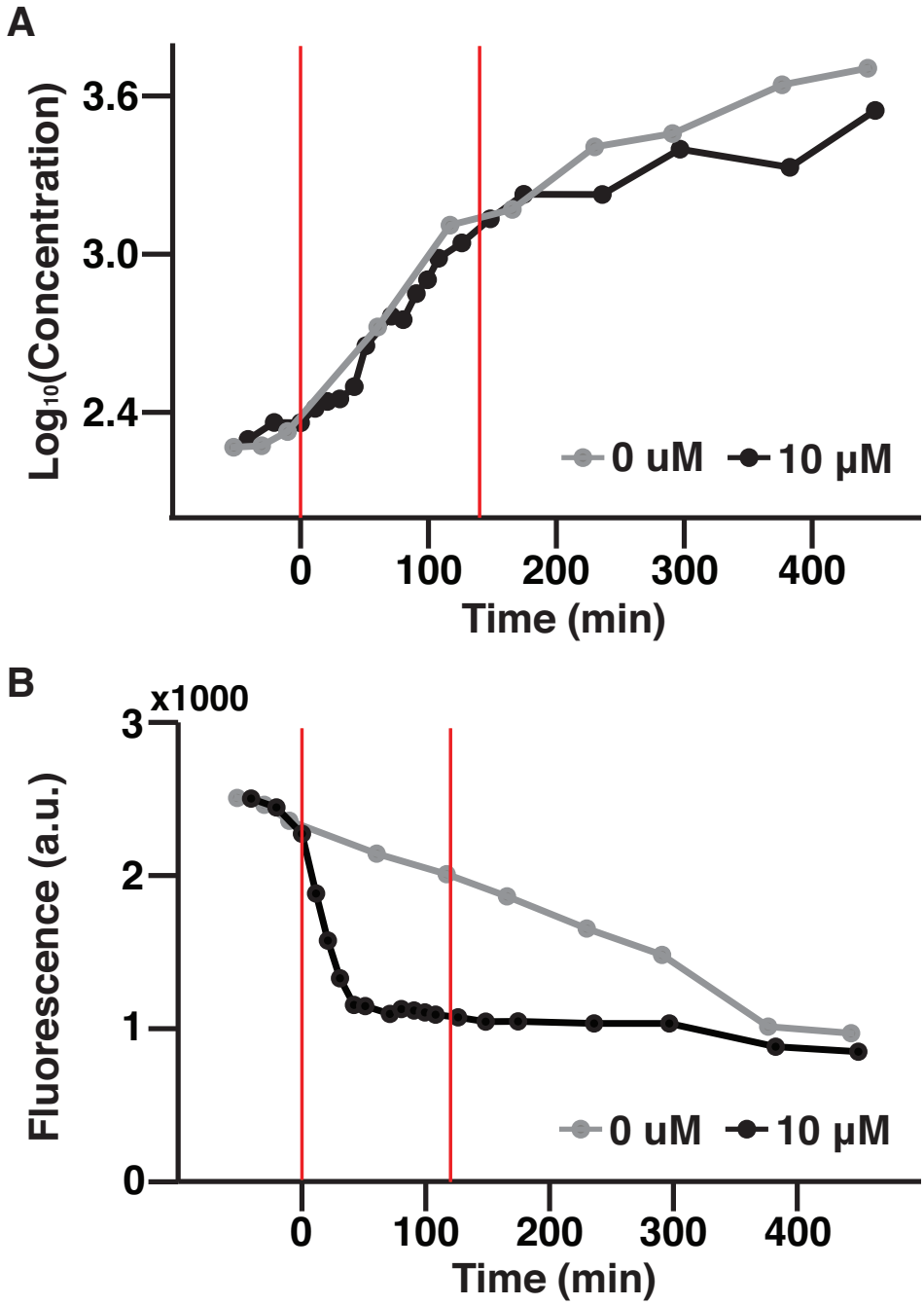

Supplementary Figure 2: Fluorescence levels decrease drastically as yeast cells enter stationary phase. (A) Representative graphs of yeast growth over time of cells containing IAA1|TIR1 treated with mock (grey) or with 10μM auxin (black). (B) Fluorescence in the same cells over time. Red lines demarcate window of experimental data collection.

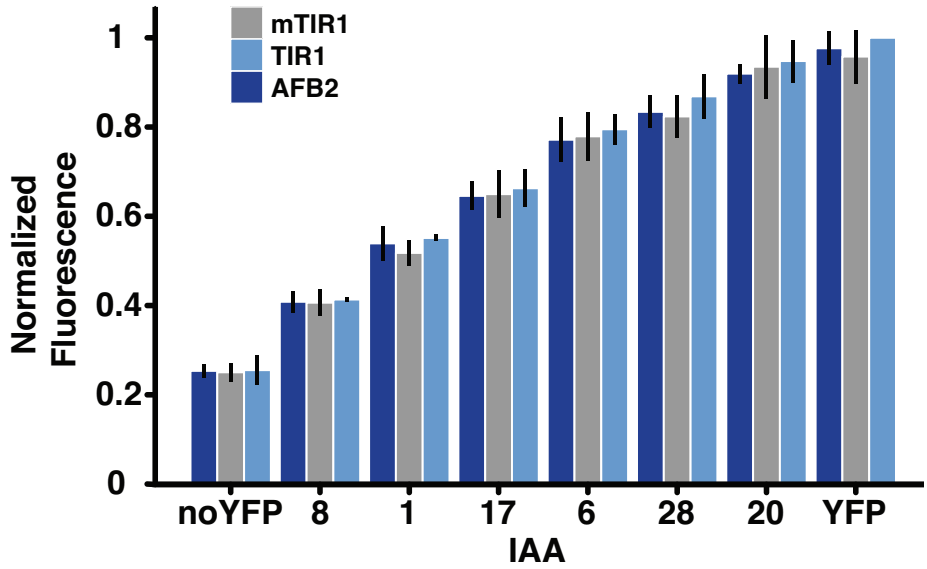

Supplementary Figure 3: AFBs do not have differential effects on basal degradation of IAAs. A sample set of IAAs was co-expressed with mTIR1, TIR1, or AFB2. Fluorescence at steady state, prior to auxin addition, was measured. These IAAs were chosen as they span the range of observed initial steady state intensity values. The noYFP strain expresses an allele of IAA17 without a YFP fusion. Regardless of AFB identity, initial fluorescence levels were indistinguishable for a given IAA. Strains were prepared as in Figure 1C. Each experiment was normalized to the YFP—TIR1 expression level. Error bars are ± one standard deviation between three experiments performed on different days.

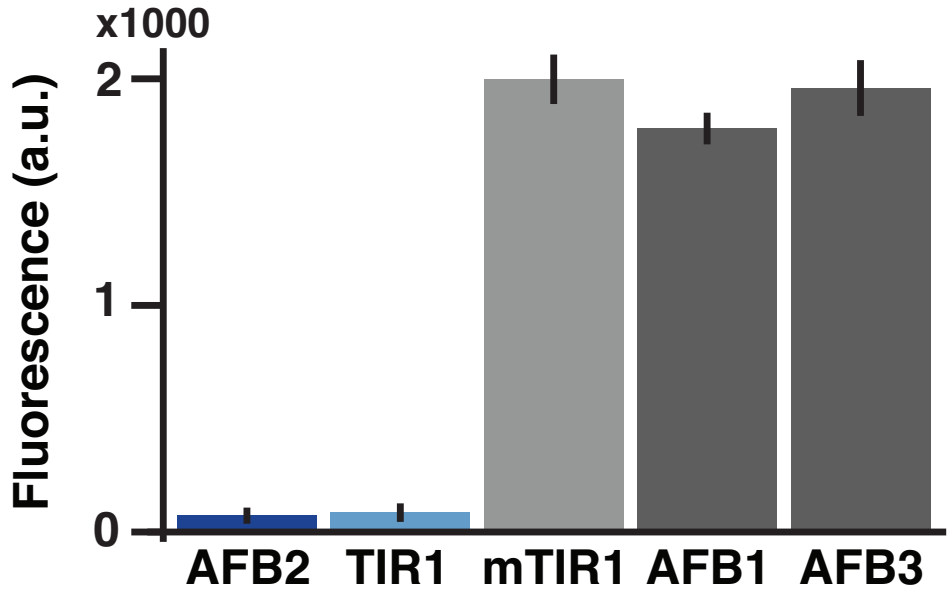

Supplementary Figure 4: AFB1 and AFB3 do not promote degradation of IAA2. IAA2 was co-expressed with each of five receptor types. Fluorescence levels were measured after a 3-hour treatment with 20μM auxin. Similar to mTIR1, AFB1 and AFB3 failed to exhibit degradation of IAA2. Error bars represent $\pm$ one standard deviation between two replicates.

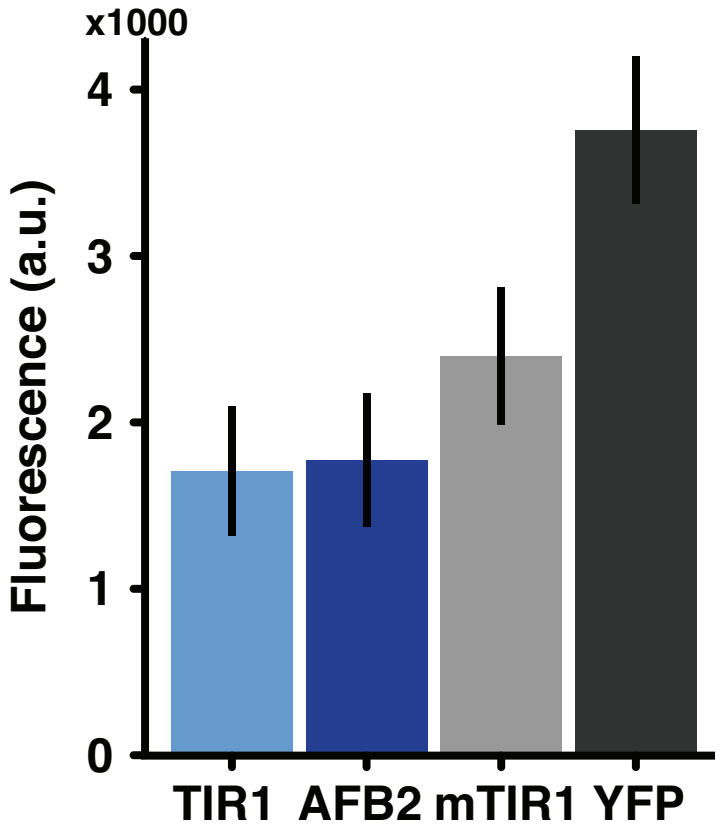

Supplementary Figure 5: TIR1 is expressed at a similar level to AFB2. AFB-YFP constructs were singly integrated into yeast, and their fluorescence intensities were compared using flow-cytometry. Error bars represent one standard deviation, between three replicates.

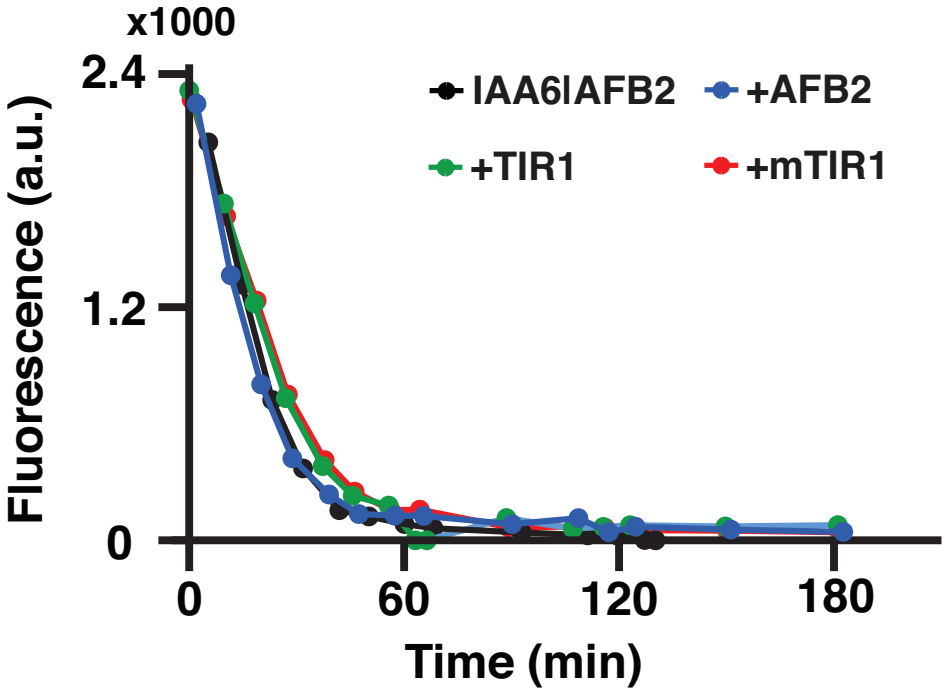

Supplementary Figure 6: AFB2 expression is not rate limiting. Additional copies of AFB (blue), TIR1 (green) or mTIR1 (red) were co-expressed with IAA6|AFB2 in diploid cells. These were compared to the original IAA6|AFB2 strain (black line). The overlapping curves indicate that the degradation rates are similar, implying that with IAA6, the effect of AFB2 is dominant relative to TIR1, and its activity is not increased with additional copies of the gene.

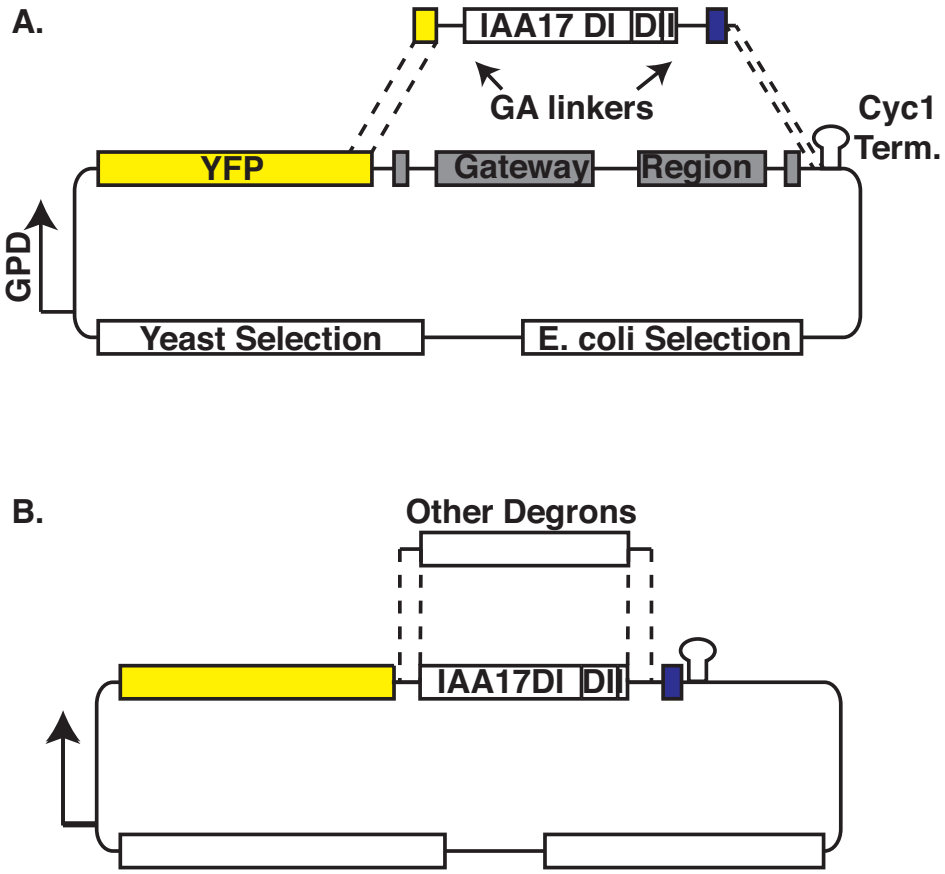

Supplementary Figure 7: Schematic of cloning strategy for domain II truncations. (A) IAA17.T1 was synthesized with Gly-Ala linkers and a 2XSV40-NLS at the C-terminus. This fragment was amplified with primers listed in Table S9 and cloned using Gibson assembly [3]. (B) Gibson assembly was then used to insert other IAA truncations into the same NLS-containing plasmid backbone.

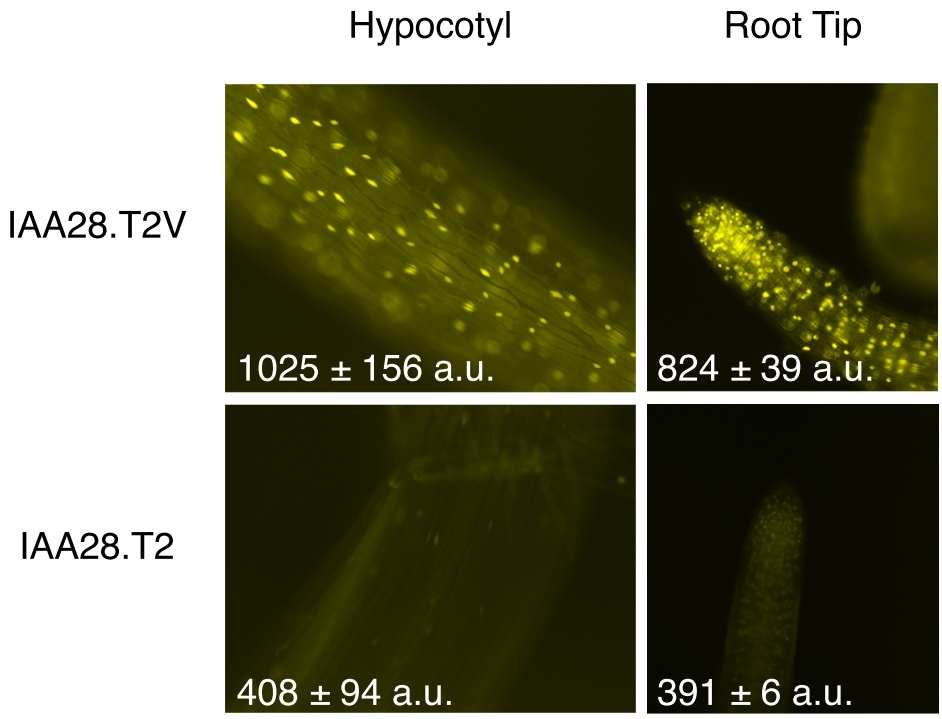

Supplementary Figure 8: Yeast degradation experiments predict relative degradation rates in plants. Consistent with the truncation degradation rates observed in yeast (Fig. 3B), hypocotyls and root tips of plants expressing IAA28.T2-VENUS accumulated lower fluorescence levels than those expressing DII-VENUS (identical to IAA28.T2V) [2]. Mean fluorescence intensity ± SEM values are shown with representative images.

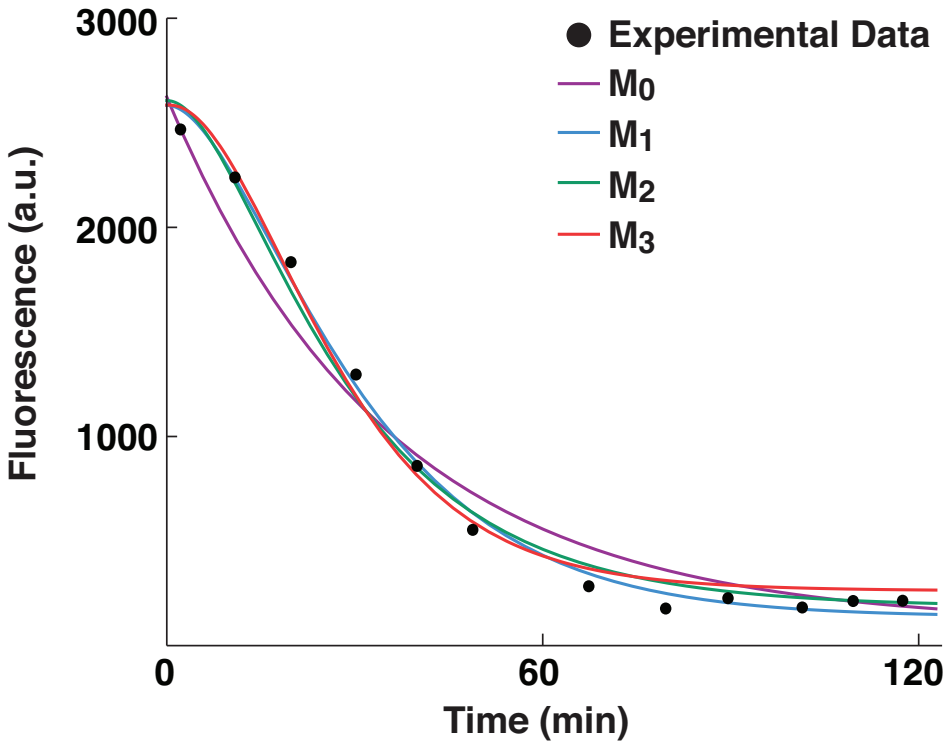

Supplementary Figure 9: Sample time-course IAA degradation data and model fits of IAA14|TIR1. Experimental data are shown in black circles, and the fits are shown in purple, blue, green and red for M_0, M_1, M_2 and M_3 models, respectively.

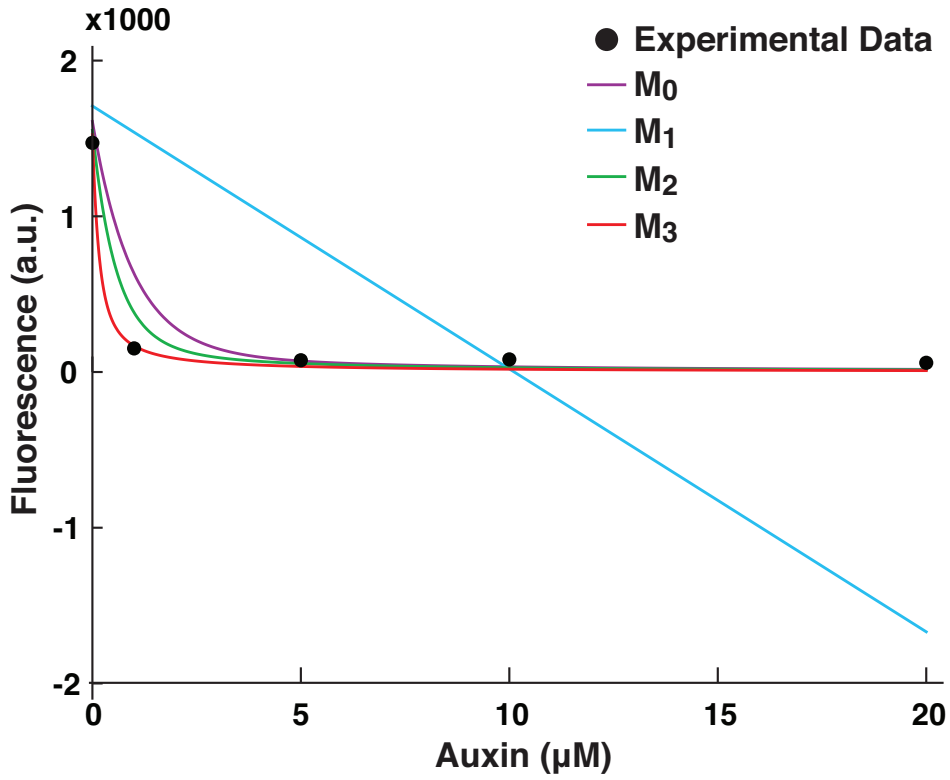

Supplementary Figure 10: Sample dose-response data and model predicted dose-response of IAA17|AFB2. Experimental data are shown in black circles, and the fits are shown in purple, blue, green and red for M_0, M_1, M_2, and M_3 models, respectively.

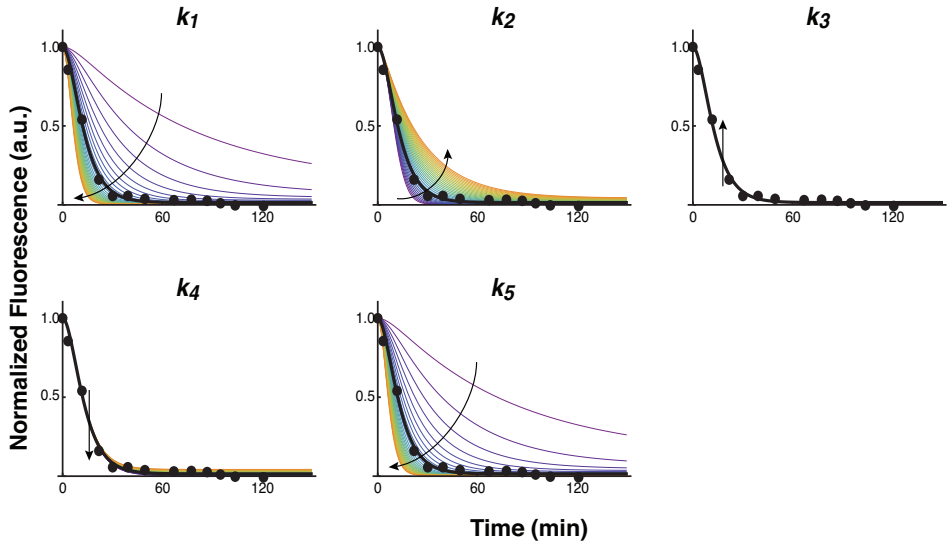

Supplementary Figure 11: Parameter variations study of M_2. Parameters of M_2 are varied from 10% to 300% of the nominal (estimated) values for IAA17|AFB2. The range was chosen based on the demonstrated range of estimated parameters shown in Supplementary Table 7. The trend demonstrated here is general for all IAA |AFB pairs. The resulting degradation curves are normalized to its initial condition. The experimental data are shown in black dots and the black arrows indicate the direction of parameter value increase.

Supplementary Table 1: A table of degradation rates, half-lives, and affinities from yeast, in vitro and plant studies.

AFB	IAA	Havens, 2012[1]		Calderon, 2012[2]	Dreher , 2006[3*]		Ramos, 2001[4*]	Quellet, 2001[5*]	Gray, 2001[6*]
		k5 mean	t 1/2 mean	Kd	basal half-life	auxin half-life	basal half-life	basal half-life	basal half-life
TIR1	1	3.94E-02	24.6	44.33	11.8	-	8	-	-
TIR1	1.1	3.49E-02	26.6	-	-	-	-	-	-
TIR1	2	3.84E-02	25.0	-	-	-	-	-	-
TIR1	3	2.90E-02	30.1	16.97	-	-	-	-	-
TIR1	4	2.59E-02	32.6	-	-	-	-	-	-
TIR1	6	2.01E-02	38.8	-	-	-	-	-	-
TIR1	7	3.52E-02	26.5	17	-	-	-	-	10.8
TIR1	8	4.10E-02	24.3	-	-	-	-	-	-
TIR1	9	3.70E-02	25.6	-	19	-	-	-	-
TIR1	10	2.65E-02	32.1	-	-	-	-	-	-
TIR1	11	1.24E-02	54.7	-	-	-	-	-	-
TIR1	12	3.06E-02	29.2	270	-	-	-	-	-
TIR1	13	3.81E-02	25.1	-	-	-	-	-	-
TIR1	14	3.11E-02	28.8	10.1	-	-	-	-	-
TIR1	15	2.02E-02	38.6	-	-	-	-	-	-
TIR1	17	3.63E-02	26.1	33	10.0	4.8	-	80.0	-
TIR1	18	3.20E-02	28.2	-	-	-	-	-	-
TIR1	19	2.82E-02	30.9	-	-	-	-	-	-
TIR1	20	2.88E-03	>>>	-	>>>	>>>	-	-	-
TIR1	26	2.75E-02	31.3	-	-	-	-	-	-
TIR1	27	3.48E-02	26.7	-	-	-	-	-	-
TIR1	28	2.55E-02	33.1	75	79.3	14.8	-	-	-
TIR1	31	5.55E-03	89.1	>1000	>20 hr	4 hr	-	-	-
TIR1	32	4.60E-03	>>>	-	-	-	-	-	

AFB	IAA	Havens, 2012[1]		Calderon, 2012[2]	Dreher , 2006[3*]		Ramos, 2001[4*]	Quellet, 2001[5*]	Gray, 2001[6*]
		k5 mean	t 1/2 mean	Kd	basal half-life	auxin half-life	basal half-life	basal half-life	basal half-life
AFB2	1	4.52E-02	19.3	-	-	-	-	-	-
AFB2	1.1	4.03E-02	20.9	-	-	-	-	-	-
AFB2	2	4.24E-02	20.3	-	-	-	-	-	-
AFB2	3	5.71E-02	16.8	-	-	-	-	-	-
AFB2	4	5.96E-02	16.3	-	-	-	-	-	-
AFB2	6	6.57E-02	15.4	-	-	-	-	-	-
AFB2	7	8.07E-02	13.6	-	-	-	-	-	-
AFB2	8	9.78E-02	12.2	-	-	-	-	-	-
AFB2	9	6.44E-02	15.7	-	-	-	-	-	-
AFB2	10	5.19E-02	17.7	-	-	-	-	-	-
AFB2	11	2.06E-02	31.8	-	-	-	-	-	-
AFB2	12	5.00E-02	18.1	-	-	-	-	-	-
AFB2	13	5.00E-02	18.3	-	-	-	-	-	-
AFB2	14	6.87E-02	15.0	-	-	-	-	-	-
AFB2	15	2.38E-02	29.0	-	-	-	-	-	-
AFB2	17	1.08E-01	11.5	-	-	-	-	-	-
AFB2	18	5.25E-02	17.7	-	-	-	-	-	-
AFB2	19	6.50E-02	15.6	-	-	-	-	-	-
AFB2	20	2.85E-03	>>>	-	-	-	-	-	-
AFB2	26	4.09E-02	20.7	-	-	-	-	-	-
AFB2	27	6.18E-02	15.9	-	-	-	-	-	-
AFB2	28	4.13E-02	20.5	-	-	-	-	-	-
AFB2	31	1.06E-02	48.9	-	-	-	-	-	-
AFB2	32	3.38E-03	>>>	-	-	-	-	-	-

[1] YFP-IAA|AFB pairs were co-expressed in yeast and YFP levels were monitored after the addition of 10 mM IAA. k5 and t 1/2 were calculated using data-driven model (Fig. 2)

[2] In vitro radio-labeled auxin binding assays were performed using purified ASK1-TIR1 complexes expressed in insect cells and GST-tagged IAAs expressed in *E.coli.*

[3] IAA:LUC transgenic seedlings were treated with cyclohexamide and LUC levels assayed at multiple time intervals. For auxin half-lives , seedlings were pretreated with 2,4-D for two hours prior to the addition of cyclohexamide The data was normalized to the mock treated samples and linearized by taking the natural log. The eqn of the linear best fit line was used to calc half-lives.

[4] IAA:LUC transgenic seedlings were treated with cyclohexamide and LUC levels assayed at multiple time intervals.

[5] Pulse-chase experiments were utlized to calculate the half-life of endogenous IAA17 in WT dark grown seedlings.

[6] Pulse-chase experiments were utlized to calculate the half-life of endogenous IAA7 in WT seedlings using the formula $t1/2 = 0.693t/\ln(N0/Nx)$, where t is time in minutes and N0 and Nx equal the amounts of AXR2 at t = 0 and t = 30min.

* Assays performed in whole seedlings: cannot distinguish receptor(s) responsible for degradation. Values are listed in the TIR1 category as TIR1 is presumed to be the dominant receptor *in planta,* though multiple receptors may play a role.

Supplementary Table 2: Table of amino acids included in each IAA truncation. The position of the conserved 13 amino acid domain II is included for comparison.

Truncation	Domains	Amino Acids		
		IAA1	IAA6	IAA28
Full Length (FL)	DI-DIV	1-168	1-189	1-175
T1	D1 and DII	1-75	1-94	1-81
T2	DII + additional aa	41-75	62-94	43-81
T2V	DII + additional aa	NA	NA	28-61
Conserved Core	DII alone	55-67	70-82	48-60

Supplementary Table 3: The residuals and the number of distinct parameters for M_0, M_1, M_2 (including its hypotheses), and M_3.

Hypothesis	$G(M)$	Number of distinct parameters for 48 IAA|Fbox pairs
H_0	49.31	144
H_1	81.68	240
H_2	24.54	240
H_{21}	32.29	168
H_{22}	46.32	168
H_{23}	48.11	102
H_{24}	27.44	102

Supplementary Table 4: Estimated parameters for IAA|TIR1 pairs using H_{23}.

Fbox	IAA	Replicate	k_1	k_2	k_3	k_4	k_5
TIR1	1	1	1.08E-01	9.22E-02	4.29E+00	3.14E-03	3.44E-02
TIR1	1.1	1	1.08E-01	9.22E-02	8.69E+00	3.14E-03	3.22E-02
TIR1	2	1	1.08E-01	9.22E-02	6.86E+00	3.14E-03	3.54E-02
TIR1	3	1	1.08E-01	9.22E-02	9.03E+00	3.14E-03	2.62E-02
TIR1	4	1	1.08E-01	9.22E-02	9.74E+00	3.14E-03	2.58E-02
TIR1	6	1	1.08E-01	9.22E-02	8.44E+00	3.14E-03	2.02E-02
TIR1	7	1	1.08E-01	9.22E-02	7.62E+00	3.14E-03	3.05E-02
TIR1	8	1	1.08E-01	9.22E-02	3.29E+00	3.14E-03	3.17E-02
TIR1	9	1	1.08E-01	9.22E-02	7.39E+00	3.14E-03	3.34E-02
TIR1	10	1	1.08E-01	9.22E-02	5.02E+00	3.14E-03	2.55E-02
TIR1	11	1	1.08E-01	9.22E-02	4.61E+00	3.14E-03	9.46E-03
TIR1	12	1	1.08E-01	9.22E-02	8.91E+00	3.14E-03	2.67E-02
TIR1	13	1	1.08E-01	9.22E-02	8.24E+00	3.14E-03	3.54E-02
TIR1	14	1	1.08E-01	9.22E-02	5.16E+00	3.14E-03	3.17E-02
TIR1	15	1	1.08E-01	9.22E-02	6.67E+00	3.14E-03	1.91E-02
TIR1	17	1	1.08E-01	9.22E-02	6.74E+00	3.14E-03	3.03E-02
TIR1	18	1	1.08E-01	9.22E-02	7.44E+00	3.14E-03	2.89E-02
TIR1	19	1	1.08E-01	9.22E-02	5.71E+00	3.14E-03	2.41E-02
TIR1	20	1	1.08E-01	9.22E-02	9.99E+00	3.14E-03	2.21E-03
TIR1	26	1	1.08E-01	9.22E-02	8.03E+00	3.14E-03	2.66E-02
TIR1	27	1	1.08E-01	9.22E-02	4.06E+00	3.14E-03	3.18E-02
TIR1	28	1	1.08E-01	9.22E-02	8.20E+00	3.14E-03	2.09E-02
TIR1	31	1	1.08E-01	9.22E-02	6.72E+00	3.14E-03	4.88E-03
TIR1	32	1	1.08E-01	9.22E-02	2.47E+00	3.14E-03	3.81E-03
TIR1	1	2	1.42E-01	1.72E-01	3.89E+00	3.19E-03	4.43E-02
TIR1	1.1	2	1.42E-01	1.72E-01	9.00E+00	3.19E-03	3.77E-02
TIR1	2	2	1.42E-01	1.72E-01	5.77E+00	3.19E-03	4.14E-02
TIR1	3	2	1.42E-01	1.72E-01	8.67E+00	3.19E-03	3.19E-02
TIR1	4	2	1.42E-01	1.72E-01	1.05E+01	3.19E-03	2.59E-02
TIR1	6	2	1.42E-01	1.72E-01	8.79E+00	3.19E-03	2.00E-02
TIR1	7	2	1.42E-01	1.72E-01	7.07E+00	3.19E-03	4.00E-02
TIR1	8	2	1.42E-01	1.72E-01	2.92E+00	3.19E-03	5.02E-02
TIR1	9	2	1.42E-01	1.72E-01	7.56E+00	3.19E-03	4.07E-02
TIR1	10	2	1.42E-01	1.72E-01	4.76E+00	3.19E-03	2.74E-02
TIR1	11	2	1.42E-01	1.72E-01	4.71E+00	3.19E-03	1.54E-02
TIR1	12	2	1.42E-01	1.72E-01	8.83E+00	3.19E-03	3.45E-02
TIR1	13	2	1.42E-01	1.72E-01	8.46E+00	3.19E-03	4.07E-02
TIR1	14	2	1.42E-01	1.72E-01	5.32E+00	3.19E-03	3.05E-02
TIR1	15	2	1.42E-01	1.72E-01	5.71E+00	3.19E-03	2.14E-02
TIR1	17	2	1.42E-01	1.72E-01	6.30E+00	3.19E-03	4.23E-02
TIR1	18	2	1.42E-01	1.72E-01	8.19E+00	3.19E-03	3.51E-02
TIR1	19	2	1.42E-01	1.72E-01	5.39E+00	3.19E-03	3.22E-02
TIR1	20	2	1.42E-01	1.72E-01	9.59E+00	3.19E-03	3.54E-03
TIR1	26	2	1.42E-01	1.72E-01	9.27E+00	3.19E-03	2.85E-02
TIR1	27	2	1.42E-01	1.72E-01	3.92E+00	3.19E-03	3.78E-02
TIR1	28	2	1.42E-01	1.72E-01	7.87E+00	3.19E-03	3.02E-02
TIR1	31	2	1.42E-01	1.72E-01	6.81E+00	3.19E-03	6.23E-03
TIR1	32	2	1.42E-01	1.72E-01	2.55E+00	3.19E-03	5.39E-03

Supplementary Table 5: Estimated parameters for IAA|AFB2 pairs using H_{23}.

Fbox	IAA	Replicate	k_1	k_2	k_3	k_4	k_5
AFB2	1	1	1.49E-01	1.18E-01	4.48E+00	3.63E-03	4.59E-02
AFB2	1.1	1	1.49E-01	1.18E-01	9.77E+00	3.63E-03	4.47E-02
AFB2	2	1	1.49E-01	1.18E-01	8.09E+00	3.63E-03	4.65E-02
AFB2	3	1	1.49E-01	1.18E-01	1.13E+01	3.63E-03	6.14E-02
AFB2	4	1	1.49E-01	1.18E-01	1.16E+01	3.63E-03	6.05E-02
AFB2	6	1	1.49E-01	1.18E-01	8.55E+00	3.63E-03	7.06E-02
AFB2	7	1	1.49E-01	1.18E-01	7.19E+00	3.63E-03	8.35E-02
AFB2	8	1	1.49E-01	1.18E-01	3.16E+00	3.63E-03	1.05E-01
AFB2	9	1	1.49E-01	1.18E-01	8.01E+00	3.63E-03	7.29E-02
AFB2	10	1	1.49E-01	1.18E-01	5.80E+00	3.63E-03	5.16E-02
AFB2	11	1	1.49E-01	1.18E-01	5.87E+00	3.63E-03	2.08E-02
AFB2	12	1	1.49E-01	1.18E-01	9.16E+00	3.63E-03	5.04E-02
AFB2	13	1	1.49E-01	1.18E-01	9.57E+00	3.63E-03	5.52E-02
AFB2	14	1	1.49E-01	1.18E-01	6.25E+00	3.63E-03	6.45E-02
AFB2	15	1	1.49E-01	1.18E-01	7.94E+00	3.63E-03	2.47E-02
AFB2	17	1	1.49E-01	1.18E-01	6.04E+00	3.63E-03	1.04E-01
AFB2	18	1	1.49E-01	1.18E-01	8.57E+00	3.63E-03	5.80E-02
AFB2	19	1	1.49E-01	1.18E-01	5.96E+00	3.63E-03	5.65E-02
AFB2	20	1	1.49E-01	1.18E-01	1.07E+01	3.63E-03	2.67E-03
AFB2	26	1	1.49E-01	1.18E-01	1.06E+01	3.63E-03	4.42E-02
AFB2	27	1	1.49E-01	1.18E-01	4.49E+00	3.63E-03	6.19E-02
AFB2	28	1	1.49E-01	1.18E-01	8.85E+00	3.63E-03	4.14E-02
AFB2	31	1	1.49E-01	1.18E-01	7.50E+00	3.63E-03	1.07E-02
AFB2	32	1	1.49E-01	1.18E-01	2.85E+00	3.63E-03	2.51E-03
AFB2	1	2	1.27E-01	8.77E-02	3.72E+00	3.25E-03	4.46E-02
AFB2	1.1	2	1.27E-01	8.77E-02	9.23E+00	3.25E-03	3.59E-02
AFB2	2	2	1.27E-01	8.77E-02	7.84E+00	3.25E-03	3.82E-02
AFB2	3	2	1.27E-01	8.77E-02	8.45E+00	3.25E-03	5.28E-02
AFB2	4	2	1.27E-01	8.77E-02	1.02E+01	3.25E-03	5.87E-02
AFB2	6	2	1.27E-01	8.77E-02	8.10E+00	3.25E-03	6.08E-02
AFB2	7	2	1.27E-01	8.77E-02	6.33E+00	3.25E-03	7.79E-02
AFB2	8	2	1.27E-01	8.77E-02	2.66E+00	3.25E-03	9.07E-02
AFB2	9	2	1.27E-01	8.77E-02	7.16E+00	3.25E-03	5.58E-02
AFB2	10	2	1.27E-01	8.77E-02	5.49E+00	3.25E-03	5.23E-02
AFB2	11	2	1.27E-01	8.77E-02	5.63E+00	3.25E-03	2.04E-02
AFB2	12	2	1.27E-01	8.77E-02	8.07E+00	3.25E-03	4.96E-02
AFB2	13	2	1.27E-01	8.77E-02	8.90E+00	3.25E-03	4.47E-02
AFB2	14	2	1.27E-01	8.77E-02	5.43E+00	3.25E-03	7.30E-02
AFB2	15	2	1.27E-01	8.77E-02	7.37E+00	3.25E-03	2.29E-02
AFB2	17	2	1.27E-01	8.77E-02	5.05E+00	3.25E-03	1.12E-01
AFB2	18	2	1.27E-01	8.77E-02	8.16E+00	3.25E-03	4.71E-02
AFB2	19	2	1.27E-01	8.77E-02	4.67E+00	3.25E-03	7.35E-02
AFB2	20	2	1.27E-01	8.77E-02	9.29E+00	3.25E-03	3.03E-03
AFB2	26	2	1.27E-01	8.77E-02	9.99E+00	3.25E-03	3.77E-02
AFB2	27	2	1.27E-01	8.77E-02	3.93E+00	3.25E-03	6.17E-02
AFB2	28	2	1.27E-01	8.77E-02	7.56E+00	3.25E-03	4.12E-02
AFB2	31	2	1.27E-01	8.77E-02	6.90E+00	3.25E-03	1.06E-02
AFB2	32	2	1.27E-01	8.77E-02	2.68E+00	3.25E-03	4.25E-03

Supplementary Table 6: Estimated parameters for Degron comparison study using H_{23}.

Fbox	IAA	Degron	Replicate	k_1	k_2	k_3	k_4	k_5
TIR1	1	FL	1	1.08E-01	9.22E-02	6.51E+00	3.14E-03	3.98E-02
TIR1	1	T1	1	1.08E-01	9.22E-02	2.80E+00	3.14E-03	3.41E-02
TIR1	1	T2	1	1.08E-01	9.22E-02	4.92E+00	3.14E-03	1.10E-02
TIR1	6	FL	1	1.08E-01	9.22E-02	6.89E+00	3.14E-03	3.59E-02
TIR1	6	T1	1	1.08E-01	9.22E-02	5.53E+00	3.14E-03	3.22E-02
TIR1	6	T2	1	1.08E-01	9.22E-02	6.06E+00	3.14E-03	1.32E-02
TIR1	28	FL	1	1.08E-01	9.22E-02	5.81E+00	3.14E-03	1.70E-02
TIR1	28	T1	1	1.08E-01	9.22E-02	5.94E+00	3.14E-03	2.96E-02
TIR1	28	T2	1	1.08E-01	9.22E-02	7.22E+00	3.14E-03	3.16E-02
TIR1	28	T2V	1	1.08E-01	9.22E-02	8.39E+00	3.14E-03	6.79E-03
TIR1	1	FL	2	1.42E-01	1.72E-01	6.70E+00	3.19E-03	4.55E-02
TIR1	1	T1	2	1.42E-01	1.72E-01	2.82E+00	3.19E-03	4.44E-02
TIR1	1	T2	2	1.42E-01	1.72E-01	4.76E+00	3.19E-03	1.24E-02
TIR1	6	FL	2	1.42E-01	1.72E-01	7.73E+00	3.19E-03	4.62E-02
TIR1	6	T1	2	1.42E-01	1.72E-01	5.97E+00	3.19E-03	4.45E-02
TIR1	6	T2	2	1.42E-01	1.72E-01	6.57E+00	3.19E-03	1.81E-02
TIR1	28	FL	2	1.42E-01	1.72E-01	5.84E+00	3.19E-03	1.98E-02
TIR1	28	T1	2	1.42E-01	1.72E-01	5.99E+00	3.19E-03	3.50E-02
TIR1	28	T2	2	1.42E-01	1.72E-01	7.28E+00	3.19E-03	3.59E-02
TIR1	28	T2V	2	1.42E-01	1.72E-01	8.14E+00	3.19E-03	7.51E-03
AFB2	1	FL	1	1.49E-01	1.18E-01	7.13E+00	3.63E-03	9.16E-02
AFB2	1	T1	1	1.49E-01	1.18E-01	3.21E+00	3.63E-03	1.05E-01
AFB2	1	T2	1	1.49E-01	1.18E-01	4.91E+00	3.63E-03	2.35E-02
AFB2	6	FL	1	1.49E-01	1.18E-01	7.43E+00	3.63E-03	1.25E-01
AFB2	6	T1	1	1.49E-01	1.18E-01	6.03E+00	3.63E-03	1.82E-01
AFB2	6	T2	1	1.49E-01	1.18E-01	6.32E+00	3.63E-03	6.81E-02
AFB2	28	FL	1	1.49E-01	1.18E-01	6.21E+00	3.63E-03	4.02E-02
AFB2	28	T1	1	1.49E-01	1.18E-01	6.70E+00	3.63E-03	7.67E-02
AFB2	28	T2	1	1.49E-01	1.18E-01	7.84E+00	3.63E-03	7.03E-02
AFB2	28	T2V	1	1.49E-01	1.18E-01	8.97E+00	3.63E-03	1.97E-02
AFB2	1	FL	2	1.27E-01	8.77E-02	7.63E+00	3.25E-03	7.44E-02
AFB2	1	T1	2	1.27E-01	8.77E-02	3.15E+00	3.25E-03	8.17E-02
AFB2	1	T2	2	1.27E-01	8.77E-02	4.88E+00	3.25E-03	1.69E-02
AFB2	6	FL	2	1.27E-01	8.77E-02	7.14E+00	3.25E-03	1.30E-01
AFB2	6	T1	2	1.27E-01	8.77E-02	5.83E+00	3.25E-03	1.87E-01
AFB2	6	T2	2	1.27E-01	8.77E-02	6.10E+00	3.25E-03	7.32E-02
AFB2	28	FL	2	1.27E-01	8.77E-02	5.83E+00	3.25E-03	2.91E-02
AFB2	28	T1	2	1.27E-01	8.77E-02	6.68E+00	3.25E-03	5.88E-02
AFB2	28	T2	2	1.27E-01	8.77E-02	7.65E+00	3.25E-03	5.35E-02
AFB2	28	T2V	2	1.27E-01	8.77E-02	8.64E+00	3.25E-03	1.39E-02

Supplementary Table 7: Average, minimum and maximum values of the estimated parameters in Supplementary Tables 4 and 5.

	average	min (% of average)	max (% of average)
k_1	0.13	0.11 (82)	0.15 (138)
k_2	0.12	8.8E-2 (74)	0.17 (195)
k_3	6.98	2.47 (35)	11.6 (468)
k_4	3.3E-3	3.1E-3 (95)	3.6E-3 (116)
k_5	3.87E-2	2.2-3 (5.7)	0.11 (51)

Supplemental Table 8: Oligonucleotides used in this study

ORF	Forward primer	Reverse primer
IAA1	ATGGAAGTCACCAATGGGCTTAACCTTAAG	TCATAAGGCAGTAGGAGCTTCGGATCC
IAA2	ATGGCGTACGAGAAAGTCAACGAGCTTAAC	TCATAAGGAAGAGTCTAGAGCAGGAGCGTC
IAA3	ATGGATGAGTTTGTTAACCTCA	TTATCATACACCACAGCCTAAAC
IAA4	ATGGAAAAAGTTGATGTTTATGATGAGCTTGTTAACCTAAAG	TTAAAGACCACCACAACCTAAACCTTTAACTTCAGATC
IAA5	ATGGCGAATGAGAGTAATAATCTTGGACTCG	TCATCCTCTGTTACATGATCTCTTCATAATCCTTAACC
IAA6	ATGGCAAAGGAAGGTCTAGCACTCGAG	TTAATCTTGCTGGAGACCAAAACCAGTTG
IAA7	ATGATCGGCCAACTTATGAACCTCAAG	TCAAGATCTGTTCTTGCAGTACTTCTCCATTG
IAA8	ATGAGTTCTGGGAACGATAAGATAAAACAAGTCC	TCAAACCCGCTCTTTGTTCTTCGATTTC
IAA9	ATGTCCCCGGAAGAGGAGCTACAGAG	TTAAGCTCTCATCTTCGATTTCTCCATTGC
IAA10	ATGAATGGTTTGCAAGAAGTTTGTTCGTC	CTACTTACCTACTCCAGCTCCAATTGATGTCTTCATG
IAA11	ATGGAAGGCGGTTCCGCTAGTG	TCATAATATCATCTGAGCTTTACCAGTAGCCTCC
IAA12	ATGCGTGGTGTGTCAGAATTGGAG	CTAAACAGGGTTGTTTCTTTGTCTATCCTTCTGC
IAA13	ATGATTACTGAACTTGAGATGGGGAAAGGTG	CTAAACCGGCTGCTTTCGCTGTC
IAA14	ATGAACCTTAAGGAGACGG	TTATCATGATCTGTTCTTGAACTTC
IAA15	ATGTCACCGGAGGAATACGTTAGGGTTTG	CTATAATCCAATAGCATCTCCGGTTTTCATTAACCTC
IAA17	ATGATGGGCAGTGTCGAGCTGAATC	TCAAGCTCTGCTCTTGCACTTCTCCATC
IAA18	ATGGAGGGTTATTCAAGAAAC	TTATCATCTTCTCATTTTCTCTTGC
IAA19	ATGGAGAAGGAAGGACTC	TTATCACTCGTCTACTCCTCTAGG
IAA20	ATGGGAAGAGGGAGAAGTTCATCGTC	TCAGTAGTGGTAATTAGCTCTTGAAATCTTCAGTCTTCTC
IAA26	ATGGAAGGTTGTCCAAGAAACAGAGAAATC	TCAGTGCATCATCTTCTCTTGCTTACTGC
IAA27	ATGTCTGTATCTGTAGCAGCAGAGCATGATTACATAG	CTAGTTCCTGCTTCTGCACTTCTCCATCAC
IAA28	ATGGAAGAAGAAAAGAGATTGG	TTACTATTCCTTGCCATGTTTTC
IAA31	ATGGAGGTCTCTAACTCTTGTTCTTCATTTTCTTCATC	TTAATACCTCTCCGGTCTCGTGATCTTTAGTCTTC
IAA32	ATGGACCCAAACACACCTGCAGAC	TTAAAAGGGAAGAAGAGCATCGTTTCTTCTTG
TIR1	ATGCAGAAGCGAATAGCCTTGTCG	TTATAATCCGTTAGTAGTAATGATTTGCCTGGAAAACC
AFB2	ATGAATTATTTCCCAGATGAAGTAATAGAGCATGTATTC	TTAGAGAATCCACACAAATGGCGG
mTIR1	ATGGTCTTCATCGGGAACTGCTACGC	TTATAATCCGTTAGTAGTAATGATTTGCCTGGAAAACC
AFB1	ATGGGTCTCCGATTCCCACCTAAG	TTACTTTATGGCTAGATGTGAAACTCCATTCTCAG
AFB3	ATGAATTATTTCCCAGACGAGGTTATAGAGCAC	CTAAAGAATCCTAACATATGGTGGTGCATCTTTTC

*all forward primers had AAAAAGCAGGCTTCAAA appended to the 5' end

**all reverse primers had AGAAAGCTGGGTG appended to the 5' end

Sequencing Primers

All Coding - M13F	GTAAAACGACGGCCAGT
All Coding - M13R	GGAAACAGCTATGACCATG
TIR1, mTIR1 (bp 663-682)	TGTTCCACTTGAAAAATTGG
TIR1, mTIR1 (bp 751-734)	GTCGCACTTCTGCAGTGT
AFB2	CTGATGGTCTTGCCTCTATTG
AFB1 (bp 478-501)	CGAGAGTGTATTGTTGAAGATTTA
AFB3 (bp 404-424)	GTGAAGGGTTTACCACTGATG

Primers used for Gibson Assembly of truncations

Template or construct	Forward	Reverse
YFP-IAA17.T1-NLS	ATCACTCTCGGCATGGACGAG	AGCGTGACATAACTAATTACATGACATCGATT
pGP4GY	GTTATGTCACGCTTACATTCACGCCC	GAGAGTGATCCCGGCGGC
IAA1.FL	TGCCGGGCCCATGGAAGTCACCAATGGGCTTAACC	GGGGGCGCCAGCACCTAAGGCAGTAGGAGCTTCGGATCCT
pGP4GY:IAA1.FL	GGTGCTGGCGCCCCCA	CCATTGGTGACTTCCATGGGCCCGGCACCC
IAA1.T1	TGCCGGGCCCATGGAAGTCACCAATGGGCTTAACC	AGCACCACTCACGTTTTTGTTGTTGTTGTTCTTACG
pGP4GY:IAA1.T1	AACAAAAACGTGAGTGGTGCTGGCGCCCC	CCATTGGTGACTTCCATGGGCCCGGCACCC
IAA1.T2	CCGGGCCCAACGACTCAACAGAAGAATCTGCTCCTC	AGCACCACTCACGTTTTTGTTGTTGTTGTTCTTACG
pGP4GY:IAA1.T2	AACAAAAACGTGAGTGGTGCTGGCGCCCC	TCTTCTGTTGAGTCGTTGGGCCCGGCACCC
IAA6.FL	TGCCGGGCCCATGGCAAAGGAAGGTCTAGCACTCG	GGGGGCGCCAGCACCATCTTGCTGGAGACCAAAACCAGTT
pGP4GY:IAA6.FL	GGTGCTGGCGCCCCCA	AGACCTTCCTTTGCCATGGGCCCGGCACCC
IAA6.T1	TGCCGGGCCCATGGCAAAGGAAGGTCTAGCACTCG	CCAGCACCGCCTATAGCTTTCGATGCTTCCTCATTG
pGP4GY:IAA6.T1	TCGAAAGCTATAGGCGGTGCTGGCGCCCC	AGACCTTCCTTTGCCATGGGCCCGGCACCC
IAA6.T2	TGCCGGGCCCGAATCACTGCCGGTTGTGAAGAGTC	CCAGCACCGCCTATAGCTTTCGATGCTTCCTCATTG
pGP4GY:IAA6T2	TCGAAAGCTATAGGCGGTGCTGGCGCCCC	ACAACCGGCAGTGATTCGGGCCCGGCACCC
IAA28.FL	GGCCCATGGAAGAAGAAAAGAGATTGGAGCTAAGGC	GGGGGCGCCAGCACCTTCCTTGCCATGTTTTCTAGGTGAGA
pGP4GY:IAA28.FL	GGTGCTGGCGCCCCCA	CTCTTTTCTTCTTCCATGGGCCCGGCACCC
IAA28.T1	GGCCCATGGAAGAAGAAAAGAGATTGGAGCTAAGGC	GCACCCAATTCCTTCTCTTCATCACTCTCCTTCTTC
pGP4GY:IAA28.T1	GAAGAGAAGGAATTGGGTGCTGGCGCCCC	CTCTTTTCTTCTTCCATGGGCCCGGCACCC
IAA28.T2	GTGCCGGGCCCAGGGTTGAGGTAGCTCCAGTGGTG	GCACCCAATTCCTTCTCTTCATCACTCTCCTTCTTC
pGP4GY:IAA28.T2	GAAGAGAAGGAATTGGGTGCTGGCGCCCC	GGAGCTACCTCAACCCTGGGCCCGGCACCC
IAA28.T2V	TGCCGGGCCCAAACAAAAAAGCTCGACCAAAGAAACA	GCGCCAGCACCGTTTCTCCGGGATGATCTCACCG
pGP4GY:IAA28.T2V	ATCATCCCGGAGAAACGGTGCTGGCGCCCC	GTCGAGCTTTTTTGTTTGGGCCCGGCACCC

Primers used for Gibson Assembly of the plant expression vector

IAA28.T2:DII-VENUS	TGTACAAAAAAGCAGGCTATGAGGGTTGAGGTAGCTCCAGTGG	GCAGCTGCCGCACAATTCCTTCTCTTCATCACTCTCCTT
DII-VENUS	TGCGGCAGCTGCGACCC	CATAGCCTGCTTTTTTGTACAAACTTGACTAGTGG

*primer names = annealing template sequence name:overlap for homologous assembly

**undelined regions anneal to the template, while the non-underlined are the additional sequence for homologous assembly

Supplementary Table 9: Yeast strains used in this study

Strain Name	Relevant Genotype
W303-1A	*MAT***a** *leu2-3,112 trp1-1 can1-100 ura3-1 ade2-1 his3-11,15*
W303-1B	*MATα leu2-3,112 trp1-1 can1-100 ura3-1 ade2-1 his3-11,15*
TIR1|IAA1	*MAT***a***/MATα LEU2:pGPD-TIR1/leu2-3,112 trp1-1/TRP1:pGPD-YFP-IAA1*
TIR1|IAA2	*MAT***a***/MATα LEU2:pGPD-TIR1/leu2-3,112 trp1-1/TRP1:pGPD-YFP-IAA2*
TIR1|IAA3	*MAT***a***/MATα LEU2:pGPD-TIR1/leu2-3,112 trp1-1/TRP1:pGPD-YFP-IAA3*
TIR1|IAA4	*MAT***a***/MATα LEU2:pGPD-TIR1/leu2-3,112 trp1-1/TRP1:pGPD-YFP-IAA4*
TIR1|IAA5	*MAT***a***/MATα LEU2:pGPD-TIR1/leu2-3,112 trp1-1/TRP1:pGPD-YFP-IAA5*
TIR1|IAA6	*MAT***a***/MATα LEU2:pGPD-TIR1/leu2-3,112 trp1-1/TRP1:pGPD-YFP-IAA6*
TIR1|IAA7	*MAT***a***/MATα LEU2:pGPD-TIR1/leu2-3,112 trp1-1/TRP1:pGPD-YFP-IAA7*
TIR1|IAA8	*MAT***a***/MATα LEU2:pGPD-TIR1/leu2-3,112 trp1-1/TRP1:pGPD-YFP-IAA8*
TIR1|IAA9	*MAT***a***/MATα LEU2:pGPD-TIR1/leu2-3,112 trp1-1/TRP1:pGPD-YFP-IAA9*
TIR1|IAA10	*MAT***a***/MATα LEU2:pGPD-TIR1/leu2-3,112 trp1-1/TRP1:pGPD-YFP-IAA10*
TIR1|IAA11	*MAT***a***/MATα LEU2:pGPD-TIR1/leu2-3,112 trp1-1/TRP1:pGPD-YFP-IAA11*
TIR1|IAA12	*MAT***a***/MATα LEU2:pGPD-TIR1/leu2-3,112 trp1-1/TRP1:pGPD-YFP-IAA12*
TIR1|IAA13	*MAT***a***/MATα LEU2:pGPD-TIR1/leu2-3,112 trp1-1/TRP1:pGPD-YFP-IAA13*
TIR1|IAA14	*MAT***a***/MATα LEU2:pGPD-TIR1/leu2-3,112 trp1-1/TRP1:pGPD-YFP-IAA14*
TIR1|IAA15	*MAT***a***/MATα LEU2:pGPD-TIR1/leu2-3,112 trp1-1/TRP1:pGPD-YFP-IAA15*
TIR1|IAA17	*MAT***a***/MATα LEU2:pGPD-TIR1/leu2-3,112 trp1-1/TRP1:pGPD-YFP-IAA17*
TIR1|IAA18	*MAT***a***/MATα LEU2:pGPD-TIR1/leu2-3,112 trp1-1/TRP1:pGPD-YFP-IAA18*
TIR1|IAA19	*MAT***a***/MATα LEU2:pGPD-TIR1/leu2-3,112 trp1-1/TRP1:pGPD-YFP-IAA19*
TIR1|IAA20	*MAT***a***/MATα LEU2:pGPD-TIR1/leu2-3,112 trp1-1/TRP1:pGPD-YFP-IAA20*
TIR1|IAA26	*MAT***a***/MATα LEU2:pGPD-TIR1/leu2-3,112 trp1-1/TRP1:pGPD-YFP-IAA26*
TIR1|IAA27	*MAT***a***/MATα LEU2:pGPD-TIR1/leu2-3,112 trp1-1/TRP1:pGPD-YFP-IAA27*
TIR1|IAA28	*MAT***a***/MATα LEU2:pGPD-TIR1/leu2-3,112 trp1-1/TRP1:pGPD-YFP-IAA28*
TIR1|IAA29	*MAT***a***/MATα LEU2:pGPD-TIR1/leu2-3,112 trp1-1/TRP1:pGPD-YFP-IAA29*
TIR1|IAA31	*MAT***a***/MATα LEU2:pGPD-TIR1/leu2-3,112 trp1-1/TRP1:pGPD-YFP-IAA31*
TIR1|IAA32	*MAT***a***/MATα LEU2:pGPD-TIR1/leu2-3,112 trp1-1/TRP1:pGPD-YFP-IAA32*
AFB2|IAA1	*MAT***a***/MATα LEU2:pGPD-AFB2/leu2-3,112 trp1-1/TRP1:pGPD-YFP-IAA1*

Strain Name	Relevant Genotype
AFB2|IAA2	*MAT**a**/MATα LEU2:pGPD-AFB2/leu2-3,112 trp1-1/TRP1:pGPD-YFP-IAA2*
AFB2|IAA3	*MAT**a**/MATα LEU2:pGPD-AFB2/leu2-3,112 trp1-1/TRP1:pGPD-YFP-IAA3*
AFB2|IAA4	*MAT**a**/MATα LEU2:pGPD-AFB2/leu2-3,112 trp1-1/TRP1:pGPD-YFP-IAA4*
AFB2|IAA5	*MAT**a**/MATα LEU2:pGPD-AFB2/leu2-3,112 trp1-1/TRP1:pGPD-YFP-IAA5*
AFB2|IAA6	*MAT**a**/MATα LEU2:pGPD-AFB2/leu2-3,112 trp1-1/TRP1:pGPD-YFP-IAA6*
AFB2|IAA7	*MAT**a**/MATα LEU2:pGPD-AFB2/leu2-3,112 trp1-1/TRP1:pGPD-YFP-IAA7*
AFB2|IAA8	*MAT**a**/MATα LEU2:pGPD-AFB2/leu2-3,112 trp1-1/TRP1:pGPD-YFP-IAA8*
AFB2|IAA9	*MAT**a**/MATα LEU2:pGPD-AFB2/leu2-3,112 trp1-1/TRP1:pGPD-YFP-IAA9*
AFB2|IAA10	*MAT**a**/MATα LEU2:pGPD-AFB2/leu2-3,112 trp1-1/TRP1:pGPD-YFP-IAA10*
AFB2|IAA11	*MAT**a**/MATα LEU2:pGPD-AFB2/leu2-3,112 trp1-1/TRP1:pGPD-YFP-IAA11*
AFB2|IAA12	*MAT**a**/MATα LEU2:pGPD-AFB2/leu2-3,112 trp1-1/TRP1:pGPD-YFP-IAA12*
AFB2|IAA13	*MAT**a**/MATα LEU2:pGPD-AFB2/leu2-3,112 trp1-1/TRP1:pGPD-YFP-IAA13*
AFB2|IAA14	*MAT**a**/MATα LEU2:pGPD-AFB2/leu2-3,112 trp1-1/TRP1:pGPD-YFP-IAA14*
AFB2|IAA15	*MAT**a**/MATα LEU2:pGPD-AFB2/leu2-3,112 trp1-1/TRP1:pGPD-YFP-IAA15*
AFB2|IAA17	*MAT**a**/MATα LEU2:pGPD-AFB2/leu2-3,112 trp1-1/TRP1:pGPD-YFP-IAA17*
AFB2|IAA18	*MAT**a**/MATα LEU2:pGPD-AFB2/leu2-3,112 trp1-1/TRP1:pGPD-YFP-IAA18*
AFB2|IAA19	*MAT**a**/MATα LEU2:pGPD-AFB2/leu2-3,112 trp1-1/TRP1:pGPD-YFP-IAA19*
AFB2|IAA20	*MAT**a**/MATα LEU2:pGPD-AFB2/leu2-3,112 trp1-1/TRP1:pGPD-YFP-IAA20*
AFB2|IAA26	*MAT**a**/MATα LEU2:pGPD-AFB2/leu2-3,112 trp1-1/TRP1:pGPD-YFP-IAA26*
AFB2|IAA27	*MAT**a**/MATα LEU2:pGPD-AFB2/leu2-3,112 trp1-1/TRP1:pGPD-YFP-IAA27*
AFB2|IAA28	*MAT**a**/MATα LEU2:pGPD-AFB2/leu2-3,112 trp1-1/TRP1:pGPD-YFP-IAA28*
AFB2|IAA29	*MAT**a**/MATα LEU2:pGPD-AFB2/leu2-3,112 trp1-1/TRP1:pGPD-YFP-IAA29*
AFB2|IAA31	*MAT**a**/MATα LEU2:pGPD-AFB2/leu2-3,112 trp1-1/TRP1:pGPD-YFP-IAA31*
AFB2|IAA32	*MAT**a**/MATα LEU2:pGPD-AFB2/leu2-3,112 trp1-1/TRP1:pGPD-YFP-IAA32*
TIR1|IAA1.FL-NLS	*MAT**a**/MATα LEU2:pGPD-TIR1/leu2-3,112 trp1-1/TRP1:pGPD-YFP-IAA1-NLS*
TIR1|IAA1.T1-NLS	*MAT**a**/MATα LEU2:pGPD-TIR1/leu2-3,112 trp1-1/TRP1:pGPD-YFP-IAA1.T1-NLS*
TIR1|IAA1.T2-NLS	*MAT**a**/MATα LEU2:pGPD-TIR1/leu2-3,112 trp1-1/TRP1:pGPD-YFP-IAA1.T2-NLS*
TIR1|IAA6.FL-NLS	*MAT**a**/MATα LEU2:pGPD-TIR1/leu2-3,112 trp1-1/TRP1:pGPD-YFP-IAA6-NLS*
TIR1|IAA6.T1-NLS	*MAT**a**/MATα LEU2:pGPD-TIR1/leu2-3,112 trp1-1/TRP1:pGPD-YFP-IAA6.T1-NLS*
TIR1|IAA6.T2-NLS	*MAT**a**/MATα LEU2:pGPD-TIR1/leu2-3,112 trp1-1/TRP1:pGPD-YFP-IAA6.T2-NLS*

Strain Name	**Relevant Genotype**
TIR1|IAA28.FL-NLS	*MAT***a***/MATα LEU2:pGPD-TIR1/leu2-3,112 trp1-1/TRP1:pGPD-YFP-IAA28-NLS*
TIR1|IAA28.T1-NLS	*MAT***a***/MATα LEU2:pGPD-TIR1/leu2-3,112 trp1-1/TRP1:pGPD-YFP-IAA28.T1-NLS*
TIR1|IAA28.T2-NLS	*MAT***a***/MATα LEU2:pGPD-TIR1/leu2-3,112 trp1-1/TRP1:pGPD-YFP-IAA28.T2-NLS*
TIR1|IAA28.T2V-NLS	*MAT***a***/MATα LEU2:pGPD-TIR1/leu2-3,112 trp1-1/TRP1:pGPD-YFP-IAA28.T2V-NLS*
AFB2|IAA1.FL-NLS	*MAT***a***/MATα LEU2:pGPD-AFB2/leu2-3,112 trp1-1/TRP1:pGPD-YFP-IAA1-NLS*
AFB2|IAA1.T1-NLS	*MAT***a***/MATα LEU2:pGPD-AFB2/leu2-3,112 trp1-1/TRP1:pGPD-YFP-IAA1.T1-NLS*
AFB2|IAA1.T2-NLS	*MAT***a***/MATα LEU2:pGPD-AFB2/leu2-3,112 trp1-1/TRP1:pGPD-YFP-IAA1.T2-NLS*
AFB2|IAA6.FL-NLS	*MAT***a***/MATα LEU2:pGPD-AFB2/leu2-3,112 trp1-1/TRP1:pGPD-YFP-IAA6-NLS*
AFB2|IAA6.T1-NLS	*MAT***a***/MATα LEU2:pGPD-AFB2/leu2-3,112 trp1-1/TRP1:pGPD-YFP-IAA6.T1-NLS*
AFB2|IAA6.T2-NLS	*MAT***a***/MATα LEU2:pGPD-AFB2/leu2-3,112 trp1-1/TRP1:pGPD-YFP-IAA6.T2-NLS*
AFB2|IAA28.FL-NLS	*MAT***a***/MATα LEU2:pGPD-AFB2/leu2-3,112 trp1-1/TRP1:pGPD-YFP-IAA28-NLS*
AFB2|IAA28.T1-NLS	*MAT***a***/MATα LEU2:pGPD-AFB2/leu2-3,112 trp1-1/TRP1:pGPD-YFP-IAA28.T1-NLS*
AFB2|IAA28.T2-NLS	*MAT***a***/MATα LEU2:pGPD-AFB2/leu2-3,112 trp1-1/TRP1:pGPD-YFP-IAA28.T2-NLS*
AFB2|IAA28.T2V-NLS	*MAT***a***/MATα LEU2:pGPD-AFB2/leu2-3,112 trp1-1/TRP1:pGPD-YFP-IAA28.T2V-NLS*

References

[1] Caldern-Villalobos LIA, Lee S, Oliveira CD, Ivetac A, Brandt W, Armitage L, Sheard LB, Tan X, Parry G, Mao H, Zheng N, Napier R, Kepinski S & Estelle M (2012) A combinatorial TIR1/AFB-Aux/IAA co-receptor system for differential sensing of auxin. Nat Chem Biol 8: 477-485

[2] Brunoud G, Wells DM, Oliva M, Larrieu A, Mirabet V, Burrow AH, Beeckman T, Kepinski S, Traas J, Bennett MJ & Vernoux T (2012) A novel sensor to map auxin response and distribution at high spatio-temporal resolution. Nature 482: 103-6

[3] Gibson DG, Young L, Chuang R-Y, Venter JC, Hutchison CA & Smith HO (2009) Enzymatic assembly of DNA molecules up to several hundred kilobases. Nat Methods 6: 343-345

[4] Dreher KA, Brown J, Saw RE & Callis J (2006) The Arabidopsis Aux / IAA Protein Family Has Diversified in Degradation and Auxin Responsiveness. Plant Cell 18: 699-714

[5] Ramos J, Zenser N, Leyser O & Callis J (2001) Rapid degradation of auxin/indoleacetic acid proteins requires conserved amino acids of domain II and is proteasome dependent. Plant Cell 13: 2349-2360

[6] Ouellet F, Overvoorde PJ & Theologis A (2001) IAA17/AXR3: biochemical insight into an auxin mutant phenotype. Plant Cell. 13: 829-41.

[7] Gray WM, Kepinski S, Rouse D, Leyser O & Estelle M (2001) Auxin regulates SCF(TIR1)-dependent degradation of AUX/IAA proteins. Nature 414: 271-6.

Chapter 3

A heat shock-inducible system to measure Aux/IAA degradation rates *in planta*

INTRODUCTION

The phytohormone auxin regulates myriad processes in plant development. Many of these require the nuclear auxin signaling pathway, in which degradation of the Aux/IAA repressor proteins allows for transcription of auxin-responsive genes (Pierre-Jerome et al., 2013). Aux/IAA degradation is a crucial event, evidenced by the range of aberrant phenotypes resulting from stabilization of these proteins (Reed, 2001).

An emerging theme in biology is the importance of signaling dynamics. Information can be encoded in signal transduction through changing the temporal properties of signaling components (Purvis and Lahav, 2013). Using a heterologous yeast system, our group recently found that Aux/IAAs exhibit a range of auxin-induced degradation rates when co-expressed in isolation with F-box proteins. This phenomenon may contribute to the variety of distinct auxin responses that are seen *in planta*. However, confirmation that Aux/IAAs show similar differences in plants as we have observed in yeast is critical for future studies connecting signaling dynamics to plant growth and development. To this end, I designed a heat-shock-inducible fluorescence degradation system to capture real-time degradation of the Aux/IAAs in plants. My assay was based on a previously developed colorimetric assay (Gray et al., 2001). Using this assay, Aux/IAAs could be shown to exhibit a range of auxin-induced degradation rates in plants. In addition, the rank order of degradation rates in plants is maintained from our yeast system in some cases, but not all.

RESULTS

A heat-shock-inducible fluorescent reporter system was employed to obtain similar levels of expression across the Aux/IAA repressors and to enable monitoring of reporter degradation in real time. Previous attempts to express tagged Aux/IAA proteins under a constitutive 35S promoter resulted in weak or no visible expression (Gray et al., 2001).

This is likely due to constant turnover of the Aux/IAAs, feedback in the auxin signaling pathway, and/or transcriptional silencing. Previously, the Leyser lab employed a heat-shock promoter to induce high expression of the Aux/IAA proteins in Arabidopsis (Gray et al., 2001). In their system, Aux/IAAs were tagged with the GUS enzyme. The degradation assay required sacrifice of populations of seedlings to stain for GUS activity after adding auxin. To monitor degradation of tagged proteins *in vivo*, I developed a similar system using a VENUS fluorescent protein instead of GUS (Fig 1A). Week-old vertically grown plants were subjected to a 2-hour 37C heat shock to induce high, even expression of the tagged proteins, as evidenced by VENUS fluorescence. Following heat shock plants were sprayed with either a 5μM IAA or mock solution to induce Aux/IAA degradation (Fig 1B). Immediately following auxin treatment, plants were imaged to obtain a 0-minute time point, and then subsequently imaged at 10-minutes intervals for an hour (Fig 1C-D). Images were taken in plant root tips, as they highly similar in size across individuals and lack interfering pigments (Fig 1D). Auxin-induced degradation required the Aux/IAA protein, as a VENUS control was stable in all conditions (Fig 1C-D). Addition of exogenous auxin increased the rate of degradation compared to a mock treatment (Fig 1C).

With a real-time degradation system in plants, I sought to test whether Aux/IAAs that exhibit a range of auxin-induced degradation rates in yeast maintain this range in plants. I first tested a series of IAA14 degradation rate variants, whose differential dynamics in yeast are due to changes made only in domain II, or the degron (Chapter 4, Fig 1B). When assayed in plants, the rank order of auxin-induced degradation rates was maintained from yeast (Chapter 4, Fig 1C-E). This suggested that our yeast degradation system was a good predictor of altered degradation rates due to changes in the degron.

To address whether different members of the Aux/IAA family exhibited a range of degradation rates in plants, I tested full-length versions of IAA1, IAA14, and IAA28. In our yeast system these three Aux/IAAs degrade at different rates (Havens et al., 2012). When co-expressed in yeast with TIR1, IAA1 is the most quickly degraded, while IAA14 and IAA28 are slower and similar to one another. In contrast, when co-expressed with

AFB2, IAA14 is the fastest degrading Aux/IAA, while the other two are slower, with IAA1 degrading slight faster than IAA28 (Havens et al., 2012). In plants, degradation of these three Aux/IAAs in response to endogenous auxin levels (mock treatment) recapitulated the rank order seen in yeast with the TIR1 receptor: IAA1 degraded fastest, and IAA28 and IAA14 were slower and similar to one another (Fig 2). In response to exogenous auxin treatment, however, IAA28 degrades faster than IAA14, with IAA1 still degrading fastest (Fig 2). In Arabidopsis, both F-box proteins are present. However, the similarity of degradation rate rank order between mock-treated plants and yeast expressing TIR1 may support a stronger role for TIR1 in this tissue. These assay confirm that these Aux/IAAs exhibit a range of degradation rates in a plant context, and in addition highlight a difference in auxin sensitivities between the proteins tested.

Once we determined that the Aux/IAAs exhibited a range of degradation rates, we asked what molecular features determine these specific degradation rates. To address this question, we made a series of degron-containing truncations of IAA1 and IAA28, one of the fastest and slowest degrading Aux/IAAs in yeast, respectively. Large truncations revealed that regions both N- and C- terminal to the degron contributed to the specific degradation rates, but that the required regions are not the same for each protein (Havens 2012). Recently, more precise truncations identified a minimal region for each IAA that degrades at the same rate as the wild-type protein in yeast (Moss et al., in prep). In IAA1, this region starts at the conserved KR domain (Dreher et al., 2006) and terminates before domain III (NdC, Fig 3A), and for IAA28 includes 5 amino acids prior to and 9 amino acids after the degron (dC*, Fig 4A). Further truncations of these minimal regions have shown that loss of specific region, or rate motifs, either N- or C-terminal to the IAA1 degron results in decreased degradation rate, while only C-terminal truncations decrease the degradation rate of IAA28 (Moss et al., in prep.). To address whether the same rate motifs acts as determinants of degradation rate in plants, we tested these truncations using our heat-shock-inducible system. Comparing truncations of IAA28, we found that the same rate motifs act as determinants of degradation rates in plants and yeast. First, the protein encompassing the minimal region, dC*, degrades at a similar rate at the full length protein (Fig 3B). Second, adding C-terminal residues to this region increased

degradation rate (dC, Fig 3B), while removal of C-terminal residues led to a rate decrease (Nd, Fig 3B). In contrast, the IAA1 truncations did not behave similarly in plant cells. While removal of the N-terminal region did slow degradation of the encoded protein in plants (dC, Fig 3C), the protein encoding only the minimal region identified in yeast also degraded slower than the full length protein (NdC, Fig 3C). However, the IAA1 constructs were particularly inconsistent, with individuals within and across different lines exhibiting much variation (Fig 4), such that conclusions are difficult to draw from this data.

DISCUSSION

The development of a heat-shock-inducible fluorescence degradation system allowed for quantification of auxin-induced Aux/IAA degradation in real time. By employing this method, we were able to obtain high Aux/IAA expression and avoid the dampening long-term effects of turnover, feedback and silencing. Degradation was dependent on the presence of a degron and rates increased in response to exogenous auxin.

With this system we observed many of the same degradation properties of Aux/IAA full-length proteins and truncations as we found in yeast. First, the full-length proteins we tested exhibited a range of degradation rates and maintained the same rank order in endogenous auxin conditions. Second, we found that the same rank order of degradation dynamics was recapitulated in plants for rate variants of IAA14. Third, the yeast system was also a reliable predictor of IAA28 truncation degradation rates. The agreements between the two systems suggest that we have captured the necessary components for specific degradation dynamics in these cases.

With the examples in which the plant and yeast degradation systems give differing results, we can hypothesize what causes these differences. For example, truncations of IAA1 behaved more variably and did not recapitulate dynamics observed in the yeast system. Due to these proteins lacking their domains III/IV, it is possible that IAA1 needs these protein-protein interaction domains to function properly in the plant context. With the full-length Aux/IAAs tested, increasing the auxin concentration caused their

degradation dynamics to switch rank order. This could suggest difference in their dynamics ranges. This might occur if one Aux/IAA has a binding partner that becomes saturated, while the other does not. Another possible explanation is that increasing auxin in the plant cells may turn on or release proteins (such as ARFs) that interact differentially with these three Aux/IAAs, leading to changes in degradation properties. More careful analysis of dose-response of each Aux/IAA in the yeast system, in combination with altered levels of F-box proteins, could help distinguish between some of these possibilities.

MATERIALS AND METHODS

Generation and analysis of transgenic plants

HS::VENUS-IAA-NLS vectors were constructed by fusing IAA truncations to an N-terminal VENUS and C-terminal SV40 NLS repeat using Gly-Ala linkers (GAGAGAGAGAGP and GAGA, respectively; Nishimura et al., 2009) via Gibson cloning (Gibson et al. 2009). The resulting fragments were restriction cloned into pGREEN vectors containing the soybean heat shock promoter HS6871 (Gray et al. 2001). Primers are listed in Supplemental Table X.

Columbia ecotype plants were transformed using the floral dip method (Clough and Bent, 1998). Plants were selected on 0.5x LS agar plates containing 50 mg/mL Kanamycin. 2-3 independent T2 lines for each construct were used for heat shock degradation assays.

Heat Shock induction and degradation assays

Seedlings were stratified at 4C for 2 days on plates containing 0.5xLS and 0.8% agar, and then grown in 16L:8D conditions for 7 days. Plates were placed on a slide warmer set at 37C for 2 hours to induce expression. Seedlings were then arranged on agar blocks containing either 5μM IAA or mock treatment, and sprayed with liquid 0.5xLS containing either 5μM IAA or vehicle. A coverslip was placed over the agar blocks and plants were imaged at 0, 10, 20, 30, 40, and 60 minutes post-treatment.

Plants were imaged using a Leica DMI 3000B microscope fitted with a Leica long-working 40x HCX PL FLUORTAR objective and illuminated with a Lumencor SOLA light source. Images were captured using Leica LAS AF version 2.6.0 software and a Leica DFC 345FX camera. Fiji software was used to quantify fluorescence in a region of interest centered on each image. Non-fluorescent siblings were used to calculate background levels. Fluorescence for each plant was analyzed by subtracting the background level of fluorescence and then normalizing to the initial time point.

REFERENCES

Dreher KA, Brown J, Saw RE, Callis J (2006) The Arabidopsis Aux / IAA Protein Family Has Diversified in Degradation and Auxin Responsiveness. Plant Cell **18**: 699–714

Gray WM, Kepinski S, Rouse D, Leyser O, Estelle M (2001) Auxin regulates SCF(TIR1)-dependent degradation of AUX/IAA proteins. Nature **414**: 271–6

Havens K a, Guseman JM, Jang SS, Pierre-Jerome E, Bolten N, Klavins E, Nemhauser JL (2012) A synthetic approach reveals extensive tunability of auxin signaling. Plant Physiol **160**: 135–42

Pierre-Jerome E, Moss BL, Nemhauser JL (2013) Tuning the auxin transcriptional response. J Exp Bot **64**: 2557–63

Purvis JE, Lahav G (2013) Encoding and decoding cellular information through signaling dynamics. Cell **152**: 945–56

Reed JW (2001) Roles and activities of Aux/IAA proteins in Arabidopsis. Trends Plant Sci **6**: 420–5

FIGURE LEGENDS

Figure 1. A heat-shock-induced fluorescence assay allows observation and quantification of Aux/IAA degradation in planta.

A. Schematic of the vector used for heat-shock-inducible fluorescence degradation assays. B. Cartoon describing our experimental method. Plants grown vertically on 0.5x LS plates were heat-shocked for 2 hours at 37C. Following heat-shock, plants were sprayed with a solution containing 5μM IAA or a mock treatment and imaged at 10-minutes intervals to assay degradation. C. Auxin-induced degradation depended on the presence of an Aux/IAA protein. IAA1 degraded rapidly in response to auxin, while Venus alone was completely stable. Addition of exogenous auxin increased IAA1 degradation. Error bars represent S.E.M. D. Images of representative plants containing heat-shock-inducible VENUS or VENUS-IAA1. Treatments are as in 1C.

Figure 2. IAAs exhibit a range of degradation rates in plants.

With endogenous levels of auxin (mock treatment), IAA1 degrades fastest, while IAA14 and IAA28 degrade at similar rates. When treated with 5μM IAA, all three Aux/IAAs degrade faster, but IAA28 degrades faster than IAA14, suggesting greater sensitivity to this level of auxin. Error bars represent S.E.M.

Figure 3. Identified rate motifs predictably alter the degradation rate of IAA28 in plants, but not of IAA1.

A. Schematic of IAA1 and IAA28 truncations tested in yeast and plants. B. IAA28 truncations demonstrate that the same rate motifs influence degradation rate in yeast and plants. The dC* truncation degrades similarly to the full length protein in both treatments. The dC truncation degrades faster, while Nd degrades slower. C. IAA1 truncations do not maintain the same relative degradation rates in plants. In our system, the NdC minimal region identified in yeast degrades slightly slower than the full-length protein under mock conditions. Inconsistencies among plant lines, however, led to large error bars. Error bars represent S.E.M.

Figure 4. Experimental variation between individual transgenic lines containing IAA1 truncations.

After heat shock, individual lines containing IAA1.dC (upper graph) and IAA1.NdC (lower graph) exhibited large variation in auxin-induced degradation rates when compared to one another, making conclusions difficult to draw from the data. Three individual lines with two replicates each are shown for IAA1.dC. Five individual lines with one to three replicates each are shown for IAA1.NdC.

Figure 1

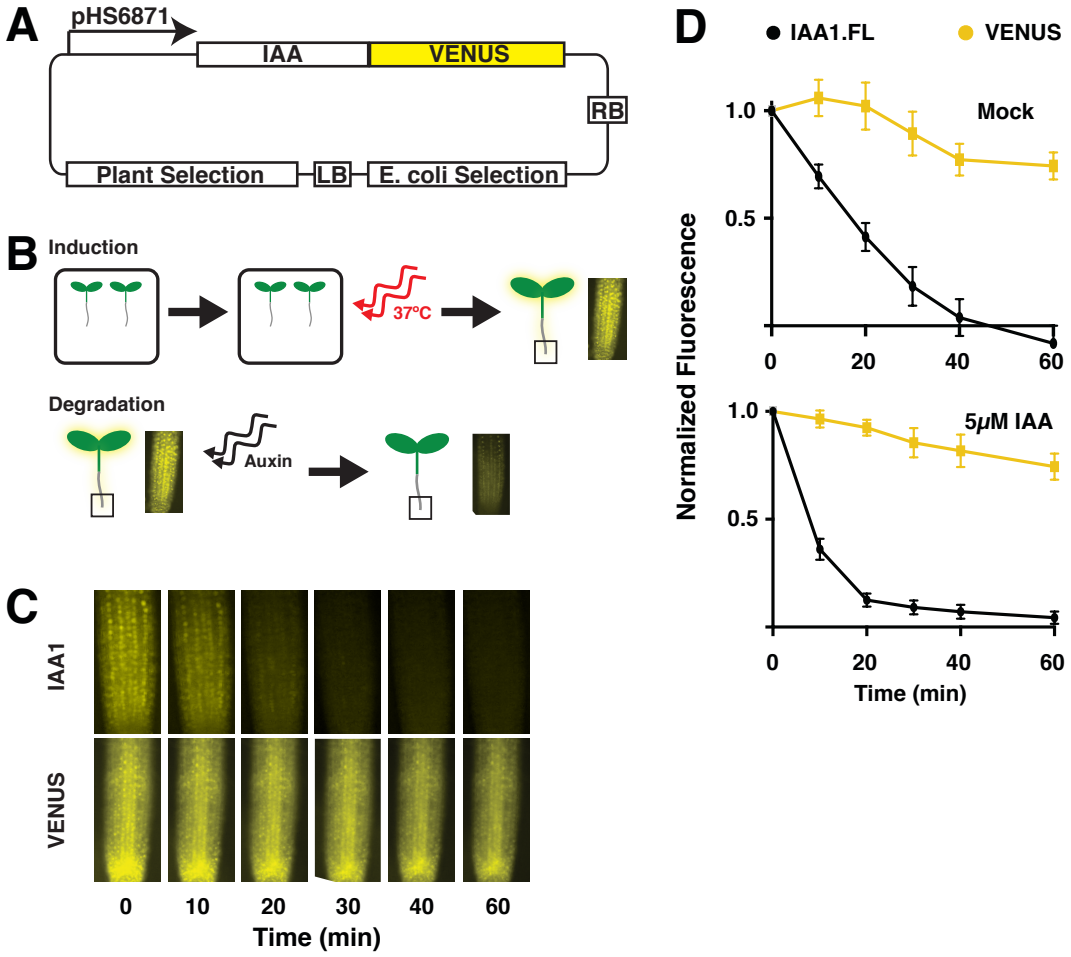
A
pHS6871
IAA
VENUS
RB
Plant Selection
LB
E. coli Selection
B
Induction
37°C
Degradation
Auxin
C
IAA1
VENUS
0
10
20
30
40
60
Time (min)
D
IAA1.FL
VENUS
Mock
5μM IAA
Normalized Fluorescence
1.0
0.5
0
20
40
60
Time (min)

Figure 2

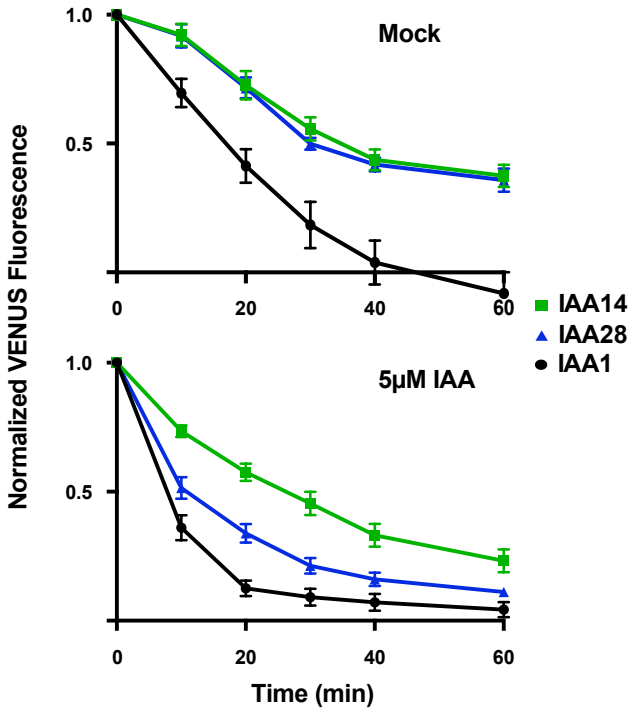
Mock
5μM IAA
Normalized VENUS Fluorescence
Time (min)
1.0
0.5
0
20
40
60
IAA14
IAA28
IAA1

Figure 3

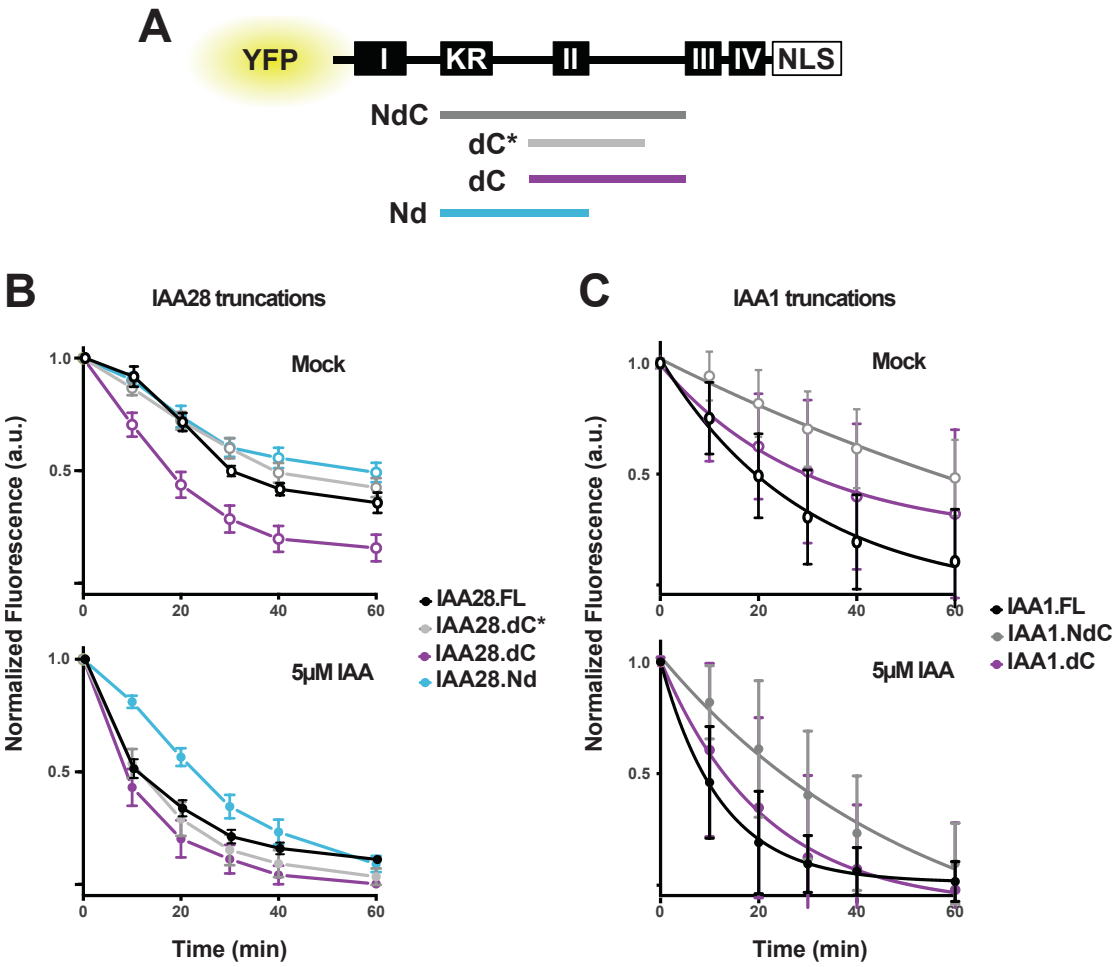
A
YFP
I
KR
II
III
IV
NLS
NdC
dC*
dC
Nd
B
IAA28 truncations
Mock
5μM IAA
Normalized Fluorescence (a.u.)
Time (min)
IAA28.FL
IAA28.dC*
IAA28.dC
IAA28.Nd
C
IAA1 truncations
Mock
5μM IAA
Normalized Fluorescence (a.u.)
Time (min)
IAA1.FL
IAA1.NdC
IAA1.dC

Figure 4

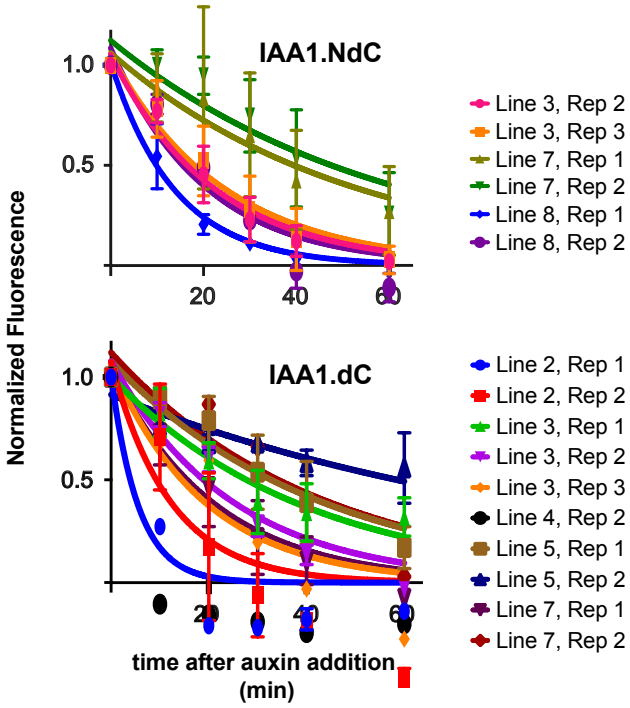
IAA1.NdC
1.0
0.5
20
40
60
Line 3, Rep 2
Line 3, Rep 3
Line 7, Rep 1
Line 7, Rep 2
Line 8, Rep 1
Line 8, Rep 2
IAA1.dC
1.0
0.5
20
40
60
Line 2, Rep 1
Line 2, Rep 2
Line 3, Rep 1
Line 3, Rep 2
Line 3, Rep 3
Line 4, Rep 2
Line 5, Rep 1
Line 5, Rep 2
Line 7, Rep 1
Line 7, Rep 2
Normalized Fluorescence
time after auxin addition
(min)

Chapter 4

Auxin-induced degradation dynamics set the pace for lateral root development

Jessica M. Guseman, Antje Hellmuth, Amy Lanctot, Tamar P. Feldman, Britney L. Moss, Eric Klavins, Luz Irina A. Calderón Villalobos, Jennifer L. Nemhauser. Auxin-induced degradation dynamics set the pace for lateral root development. Submitted.

ABSTRACT

Auxin elicits diverse cell behaviors through a simple nuclear signaling pathway initiated by degradation of Aux/IAA co-repressors. Our previous work revealed that members of the large *Arabidopsis* Aux/IAA family exhibit a range of degradation rates in synthetic contexts. However, it remained an open question whether differences in Aux/IAA turnover rates played a significant role in plant responses to auxin. Here, we use the well-established model of lateral root development to directly test the hypothesis that the rate of auxin-induced Aux/IAA turnover sets the pace for auxin-regulated developmental events. We did this by generating transgenic plants expressing degradation rate variants of IAA14, a critical determinant of lateral root initiation. Progression through the well-established stages of lateral root development was strongly correlated with the engineered rates of IAA14 turnover, leading to the conclusion that Aux/IAAs are auxin-initiated timers that synchronize developmental transitions.

INTRODUCTION

The plant hormone auxin directs many developmental responses, including the elaboration of branching patterns in the root. Among the first steps in auxin signal transduction is the ubiquitylation and degradation of transcriptional co-repressor proteins called Aux/IAAs (Chapman and Estelle, 2009). The Aux/IAA co-repressors belong to a large gene family, with 29 members in Arabidopsis. Auxin induces a high-affinity interaction between a degron sequence in the Aux/IAA (DII) and an F-box protein belonging to the TIR1/AFB family (Dharmasiri et al., 2005; Kepinski and Leyser, 2005; Tan et al., 2007). Stabilizing mutations in degrons of different Aux/IAAs provoke distinct phenotypes, suggesting there is functional specificity within the family (Lokerse and Weijers, 2009). Further support of this model comes from experiments where stabilized versions of one Aux/IAA cannot fully recapitulate the phenotype of stabilized

versions of a different family member, even when expressed from the same promoter (Muto et al., 2007; Weijers et al., 2005).

The dynamics of cellular signaling, in addition to absolute changes in signal abundance, can play a critical role in determining cellular outcomes (Purvis and Lahav, 2013). For example, calcium dynamics have recently been shown to play a critical role in communication among gametophytic cells during fertilization (Ngo et al., 2014). There is significant variation among Aux/IAAs in both auxin-induced affinity for TIR1/AFBs and degradation rates (Calderón Villalobos et al., 2012; Havens et al., 2012). This variation may be translated into quantitative differences in Aux/IAA function in plants.

Lateral root development has a well-defined sequence of developmental stages, many of which are controlled by auxin, and is non-essential for plant survival in laboratory conditions (Fig. 1A; (Malamy and Benfey, 1997)). These attributes make it an ideal testing ground to interrogate the possibility that nuclear auxin signaling dynamics act as a checkpoint to set the timing of auxin-regulated cell behaviors. To test this hypothesis, we used a synthetic yeast system to guide the engineering of plants expressing degradation rate variants of IAA14, an Aux/IAA that is critical for the first asymmetric divisions that mark the initiation of new root primordia. By expressing these variants in plants under the native *IAA14* promoter, we found that the dynamics of lateral root development were plastic and could be tuned by altering the pace of auxin-induced IAA14 turnover.

RESULTS

IAA14 degradation rate and auxin sensitivity can be tuned by single point mutations

Analysis of DII-Luciferase fusions in plants identified a number of specific amino acid substitutions that slowed or abolished protein turnover (Ramos et al., 2001). We generated IAA14 mutants with a subset of these mutations and found that they exhibited a range of auxin-induced degradation dynamics in a synthetic yeast degradation assay (Figure 1B and 1C, Figure S1A and S1B; (Havens et al., 2012)). Based on their degradation rates, we designated the variants as wild-type (14), Fast (F), Medium (M), Slow (S), or Insensitive (I). The I-variant protein harbors the same mutation found in the *solitary root* (*slr-1*) mutant (Fukaki et al., 2002).

As in *slr-1* mutant plants, the I-variant was auxin-insensitive in yeast (Figure 1B and 1C). As expected, auxin binding was reduced by mutations in DII and showed an inverse relationship with protein stability (Figure 1D, (Calderón Villalobos et al., 2012)). Auxin dose response assays provided additional evidence that auxin sensitivity of the IAA14 variants was well correlated with observed degradation rates (Figure S1C).

To test whether the differences in degradation rates among the IAA14 variants observed in yeast were maintained in their native context, we developed a fluorescent Aux/IAA degradation assay in plants (Fig. 1E and 1F). Expression levels of *Aux/IAA*s are generally quite low, so we employed a previously characterized heat-shock-inducible promoter to provide detectable levels of initial fluorescence (Gray et al., 2001). Heat shock treatment at 37^{o}C led to a high and largely equal induction of all VENUS-IAA fusion proteins across plant lines (Figure 1F). Quantification of fluorescence over time led to a relative rate of degradation that was strikingly similar to that observed in yeast (Figure 1E).

Lateral root density is quantitatively decreased by slowing the rate of IAA14 degradation

Next, we analyzed root architecture of transgenic plants expressing 14-, F-, M-, S-, or I-variants of IAA14 from the native IAA14 promoter. Relative stability of the IAA14 variants was inversely proportional to lateral root density (Figure 2A). Expressing additional copies of wild-type IAA14 had no effect on root development, as 14-variant lines were indistinguishable from untransformed controls (Figure S2A), and expression of IAA14 was similar across variant lines (Figure S2B). This is consistent with few descriptions of Aux/IAA overexpression phenotypes, and several reports that overexpression has little to no effect phenotype (Reed, 2001). Plants expressing the F-variant of IAA14 had similar lateral root densities as the IAA14 control, consistent with the similar degradation dynamics of the two constructs. Complete stabilization of IAA14 in the I-variant fully inhibited lateral root development, as has been described in *slr-1* mutants carrying the identical proline to serine substitution in the native IAA14. With intermediate degradation rate constructs, plants developed fewer and fewer lateral roots as degradation rate slowed. Over time, this trend was accentuated. In addition to their lateral root defect, *slr* mutants lack root hairs (Fukaki et al., 2002). Consistent with this phenotype, root hair density was correlated with degradation rates in the plants expressing IAA14 variants (Figure

S2C). Also consistent with the *slr* mutant phenotype, neither hypocotyl elongation nor shoot branching were strongly affected by changes in IAA14 stability (Figure S2C). By 14 days post germination (dpg), the density of roots of the M- and S-variant plants was similar to the densities of 14- and M-variant plants at 7dpg, respectively. These findings suggest that slowing the dynamics of IAA14 degradation translates into a delay in lateral root emergence.

Lateral roots are continually formed near the root tip, producing a standing developmental sequence of lateral root stages (I-VII) along the length of the primary root. To further parse the effect of slowing IAA14 degradation rate, we analyzed the distribution of developmental stages of lateral root primordia in our transgenic lines (Figure 2B). As expected, I-variant lines had no primordia at any stage. The density of primordia in S-variant lines was approximately a quarter of that observed in 14-control plants, and all were in the earliest stages (I-IV). The distribution of primordia at stages II-VI was quite similar in plants expressing 14-, F-, and M-variants. However, M-variant plants had higher numbers of stage I primordia and a reduced number of stage VII primordia, consistent with a developmental delay leading to fewer emerged roots.

IAA14 degradation dynamics determine the dynamics of lateral root development

To directly assess developmental dynamics, we used gravistimulation to synchronize the location and timing of primordia initiation (Lucas et al., 2008; De Smet et al., 2007). Briefly, when plants grown vertically on plates are turned 90 degrees, roots reorient towards the new gravity vector. A lateral root primordium is induced at high frequency on the outer side of the bend. By 18 hours-post-induction (hpi), all of the plants transformed with wild-type IAA14 had initiated a new lateral root at the expected position. Half of the primordia were stage I and the other half had progressed to stage II (Figure 3A). In M-variant plants, initiation was delayed with several roots lacking primordia altogether at 18 hpi. This delay became even more apparent over time (Movie S1A and S1B). In addition, many late stage primordia in M-variant plants exhibited morphological defects. These primordia were elongated, and they appeared to displace both the surrounding vasculature and endodermal layers (Figure 3B). These phenotypes are reminiscent of those seen in mutants blocked in lateral root emergence (Kumpf et al., 2013; Vermeer et al., 2014). These defects suggest that early developmental delays might disrupt coordination between the primordia and the overlaying cell layers. For plants with even slower IAA14 degradation

dynamics, developmental progression was further compromised. No primordia were detected in S-variant plants at 18 hpi, and, by 66 hpi, only a small subset of roots had even stage I primordia. This is consistent with delayed induction of the auxin-responsive DR5-VENUS reporter (Brunoud et al., 2012) in these lines (Figure 3C). While a peak of reporter expression was detected in the outer bend of 14-control roots as early as 10 hpi, induction was delayed until 13 hpi in many M-variant plants. Little to no induction of reporter expression was observed in S-variant plants even as late as 24 hpi. As expected, no primordia were detected in any I-variant roots at any time (Figure 3A).

DISCUSSION

This study draws a direct molecular connection between the dynamics of auxin signaling and the dynamics of organogenesis. By engineering Aux/IAA variants with reduced auxin sensitivity, we discovered that timing of organ initiation was plastic and could be tuned. The synthetic engineering of degradation rates applied here may be analogous to a natural evolutionary process of selecting Aux/IAA properties to optimally tune emergent auxin signaling modules in new contexts. Optimization of auxin sensitivity among co-expressed Aux/IAAs could produce a hierarchical action (Pierre-Jerome et al., 2014), including sequential induction of specific target genes. Sequential degradation of Aux/IAAs could lead to a wave of gene expression, similar to the temporal gradation of gene expression observed for Dpp signaling during *Drosophila* wing development (O'Keefe et al., 2014). Higher order transcriptional complexes between Aux/IAAs and their target transcription factors the AUXIN RESPONSE FACTORS (ARFs) (Korasick et al., 2014; Nanao et al., 2014) are likely to influence Aux/IAA degradation rates, further modulating the dynamics of downstream transcription of target genes.

From an engineering perspective, ready modification of the auxin sensitivity of Aux/IAAs may reduce noise by contributing to a multiple feedback-controlled system. In such a system, linked controllers minimize variation at different time and/or spatial scales. In auxin signaling, auxin transport, synthesis and conjugation would contribute to the total amount of auxin in the nucleus, constituting one controller. Aux/IAAs would act as an additional controller, regulating transcription of target genes, including many of those involved in auxin transport, synthesis and conjugation. Thus, the ability to tune Aux/IAA degradation rates is an essential part of

optimizing the overall auxin response for a particular cellular context, and provides a target for engineering synthetic and natural systems.

MATERIALS AND METHODS

Yeast growth and transformation

Yeast were grown on Yeast Peptone Dextrose (YPD) and Synthetic Complete (SC) medium supplemented with 80 mg/mL adenine and made according to standard protocols. Transformations were performed using a standard lithium acetate protocol (Gietz and Woods, 2002) into MATa W303-1A or MATa W814-29B, a gift from laboratory of D. Gottschling.

Yeast strain construction

Amino acids substitutions were introduced into the coding region of IAA14 in pDONR entry vectors via Gibson cloning (Gibson et al., 2009). IAA14 variant coding regions were then cloned into pGP4GY-ccdB destination vectors (Havens et al., 2012) using an LR clonase reaction. 200 ng of the resulting pGP4GY-IAA14 variant constructs were digested with PmeI for 1 h at 37C and transformed into W303-1A yeast cells. W814-29B cells containing pGP5G-TIR1 or AFB2 constructs were mated with cells containing IAA14 constructs using standard procedures. Strains to be mated were co-inoculated at low density into YPD medium, grown overnight at 30°C, and struck out to single colonies on SC-His-Trp to select for diploids.

Yeast degradation assays

Cell cultures were prepared for degradation assays as described (Havens et al., 2012). Briefly, cells were cultured to log-phase of growth and two measurements were taken at prior to the addition of treatment. For each strain, one replicate was mock treated (95% [v/v] ethanol) and one replicate was treated with 10 mM indole-3-acetic acid. Time 0 readings were taken immediately after auxin addition. Subsequent readings were taken at 10 minutes intervals over 2 h. Control experiments with mock treated cells were measured every hour for the duration of the experiment.

Auxin binding assays

Radioligand binding assays were performed as previously described (Calderón Villalobos et al., 2012). In brief, recombinant TIR1-ASK1 protein complex and N-terminal GST-tagged IAA14 variant proteins were purified to high purity. Duplicate samples containing both proteins, radiolabeled indole-3-acetic acid (IAA) and cold competitor (unlabeled IAA) were incubated for 1 h on ice, subsequently filter-immobilized, and washed with binding buffer. Filters were incubated overnight and retained radiolabeled auxin was measured via scintillation counting. Nonspecific binding was determined using a 10,000-fold excess of cold IAA with respect to [^{3}H]-IAA. Data analysis was performed using GraphPad Prism 5 software. K_d values were obtained applying One-site binding (hyperbola) model. Specific binding was calculated as the difference of average total binding and nonspecific binding. Samples for total and non-specific binding were in duplicates. Experiments were repeated twice either as saturation or competition binding with consistent results.

Plant material

All IAA14 constructs were transformed into Columbia (Col-0) wild-type plants. DR5::VENUS-N7 seeds were provided by T. Vernoux. Seeds were sown on 0.5x LS media, stratified at 4°C for 2 days, and grown in continuous light conditions for 7 or 14 dpg. For lateral root induction assays, plants were stratified for 2 days at 4°C and grown in continuous light for 4 days. On the 4th day, the plates were rotated 90 degrees. Plants were cleared and imaged 18, 42, and 66 h after rotation.

Transgenic plant lines

For IAA14 constructs used in plants, a 2 kb region containing the IAA14 promoter (Fukaki et al., 2002) was cloned into pGREEN vectors via restriction cloning. Coding regions of IAA14 variants were subsequently cloned downstream of the IAA14 promoter. Plants containing the IAA14 variants were crossed with DR5::VENUS-N7 plants. HS::VENUS-IAA-NLS constructs were generated by fusing Aux/IAA truncations to an N-terminal VENUS and C-terminal SV40 NLS repeat using Gly-Ala linkers (GAGAGAGAGAGP and GAGA, respectively; (Nishimura et al., 2009)) via Gibson cloning. The resulting fragments were cloned into pGREEN vectors containing the soybean heat shock promoter HS6871 (Gray et al., 2001). All constructs were transformed into plants using the floral dip method (Clough and Bent, 1998).

Time-lapse fluorescence detection following heat-shock

Agar plates containing plants were placed on a slide warmer set at 37°C for 2 h to induce expression. Seedlings were then arranged on agar blocks containing either 5 μM IAA or mock treatment, and sprayed with liquid 0.5x LS containing either 5 μM IAA or vehicle. A coverslip was placed over the agar blocks and plants were imaged at 0, 10, 20, 30, 40, and 60 m post-treatment.

Histology and Microscopy

Plants containing IAA14 variants constructs were cleared and prepared for phenotyping as described previously (Malamy and Benfey, 1997). Plants were imaged using a Leica DMI 3000B microscope fitted with a Leica long working 40x HCX PL FLUORTAR objective and illuminated with a Lumencor SOLA light source. Images were captured using Leica LAS AF version 2.6.0 software and a Leica DFC 345FX camera. For fluorescent images, Fiji software was used to quantify fluorescence in a region of interest centered on each image. Non-fluorescent siblings were used to calculate background levels. Fluorescence for each plant was analyzed by subtracting the background level of fluorescence and then normalizing to the initial time point.

RNA isolation and qPCR

Variant plants were grown vertically on 0.5x LS plates with 1.8% agar for 7 days and roots were excised and flash frozen at -80^{o}C. RNA was extracted from roots using an Illustra kit (GE Healthcare), and 1μg of complementary DNA was prepared using iScript kit (Bio-Rad). Samples were analyzed using SYBR Green Supermix (Bio-Rad) reactions run in a CFX96 Real-Time System (Bio-Rad). Expression for each gene was calculated using the formula $(E_{target})^{-\Delta CPtarget(control-sample)}/(E_{ref})^{-\Delta CPref(control-sample)}$ and normalized to the reference gene At1g13320 (Pfaffl, 2001).

Time lapse imaging of whole seedlings

Plants were grown vertically on 0.5x LS plates in Percival chambers under continuous light. At 4 dpg, plates were rotated 90º to induce lateral roots. Images were captured every hour using an

infrared camera system as previously described (Stewart et al., 2011). Images were processed using Image J (NIH).

Root hair density and hypocotyl measurements

Vertically-grown 7 dpg plants were imaged on a Leica dissecting microscope (S8APO, Leica Microsystems) and camera (DFC290, Leica Microsystems) for root hairs or scanned for hypocotyl measurement. Root hair number and hypocotyl length was determined using ImageJ. Two replicates were quantified, with 4-6 plants in each replicate for root hairs and 8-10 plants in each for hypocotyls.

AUTHOR CONTRIBUTIONS

JMG, BLM, AH, LACV, EK, and JLN conceived and designed experiments. JMG, AH, AL and TPF performed experiments. JMG and JLN wrote the paper.

ACKNOWLEDGEMENTS

This work was supported by the Paul G. Allen Family Foundation (JLN and EK). JMG was supported by the Developmental Biology Predoctoral Training Grant (T32HD007183) from the National Institute of Child Health and Human Development. We thank Keiko Torii, Takato Imaizumi, Christine Queitsch, David Raible, and members of the Nemhauser Lab and the Seattle Developmental Biology Group for excellent discussions and critical evaluation of this manuscript; Autumn Walker, Danny Liang, Minki Kim, Kevin Ford, and Wai Pang Chan for technical assistance; and Teva Vernoux for providing seeds.

REFERENCES

Brunoud, G., Wells, D.M., Oliva, M., Larrieu, A., Mirabet, V., Burrow, A.H., Beeckman, T., Kepinski, S., Traas, J., Bennett, M.J., et al. (2012). A novel sensor to map auxin response and distribution at high spatio-temporal resolution. Nature *482*, 103–106.

Calderón Villalobos, L.I. a, Lee, S., De Oliveira, C., Ivetac, A., Brandt, W., Armitage, L., Sheard, L.B., Tan, X., Parry, G., Mao, H., et al. (2012). A combinatorial TIR1/AFB-Aux/IAA co-receptor system for differential sensing of auxin. Nat. Chem. Biol. *8*, 477-485.

Chapman, E.J., and Estelle, M. (2009). Mechanism of auxin-regulated gene expression in plants. Annu. Rev. Genet. *43*, 265–285.

Clough, S.J., and Bent, A.F. (1998). Floral dip: a simplified method for Agrobacterium-mediated transformation of Arabidopsis thaliana. Plant J. *16*, 735–743.

De Smet, I., Tetsumura, T., De Rybel, B., Frey, N.F.D., Laplaze, L., Casimiro, I., Swarup, R., Naudts, M., Vanneste, S., Audenaert, D., et al. (2007). Auxin-dependent regulation of lateral root positioning in the basal meristem of Arabidopsis. Development *134*, 681–690.

Dharmasiri, N., Dharmasiri, S., and Estelle, M. (2005). The F-box protein TIR1 is an auxin receptor. Nature *435*, 441–445.

Fukaki, H., Tameda, S., Masuda, H., and Tasaka, M. (2002). Lateral root formation is blocked by a gain-of-function mutation in the SOLITARY-ROOT/IAA14 gene of Arabidopsis. Plant J. *29*, 153–168.

Gibson, D.G., Young, L., Chuang, R.-Y., Venter, J.C., Hutchison, C.A., and Smith, H.O. (2009). Enzymatic assembly of DNA molecules up to several hundred kilobases. Nat. Methods *6*, 343–345.

Gietz, R.D., and Woods, R.A. (2002). Transformation of yeast by lithium acetate/single-stranded carrier DNA/polyethylene glycol method. Methods Enzymol. *350*, 87–96.

Gray, W.M., Kepinski, S., Rouse, D., Leyser, O., and Estelle, M. (2001). Auxin regulates SCF(TIR1)-dependent degradation of AUX/IAA proteins. Nature *414*, 271–276.

Havens, K.A., Guseman, J.M., Jang, S.S., Pierre-Jerome, E., Bolten, N., Klavins, E., and Nemhauser, J.L. (2012). A synthetic approach reveals extensive tunability of auxin signaling. Plant Physiol. *160*, 135–142.

Kepinski, S., and Leyser, O. (2005). The Arabidopsis F-box protein TIR1 is an auxin receptor. Nature *435*, 446–451.

Korasick, D.A., Westfall, C.S., Lee, S.G., Nanao, M.H., Dumas, R., Hagen, G., Guilfoyle, T.J., Jez, J.M., and Strader, L.C. (2014). Molecular basis for AUXIN RESPONSE FACTOR protein interaction and the control of auxin response repression. Proc. Natl. Acad. Sci. U. S. A. *111*, 5427–5432.

Kumpf, R.P., Shi, C.-L., Larrieu, A., Stø, I.M., Butenko, M. a, Péret, B., Riiser, E.S., Bennett, M.J., and Aalen, R.B. (2013). Floral organ abscission peptide IDA and its HAE/HSL2 receptors control cell separation during lateral root emergence. Proc. Natl. Acad. Sci. *110*, 5235–5240.

Lokerse, A.S., and Weijers, D. (2009). Auxin enters the matrix--assembly of response machineries for specific outputs. Curr. Opin. Plant Biol. *12*, 520–526.

Lucas, M., Godin, C., Jay-Allemand, C., and Laplaze, L. (2008). Auxin fluxes in the root apex co-regulate gravitropism and lateral root initiation. J. Exp. Bot. *59*, 55–66.

Malamy, J.E., and Benfey, P.N. (1997). Organization and cell differentiation in lateral roots of Arabidopsis thaliana. Development *124*, 33–44.

Muto, H., Watahiki, M.K., Nakamoto, D., Kinjo, M., and Yamamoto, K.T. (2007). Specificity and similarity of functions of the Aux/IAA genes in auxin signaling of Arabidopsis revealed by promoter-exchange experiments among MSG2/IAA19, AXR2/IAA7, and SLR/IAA14. Plant Physiol. *144*, 187–196.

Nanao, M.H., Vinos-Poyo, T., Brunoud, G., Thévenon, E., Mazzoleni, M., Mast, D., Lainé, S., Wang, S., Hagen, G., Li, H., et al. (2014). Structural basis for oligomerization of auxin transcriptional regulators. Nat. Commun. *5*, 3617.

Ngo, Q.A., Vogler, H., Lituiev, D.S., Nestorova, A., and Grossniklaus, U. (2014). A calcium dialog mediated by the FERONIA signal transduction pathway controls plant sperm delivery. Dev. Cell *29*, 491–500.

Nishimura, K., Fukagawa, T., Takisawa, H., Kakimoto, T., and Kanemaki, M. (2009). An auxin-based degron system for the rapid depletion of proteins in nonplant cells. Nat. Methods *6*, 917–922.

O' Keefe, D.D., Thomas, S., Edgar, B.A., and Buttitta, L. (2014). Temporal Regulation of Dpp Signaling Output in the Drosophila Wing. Dev. Dyn. *243*, 818-832.

Pfaffl, M.W. (2001). A new mathematical model for relative quantification in real-time RT-PCR. Nucleic Acids Res. *29*, e45.

Purvis, J.E., and Lahav, G. (2013). Encoding and decoding cellular information through signaling dynamics. Cell *152*, 945–956.

Ramos, J. a, Zenser, N., Leyser, O., and Callis, J. (2001). Rapid degradation of auxin/indoleacetic acid proteins requires conserved amino acids of domain II and is proteasome dependent. Plant Cell *13*, 2349–2360.

Stewart, J.L., Maloof, J.N., and Nemhauser, J.L. (2011). PIF genes mediate the effect of sucrose on seedling growth dynamics. PLoS One *6*, e19894.

Tan, X., Calderon-Villalobos, L.I. a, Sharon, M., Zheng, C., Robinson, C. V, Estelle, M., and Zheng, N. (2007). Mechanism of auxin perception by the TIR1 ubiquitin ligase. Nature *446*, 640–645.

Vermeer, J.E.M., von Wangenheim, D., Barberon, M., Lee, Y., Stelzer, E.H.K., Maizel, A., and Geldner, N. (2014). A spatial accommodation by neighboring cells is required for organ initiation in Arabidopsis. Science *343*, 178–183.

Weijers, D., Benkova, E., Jäger, K.E., Schlereth, A., Hamann, T., Kientz, M., Wilmoth, J.C., Reed, J.W., and Jürgens, G. (2005). Developmental specificity of auxin response by pairs of ARF and Aux/IAA transcriptional regulators. EMBO J. *24*, 1874–1885.

FIGURE LEGENDS

Fig. 1. Engineered IAA14 variants exhibit a range of degradation rates and sensitivity to auxin.

(A) Schematic of lateral root development. **(B)** Amino acid substitutions engineered in domain II of IAA14. **(C)** IAA14 rate variants exhibited a range of auxin-induced degradation rates in yeast. YFP-tagged variants were co-expressed in yeast with the AFB2 auxin receptor. Time-lapse flow cytometry was used to monitor the YFP signal over time after auxin treatment at Time 0. Profiles were normalized to initial fluorescence. See also Fig S1A-B. **(D)** When combined with TIR1, IAA14 variants had different auxin-binding affinities. *In vitro* saturation binding experiments showed high auxin binding affinity by the TIR1:14-control (K_d=12.2 +/-5.7) and TIR1:14-Fast (K_d=13.6 +/-2.7) co-receptor complexes. Auxin binding affinity was substantially reduced in the TIR1:14-Medium complex (K_d=77.3 +/-11.4), and the TIR1:14-Slow complex (K_d=187 +/-206). A representative saturation binding experiment is shown. Error bars represent S.E.M. See also Fig S1C. **(E)** Degradation rates in plants were similar to those observed in yeast. Venus-tagged IAA14 variants were induced by 2h treatment at 37C (heat shock) after which plants were sprayed with auxin (Time 0). Error bars represent S.E.M. **(F)** Images of representative plants containing heat-shock-inducible Venus-IAA14 variants. Treatments are as in 1E.

Fig. 2. Slowing IAA14 degradation rate quantitatively decreases lateral root density.

(A) 14-control (14) and 14-Fast (F) lines had similar densities of lateral roots at 7 and 14 dpg. In contrast, plants expressing 14-Medium (M) and 14-Slow (S) variants had fewer lateral roots at both time-points, suggesting a developmental delay. No emerged lateral roots were detected at any time-point in 14-Insensitive (I) lines. Averages were calculated from three independent experiments with 6-10 seedlings per experiment. N.D. No lateral roots detected. See also Figure S2. **(B)** The density of lateral root primordia per developmental stage I-VII showed a similar overall trend as observed with emerged roots. Averages are from 7 dpg seedlings, and were calculated from three independent experiments with six seedlings per experiment. See also Figure S2.

Fig. 3. IAA14 degradation dynamics determine the rate of progression through lateral root development.

(A) Progression of lateral root development is delayed in plants containing slower IAA14 variants. Root development was synchronized using root gravitropic responses to induce root bending. Developmental stages were analyzed at 18, 42, and 66 hpi for 14-control (14), 14-Medium (M), 14-Slow (S) and 14-Insensitive (I) lines. See also Movie S1. **(B)** Late stage primordia in 14-Medium plants frequently exhibited aberrant morphology. The yellow line indicates the outer layer of the lateral root primordium. The red line indicates vascular tissue. **(C)** Expression of the auxin-responsive reporter DR5-Venus is rapidly induced by root bending in IAA14-control lines. Reporter expression is delayed in plants expressing Medium- and Slow IAA14 variants, consistent with a delay in organogenesis. The outer bend, where the primordia will initiate, is shown to the right in all panels. Two individuals are shown for each time point post-induction to illustrate the range of DR5 expression levels observed between individual plants within a line. Gray lines indicate the outside boundary of each root.

Figure S1. A synthetic system for assaying auxin-induced degradation rate variants.

(A) Degradation rates observed when IAA14 variants are co-expressed with TIR1 are similar to those observed when variants are co-expressed with AFB2. YFP-tagged variants were co-expressed in yeast with the TIR1 auxin receptor. Degradation of the YFP signal following addition of auxin at time 0 was quantified with flow cytometry. Degradation profiles were normalized to initial fluorescence. See also Figure 1C. **(B)** Degradation of IAA14 variants is auxin-dependent. YFP-tagged variants were co-expressed in yeast with either AFB2 or TIR1. Fluorescence following addition of a mock treatment at time 0 was quantified with flow cytometry. All of these strains show similar fluorescence values over time as auxin-treated strains expressing YFP without an Aux/IAA fusion (YFP). A control strain without YFP was monitored to estimate levels of background fluorescence. See also Figure 1C and S1A. **(C)** Degradation rates of IAA14 rate variants are correlated with sensitivity to auxin. Yeast expressing YFP-tagged IAA14 variants and either AFB2 or TIR1 was grown in media with the indicated concentrations of auxin. Fluorescence was measured by flow-cytometry 2 h after addition of mock or auxin treatment. See also Figure 1D.

Figure S2. **Effects of IAA14 are specific and not dose-dependent.**

(A) Additional copies of wild-type IAA14 do not affect lateral root densities. Lateral root phenotypes were compared between plants transformed with wild-type IAA14 expressed from its own promoter (pIAA14::IAA14) and untransformed plants (Col). Emerged lateral roots were counted at the end of 7dpg or 14dpg. Error bar represent S.E.M. See also Figure 2A-B. **(B)** Variant lines exhibit similar levels of IAA14 mRNA expression. Plants transformed with IAA14 variants were treated for 3 h with either mock or auxin treatments. Levels of *IAA14* mRNA in isolated roots were quantified by qPCR. See also Figure 2A-B. **(C)** Effects of variation in IAA14 degradation rate are tissue-specific Root hair density decreased when IAA14 degradation rate was slowed. See also Figure 2A-B and S2D. **(D)** Hypocotyl length of plants grown in light/dark cycles or constant conditions was not correlated with IAA14 degradation rate. Error bars represent S.E.M. See also Figure 2A-B and S2C.

Movie S1. Time-lapse imaging of lateral root emergence in a 14- and Medium variant plant.

(A) Plants were gravistimulated to induce lateral root formation and imaged every hour over 8 days. Lateral roots were detected at the outer side of the root bend between 70 and 90 hours-post-induction (hpi). A timer at the upper left indicates hpi. See also Figure 3. **(B)** Plants were grown and gravistimulated as in Movie S1. In the Medium-variant plants, a lateral root emerged at the bend in the root between 90 and 110 hours-post-induction (hpi). A small number of Medium plants had no visible primordia by the end of imaging. No plants expressing the Slow- or Insensitive variants formed roots for the duration of imaging. A timer at the upper left indicates hpi. See also Figure 3.

Figure 1

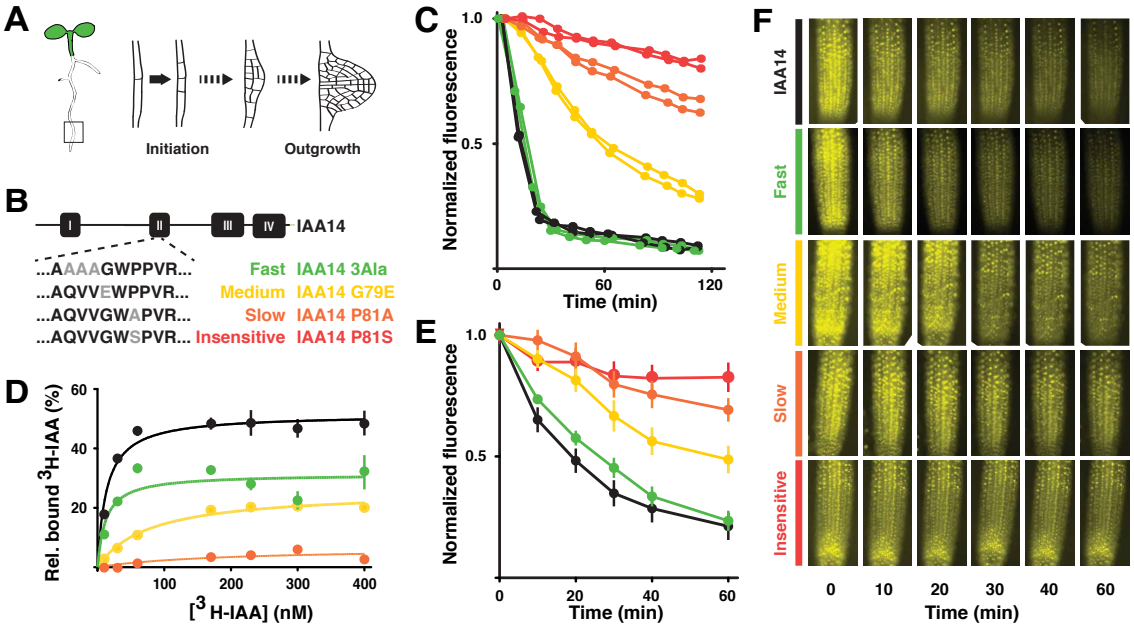
A
Initiation
Outgrowth
B
I
II
III
IV
IAA14
...AAAAGWPPVR... Fast IAA14 3Ala
...AQVVEWPPVR... Medium IAA14 G79E
...AQVVGWAPVR... Slow IAA14 P81A
...AQVVGWSPVR... Insensitive IAA14 P81S
D
Rel. bound 3H-IAA (%)
[3 H-IAA] (nM)
C
Normalized fluorescence
Time (min)
E
Normalized fluorescence
Time (min)
F
IAA14
Fast
Medium
Slow
Insensitive
Time (min)

Figure 2

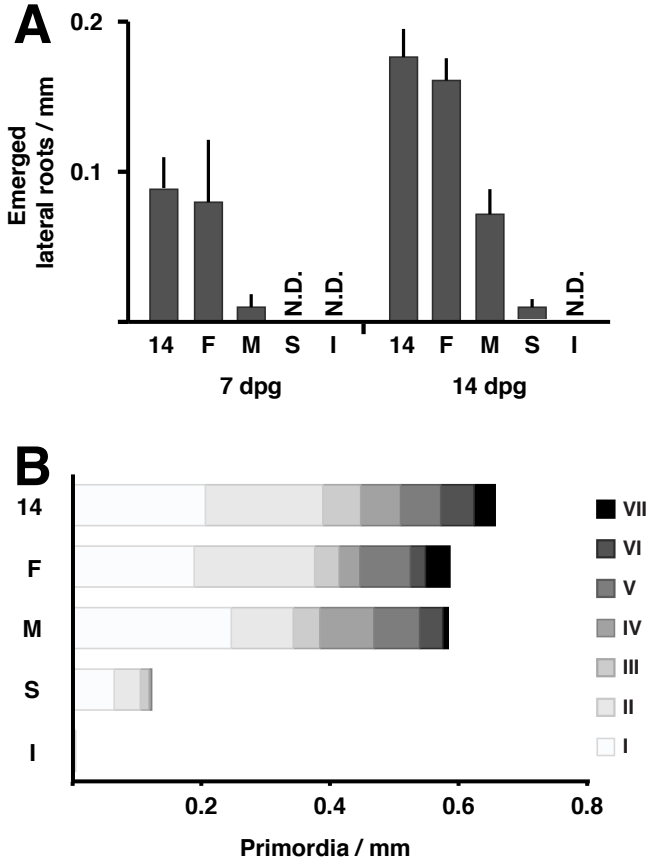
A
0.2
0.1
Emerged lateral roots / mm
N.D.
N.D.
N.D.
14 F M S I 14 F M S I
7 dpg
14 dpg
B
14
F
M
S
I
VII
VI
V
IV
III
II
I
0.2
0.4
0.6
0.8
Primordia / mm

Figure 3

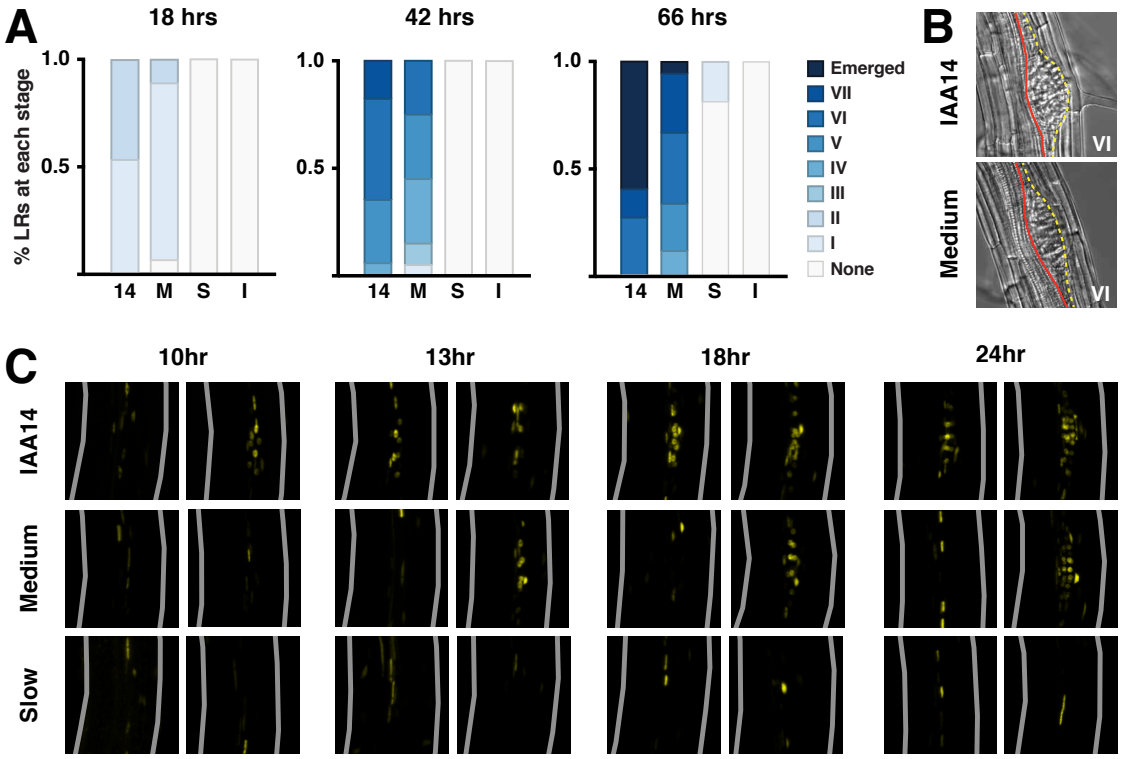
A
18 hrs
42 hrs
66 hrs
% LRs at each stage
1.0
0.5
14 M S I
Emerged
VII
VI
V
IV
III
II
I
None
B
IAA14
Medium
VI
C
10hr
13hr
18hr
24hr
IAA14
Medium
Slow

SUPPLEMENTARY INFORMATION

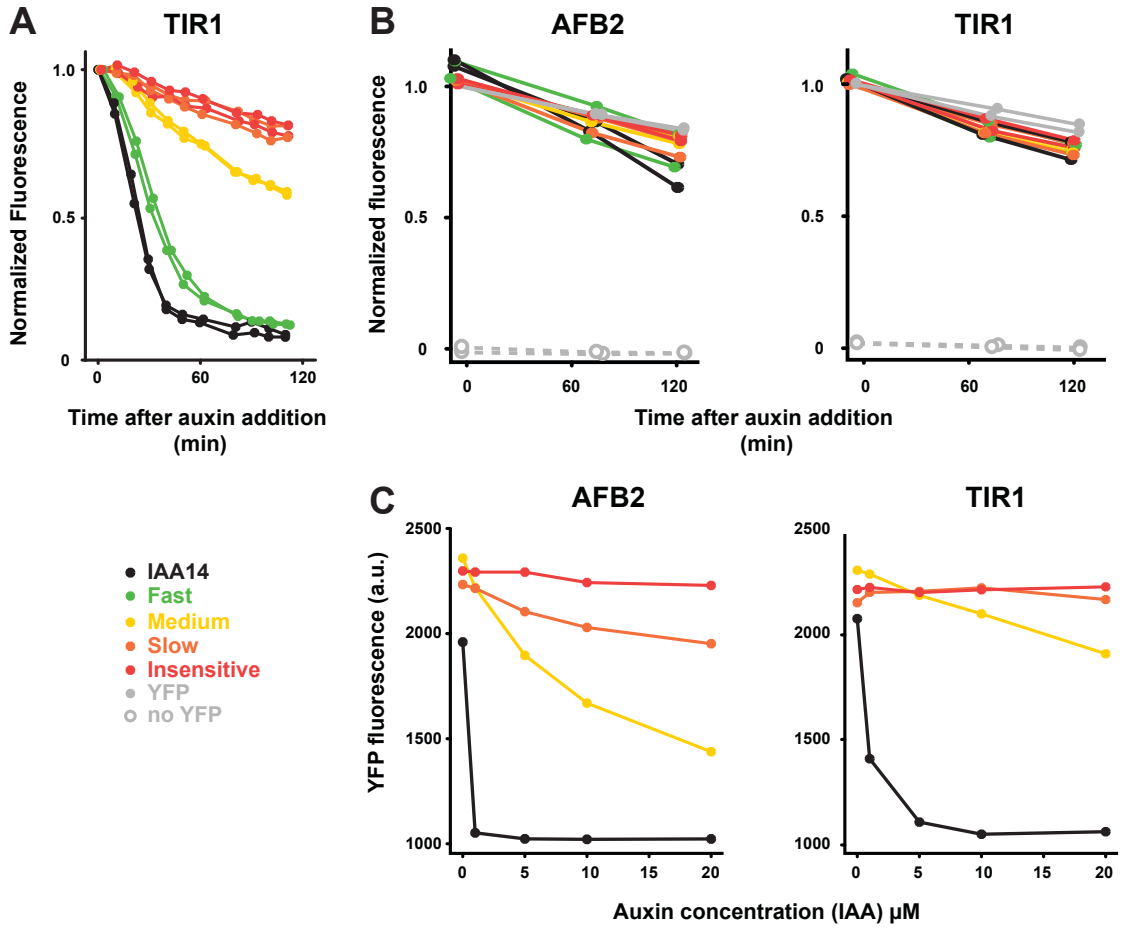

Figure S1. A synthetic system for assaying auxin-induced degradation rate variants. **(A)** Degradation rates observed when IAA14 variants are co-expressed with TIR1 are similar to those observed when variants are co-expressed with AFB2. YFP-tagged variants were co-expressed in yeast with the TIR1 auxin receptor. Degradation of the YFP signal following addition of auxin at time 0 was quantified with flow cytometry. Degradation profiles were normalized to initial fluorescence. See also Figure 1C. **(B)** Degradation of IAA14 variants is auxin-dependent. YFP-tagged variants were co-expressed in yeast with either AFB2 or TIR1. Fluorescence following addition of a mock treatment at time 0 was quantified with flow cytometry. All of these strains show similar fluorescence values over time as auxin-treated strains expressing YFP without an Aux/IAA fusion (YFP). A control strain without YFP was monitored to estimate levels of background fluorescence. See also Figure 1C and S1A. **(C)** Degradation rates of IAA14 rate variants are correlated with sensitivity to auxin. Yeast expressing YFP-tagged IAA14 variants and either AFB2 or TIR1 was grown in media with the indicated concentrations of auxin. Fluorescence was measured by flow-cytometry 2 h after addition of mock or auxin treatment. See also Figure 1D.

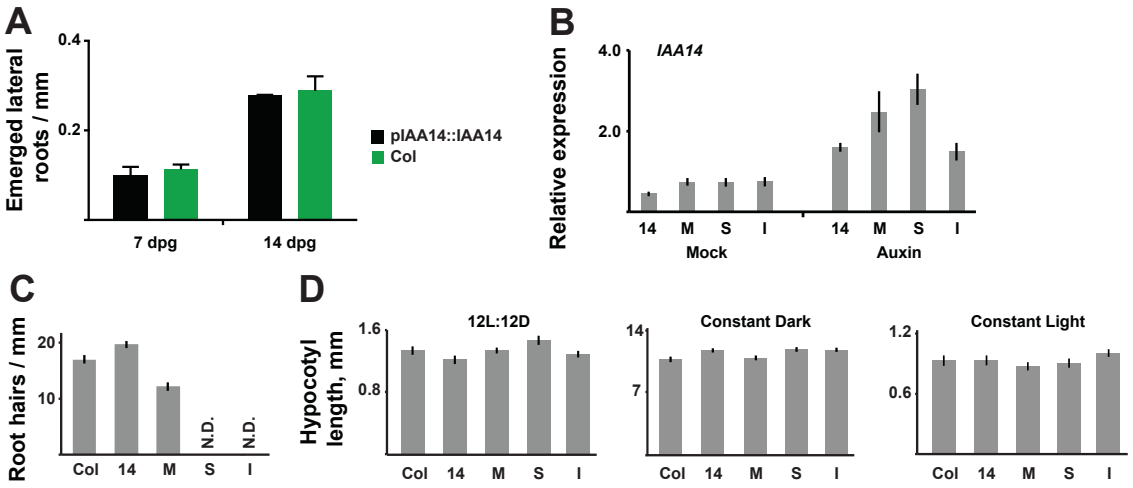

Figure S2. **Effects of IAA14 are specific and not dose-dependent.**
(A) Additional copies of wild-type IAA14 do not affect lateral root densities. Lateral root phenotypes were compared between plants transformed with wild-type IAA14 expressed from its own promoter (pIAA14::IAA14) and untransformed plants (Col). Emerged lateral roots were counted at the end of 7dpg or 14dpg. Error bar represent S.E.M. See also Figure 2A-B. **(B)** Variant lines exhibit similar levels of IAA14 mRNA expression. Plants transformed with IAA14 variants were treated for 3 h with either mock or auxin treatments. Levels of *IAA14* mRNA in isolated roots were quantified by qPCR. See also Figure 2A-B. **(C)** Effects of variation in IAA14 degradation rate are tissue-specific Root hair density decreased when IAA14 degradation rate was slowed. See also Figure 2A-B and S2D. **(D)** Hypocotyl length of plants grown in light/dark cycles or constant conditions was not correlated with IAA14 degradation rate. Error bars represent S.E.M. See also Figure 2A-B and S2C.

Movie S1. Time-lapse imaging of lateral root emergence in a 14- and Medium variant plant.
(A) Plants were gravistimulated to induce lateral root formation and imaged every hour over 8 days. Lateral roots were detected at the outer side of the root bend between 70 and 90 hours-post-induction (hpi). A timer at the upper left indicates hpi. See also Figure 3.
(B) Plants were grown and gravistimulated as in Movie S1. In the Medium-variant plants, a lateral root emerged at the bend in the root between 90 and 110 hours-post-induction (hpi). A small number of Medium plants had no visible primordia by the end of imaging. No plants expressing the Slow- or Insensitive variants formed roots for the duration of imaging. A timer at the upper left indicates hpi. See also Figure 3.

Chapter 5

CONCLUSION: Understanding biology is hard. But terribly interesting.

Auxin signaling is complicated: new tools to address long-standing questions

From the early proposal by Darwin that chemical messengers are sent from the tip of a seedling to cause it to bend towards the light, many people have studied the roles of the chemical messenger auxin in plant growth and development. In fact, the massive interest in this topic attracted me to it in the first place. Years of experimentation have led to a wealth of knowledge about how auxin sends signals about nearly every process in plant biology. We know quite a lot about the nuclear auxin signaling pathway, including: the basic structure of this pathway (Pierre-Jerome et al., 2013); the molecular structure of the auxin binding pocket (Tan et al., 2007); what proteins act as influx and efflux carriers and how they are recycled to and from the cell membrane (Zazímalová et al., 2010); how auxin is synthesized and conjugated (Korasick et al., 2013). When I started studying auxin biology in 2010, there were some major experimental challenges for moving forward and interpreting auxin-related studies in plants. Over the next few years, a number of groups, including our own, set out to develop new tools and systems to address and add clarity to questions regarding how auxin elicits responses:

A major difficulty has been the lack of tools for auxin visualization and quantification. The DR5 reporter has been very useful to visualize where auxin-responsive transcription is likely happening. More recently, DII-Venus emerged as a useful negative auxin sensor (Brunoud et al., 2012). DII-Venus employs the use of an IAA28 degron domain, and thus is degraded in the presence of auxin. A caveat for using a component of the signaling pathway itself is that it depends on the presence of the AFB auxin receptors, which are variable in different tissues. In addition, it is only as sensitive as IAA28, which is a relatively slow degrading Aux/IAA (Havens et al., 2012). An improvement on this might be to have sensors built from multiple Aux/IAA degrons with different sensitivities to auxin. This would allow us to use a dynamic range of sensitivies to better capture high

and low auxin concentrations. Even more ideal would be to develop a sensor that worked independently of the native auxin pathway, such that auxin levels could be faithfully reported regardless of the complement of signaling components present in a specific cell type.

Another challenge is that multiple Aux/IAAs and ARFs are co-expressed in many cell types, but tissue-specific expression maps are still incomplete and difficult to obtain. Over the past several years, a few organ-specific studies have mapped out the transcriptome of auxin-responsive genes over time (Vernoux et al., 2011; Bargmann et al., 2013). This is a place where bioinformatics will be very useful, adding new tools to pull existing and new data together to form a more comprehensive and dynamic picture. For example, in lateral root formation, it would be ideal to know how many Aux/IAAs and ARFs are expressed in each cell layer contributing to the process (pericycle, endodermis, cortex), and when, how long, and in what order these genes are expressed. Ideally, having this information for each cell type throughout the plant would allow us generate new hypotheses about how these proteins work together without missing pieces.

The fact that the auxin pathway is integrated with many other hormone and nutrient signaling pathways also complicates investigations of its specific roles. Many groups working on signal integration, including our own, have taken to combining mathematical modeling with biological experiments to generate hypotheses about pathway interactions: for example addressing interactions between auxin, GA, and sucrose in hypocotyl elongation (Lilley et al., unpublished); strigolactone action on auxin transport in shoot branching (Prusinkiewicz et al., 2009; Shinohara et al., 2013); and auxin-ethylene-cytokinin interactions in root growth (Liu et al., 2010).

In collaboration with the Klavins lab in the Electrical Engineering department, we developed a new approach to auxin signaling to tackle some of these challenges and gain some clarity (Havens et al., 2012). Similar to heterologous expression experiments used in the past (Mak et al., 1989; Tilley et al., 1989; Krobitsch and Lindquist, 2000; Zuo et al., 2000), we importing the auxin pathway into yeast, allowing us to express signaling components in isolation, control auxin input with precision, measure signaling dynamics with high temporal resolution, as well as monitor on a single cell level. Mathematical modeling allowed us to not only quantify degradation rate, but also to generate and test

hypotheses about other parameters in the system, such as the effects of expression level on degradation rate. Working in this collaboration cemented for me that so much of biology can benefit from intersecting with new disciplines to develop new tools to address questions.

Aux/IAAs exhibit range of degradation rates – why?

When we compare the families of auxin signaling components between early and late diverging land plants, several trends stand out. First, we see an increase in developmental and physiological complexity in more recently diverged species, as well as the number of the processes that auxin regulates. Second, there are increased numbers of Aux/IAA protein family members, not correlated with genome size (Remington et al., 2004; Paponov et al., 2009). Studies have suggested that this is likely due to retention of gene duplicates, as Aux/IAAs are not under higher selection pressure (Paponov et al., 2009). We know that a common mechanism for gene duplicate retention is subfunctionalization through divergence in expression pattern (Conant and Wolfe, 2008). Previous studies have shown that expression patterns of Aux/IAA sister pairs have diverged significantly (Duarte et al., 2006). I speculate that after post-duplication divergence in expression of Aux/IAA sisters, optimization of degradation rates offered a selective advantage in these distinct cellular contexts. For each new auxin-regulated process, this would allow for the evolution of developmental timing mechanisms and optimization of the dynamic range of auxin sensitivities.

To address this speculation, I think there are a number of experimental approaches that will be especially informative. First, do degradation rates of other Aux/IAAs act as biological timers in other developmental contexts, and does this act to separate the timing of their functions? For example, when Aux/IAAs are controlling consecutive steps of a developmental process, does a fast degrading protein regulate the earlier step and a slow degrader regulate the later one? Is this a common mechanism or particular to IAA14 or roots? Second, it would be very interesting to look at degradation rates across Arabidopsis accessions or closely related species. This would allow us to compare the range of Aux/IAA degradation rates, but also how the degradation rate of an individual

Aux/IAA family member differs, especially in the context of development. For example, in accessions that evolved/adapted to make fewer lateral roots than Columbia, does IAA14 degrade slower?

How else might we get specificity?

A set of hypotheses can be made about how we get specificity from auxin signaling. We've gathered quite a bit of evidence to support our hypothesis that Aux/IAA degradation rates differ, and that these degradation rates act as biological timers (Chapters 2 and 4). Another hypothesis that greatly interested me from the beginning was that specific ARF-Aux/IAA pairs have binding preferences for one another. This hypothesis is support in part by striking similarities between mutant phenotypes. For example, several Aux/IAA stabilized mutants phenocopy specific ARF knockout mutants (Hardtke et al., 2004; De Smet et al., 2010). I set out to test this hypothesis originally using a multi-color BiFC system to run competition experiments. While this proved difficult and I moved it to the back burner to pursue the role of Aux/IAA degradation rates in development, a number of new studies have opened up a lot of new questions on this topic. Structure and dimerization studies have provided mechanisms for how these proteins dimerize (Boer et al., 2014; Korasick et al., 2014) and suggest that explaining binding preference is more complex than previous one-IAA-one-ARF models. For example, ARFs and Aux/IAAs appear have different requirements for the binding surfaces each needs to dimerize, and Aux/IAA oligomerization might be required for repression (Korasick et al., 2014). This opens more questions about how we get specificity. Are multiple Aux/IAA family members repressing ARFs together, and if we factor in differential degradation rates among them, how does this change the behavior of the complex?

My ongoing transformation to a biologist

I recently found a piece of paper in an old notebook where I listed the pros and cons of working on the auxin synthetic biology project. A con for 2010 Jessica was that I seemed

to have an inner conflict about working in synthetic biology and that I "didn't want to change things". What I meant by this, I remembered, was that I feared synthetic biology as a tool to irreparably alter the natural world at the whim of humans. I have since realized that I was actually just afraid of the unknown. In addition, I reminded myself that I trust the other scientists I work with (so it couldn't be part of some diabolical scheme), and that humans are part of the nature, too. Initially, the idea of synthetic biology was very new to me, and I had not had time to think about its uses and consequences. After a while, I sorted out my rational thoughts and emotional feelings enough to ask, listen, and understand the innovative things we can do with synthetic biology. For example, building new circuits in bacteria, yeast or plant cells can allow for the design of organisms useful in medicine production, biofuels, disease diagnostics, and, of course, addressing biological questions. Using auxin-induced repressor degradation allows us to generate synthetic circuits that are fast and controllable, something that could be very useful for any of these applications.

Also during graduate school, I became much more familiar with the debate over genetically modified organisms (GMOs). This was a topic I thought very little about before, and decided to participate in a public reading group of Pam Ronald's book Tomorrow's Table, hosted by the Biology department. This really opened my eyes to the fact that a lot of people are very worried about GMOs. The fears of many people that I talked to were similar to my initial fears of synthetic biology. They didn't understand how the biology works, and were afraid of what they didn't know. While I've come to realize that there are real issues that are in need of discussion concerning GMOs, most of the fears of the general public seem to be focused on non-issues or mis-information. Over the past few years, I have improved my ability to rationally discuss and teach people what I know about biology and how it relates to these concerns.

I've done a lot of growing up and confidence-building throughout graduate school. A major lesson I have learned is not to fear what I don't know, but instead to ask questions and make hypotheses. Because that is what scientists do.

REFERENCES

Bargmann BOR, Vanneste S, Krouk G, Nawy T, Efroni I, Shani E, Choe G, Friml J, Bergmann DC, Estelle M, et al (2013) A map of cell type-specific auxin responses. Mol Syst Biol **9**: 688

Boer DR, Freire-Rios A, van den Berg WAM, Saaki T, Manfield IW, Kepinski S, López-Vidrieo I, Franco-Zorrilla JM, de Vries SC, Solano R, et al (2014) Structural basis for DNA binding specificity by the auxin-dependent ARF transcription factors. Cell **156**: 577–89

Brunoud G, Wells DM, Oliva M, Larrieu A, Mirabet V, Burrow AH, Beeckman T, Kepinski S, Traas J, Bennett MJ, et al (2012) A novel sensor to map auxin response and distribution at high spatio-temporal resolution. Nature **482**: 103–106

Conant GC, Wolfe KH (2008) Turning a hobby into a job: how duplicated genes find new functions. Nat Rev Genet **9**: 938–50

Duarte JM, Cui L, Wall PK, Zhang Q, Zhang X, Leebens-Mack J, Ma H, Altman N, dePamphilis CW (2006) Expression pattern shifts following duplication indicative of subfunctionalization and neofunctionalization in regulatory genes of Arabidopsis. Mol Biol Evol **23**: 469–78

Hardtke CS, Ckurshumova W, Vidaurre DP, Singh S a, Stamatiou G, Tiwari SB, Hagen G, Guilfoyle TJ, Berleth T (2004) Overlapping and non-redundant functions of the Arabidopsis auxin response factors MONOPTEROS and NONPHOTOTROPIC HYPOCOTYL 4. Development **131**: 1089–100

Havens K a, Guseman JM, Jang SS, Pierre-Jerome E, Bolten N, Klavins E, Nemhauser JL (2012) A synthetic approach reveals extensive tunability of auxin signaling. Plant Physiol **160**: 135–42

Korasick DA, Enders TA, Strader LC (2013) Auxin biosynthesis and storage forms. J Exp Bot **64**: 2541–55

Korasick DA, Westfall CS, Lee SG, Nanao MH, Dumas R, Hagen G, Guilfoyle TJ, Jez JM, Strader LC (2014) Molecular basis for AUXIN RESPONSE FACTOR protein interaction and the control of auxin response repression. Proc Natl Acad Sci U S A **111**: 5427–32

Krobitsch S, Lindquist S (2000) Aggregation of huntingtin in yeast varies with the length of the polyglutamine expansion and the expression of chaperone proteins. Proc Natl Acad Sci U S A **97**: 1589–94

Liu J, Mehdi S, Topping J, Tarkowski P, Lindsey K (2010) Modelling and experimental analysis of hormonal crosstalk in Arabidopsis. Mol Syst Biol **6**: 373

Mak P, McDonnell DP, Weigel NL, Schrader WT, O'Malley BW (1989) Expression of functional chicken oviduct progesterone receptors in yeast (Saccharomyces cerevisiae). J Biol Chem **264**: 21613–8

Paponov I a, Teale W, Lang D, Paponov M, Reski R, Rensing S a, Palme K (2009) The evolution of nuclear auxin signalling. BMC Evol Biol **9**: 126

Pierre-Jerome E, Moss BL, Nemhauser JL (2013) Tuning the auxin transcriptional response. J Exp Bot **64**: 2557–63

Prusinkiewicz P, Crawford S, Smith RS, Ljung K, Bennett T, Ongaro V, Leyser O (2009) Control of bud activation by an auxin transport switch. Proc Natl Acad Sci U S A **106**: 17431–6

Remington DL, Vision TJ, Guilfoyle TJ, Reed JW (2004) Contrasting Modes of Diversification in the Aux/IAA and ARF Gene Families. Plant Physiol **135**: 1738–1752

Shinohara N, Taylor C, Leyser O (2013) Strigolactone can promote or inhibit shoot branching by triggering rapid depletion of the auxin efflux protein PIN1 from the plasma membrane. PLoS Biol **11**: e1001474

De Smet I, Lau S, Voss U, Vanneste S, Benjamins R, Rademacher EH, Schlereth A, De Rybel B, Vassileva V, Grunewald W, et al (2010) Bimodular auxin response controls organogenesis in Arabidopsis. Proc Natl Acad Sci U S A **107**: 2705–10

Tan X, Calderon-Villalobos LI a, Sharon M, Zheng C, Robinson C V, Estelle M, Zheng N (2007) Mechanism of auxin perception by the TIR1 ubiquitin ligase. Nature **446**: 640–5

Tilley WD, Marcelli M, Wilson JD, McPhaul MJ (1989) Characterization and expression of a cDNA encoding the human androgen receptor. Proc Natl Acad Sci U S A **86**: 327–31

Vernoux T, Brunoud G, Farcot E, Morin V, Van den Daele H, Legrand J, Oliva M, Das P, Larrieu A, Wells D, et al (2011) The auxin signalling network translates dynamic input into robust patterning at the shoot apex. Mol Syst Biol **7**: 508

Zazímalová E, Murphy AS, Yang H, Hoyerová K, Hosek P (2010) Auxin transporters--why so many? Cold Spring Harb Perspect Biol **2**: a001552

Zuo J, Niu QW, Chua NH (2000) Technical advance: An estrogen receptor-based transactivator XVE mediates highly inducible gene expression in transgenic plants. Plant J **24**: 265–73